

Fall 2014

Quartz-mems: Wet chemical etching assisted by electromagnetic energy sources for the development of quartz crystal to be used for microelectromechanical systems

William J. Clower

Follow this and additional works at: <https://digitalcommons.latech.edu/dissertations>

 Part of the [Electrical and Computer Engineering Commons](#), and the [Nanoscience and Nanotechnology Commons](#)

**QUARTZ-MEMS: WET CHEMICAL ETCHING ASSISTED BY
ELECTROMAGNETIC ENERGY SOURCES FOR THE
DEVELOPMENT OF QUARTZ CRYSTAL TO BE USED FOR
MICROELECTROMECHANICAL SYSTEMS**

by

William J. Clower, B.S.

A Dissertation Presented in Partial Fulfillment
of the Requirements of the Degree
Doctor of Philosophy

COLLEGE OF ENGINEERING & SCIENCE
LOUISIANA TECH UNIVERSITY

November 2014

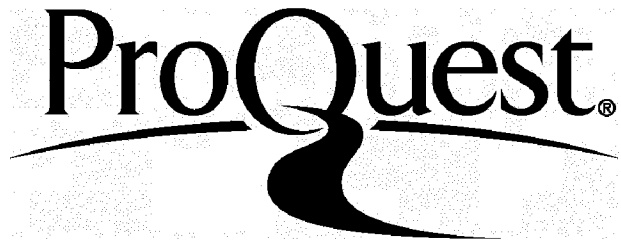
ProQuest Number: 10612785

All rights reserved

INFORMATION TO ALL USERS

The quality of this reproduction is dependent upon the quality of the copy submitted.

In the unlikely event that the author did not send a complete manuscript and there are missing pages, these will be noted. Also, if material had to be removed, a note will indicate the deletion.



ProQuest 10612785

Published by ProQuest LLC(2017). Copyright of the Dissertation is held by the Author.

All rights reserved.

This work is protected against unauthorized copying under Title 17, United States Code.
Microform Edition © ProQuest LLC.

ProQuest LLC
789 East Eisenhower Parkway
P.O. Box 1346
Ann Arbor, MI 48106-1346

LOUISIANA TECH UNIVERSITY

THE GRADUATE SCHOOL

SEPTEMBER 22, 2014

Date

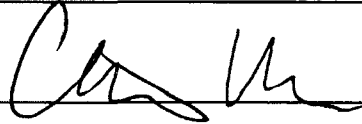
We hereby recommend that the dissertation prepared under our supervision by

William J. Clower B.S.

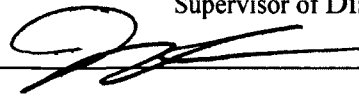
entitled QUARTZ-MEMS: WET CHEMICAL ETCHING ASSISTED BY
ELECTROMAGNETIC ENERGY SOURCES FOR THE DEVELOPMENT OF
QUARTZ CRYSTAL TO BE USED FOR MICROELECTROMECHANICAL
SYSTEMS

be accepted in partial fulfillment of the requirements for the Degree of

DOCTOR OF PHILOSOPHY IN ENGINEERING



Supervisor of Dissertation Research



Head of Department

Engineering

Department

Recommendation concurred in:

VILLE KAJAKAARI

Long Que

Patil Ramakrishnan

Karl E. ...

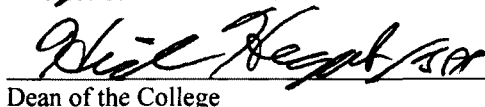
Advisory Committee

Approved:


Director of Graduate Studies

Approved:


Dean of the Graduate School


Dean of the College

ABSTRACT

Quartz crystal resonators have been the most commonly used timing devices to date. Today's timing market requires devices to be as small as possible and consume smaller amounts of energy. Because of the market demand, many startup companies have formed to develop silicon resonators as timing devices. Silicon resonators have poor noise and temperature performance (due to its linear temperature versus frequency coefficient). At the moment the only advantage that silicon resonators have over quartz crystal resonators is a small form factor. The photolithography processing method currently being used in industry is a very tedious task, requiring multiple etching steps and a final frequency trimming step for each individual resonator.

The goal of this research was to find a process that could increase the etch rate of quartz crystals beyond the current methods available. This dissertation reports the first results on x-rays assisting the electrochemical etching of quartz crystals in the development of quartz resonators. This process has shown the ability to increase the etch rate of quartz by 27%. The second method explored in this work involves the use of lasers to rapidly etch quartz crystals during the wet etching process. The etch rate with the laser setup can be varied from 3.8 $\mu\text{m/hr}$ to 278 $\mu\text{m/hr}$. These processes were integrated with a control system used to measure the resonant frequency of each individual resonator to an accuracy of $\pm 10\text{ppm}$. Using two lasers incorporated with the control system allowed for a total etching accuracy of $\pm 50\text{ppm}$ for two resonators on the same die.

APPROVAL FOR SCHOLARLY DISSEMINATION

The author grants to the Prescott Memorial Library of Louisiana Tech University the right to reproduce, by appropriate methods, upon request, any or all portions of this Dissertation. It is understood that "proper request" consists of the agreement, on the part of the requesting party, that said reproduction is for his personal use and that subsequent reproduction will not occur without written approval of the author of this Dissertation. Further, any portions of the Dissertation used in books, papers, and other works must be appropriately referenced to this Dissertation.

Finally, the author of this Dissertation reserves the right to publish freely, in the literature, at any time, any or all portions of this Dissertation.

Author William J. Clower

Date 11-03-2014

DEDICATION

I want to dedicate this dissertation work to my late Grandfather, Ernest Earl Clower.

TABLE OF CONTENTS

| | |
|--|-----|
| ABSTRACT..... | iii |
| DEDICATION..... | v |
| LIST OF TABLES..... | xi |
| LIST OF FIGURES..... | xii |
| ACKNOWLEDGEMENTS..... | xvi |
| CHAPTER 1 INTRODUCTION TO QUARTZ CRYSTAL INDUSTRY..... | 1 |
| 1.1 Quartz Crystal Industry..... | 2 |
| 1.1.1 Applications of Quartz Crystals..... | 6 |
| 1.1.2 Current Quartz Crystal Devices on Market..... | 7 |
| 1.1.3 Competitors to Quartz Crystal Resonators..... | 10 |
| 1.2 Properties of Alpha Quartz..... | 16 |
| 1.2.1 Piezoelectric Nature..... | 16 |
| 1.2.2 Quality Factor..... | 21 |
| 1.2.3 Zero Temperature Coefficient Cuts..... | 24 |
| 1.2.4 Low Solubility of Quartz Crystals..... | 26 |
| 1.3 Current Processing Methods..... | 27 |
| 1.3.1 Deep Reactive Ion Etching (DRIE)..... | 28 |

| | |
|--|-----------|
| 1.3.2 Micromachining Ion Track Etching (MITE)..... | 28 |
| 1.3.3 Mechanical Lapping..... | 29 |
| 1.3.4 Wet Etching of Quartz Resonators..... | 29 |
| 1.3.5 Commercial Wet Etching Process | 34 |
| 1.4 Research Objective..... | 36 |
| CHAPTER 2 ETCHING CONTROL SYSTEM..... | 38 |
| 2.1 PID Control Theory | 39 |
| 2.1.1 Proportional Control | 42 |
| 2.1.2 Integral Control..... | 44 |
| 2.1.3 Derivative Control | 46 |
| 2.1.4 PID Controller | 47 |
| 2.2 Implementation of PID Control In LABVIEW | 49 |
| 2.2.1 Control Interface | 50 |
| 2.3 Resonators On Same Die Simultaneously Etched..... | 52 |
| 2.3.1 Experiment Setup..... | 52 |
| 2.3.2 Results and Discussions | 53 |
| 2.4 Conclusion..... | 56 |
| CHAPTER 3 ELECTROCHEMICAL ETCHING ASSISTED BY X-RAYS..... | 58 |
| 3.1 Electrochemical Etching of Silicon | 59 |
| 3.2 Photon Effects on Etching Silicon..... | 61 |

| | |
|---|------------|
| 3.3 Photon Effects on The Energy Band Gap of Insulators..... | 63 |
| 3.4 Review of Electrochemical and UV Radiation Etching of Amorphous Silicon Dioxide..... | 65 |
| 3.5 Review of Assisted Wet Etching of Quartz Crystals..... | 69 |
| 3.6 Experimental Setup..... | 70 |
| 3.6.1 X-Ray Tube and Operational Principles..... | 74 |
| 3.7 Radiation Effects on Quartz..... | 81 |
| 3.7.1 Defects Present in Quartz Crystals..... | 81 |
| 3.7.2 Electrodiffusion of Impurity Ions in Quartz Crystals..... | 86 |
| 3.7.3 Radiation Induced Current Through Quartz..... | 87 |
| 3.7.4 Modeling of Radiation Induced Current Through Quartz..... | 91 |
| 3.7.5 Results and Discussions..... | 93 |
| 3.8 Conclusion and Future Work..... | 104 |
| CHAPTER 4 LASER ASSISTED RAPID ETCHING..... | 106 |
| 4.1 Literature Review for Laser Etching of Quartz..... | 108 |
| 4.2 Laser Etching Setup for Creating BAW QCRs..... | 111 |
| 4.3 Laser Principles of Operation..... | 114 |
| 4.3.1 Laser Pumping..... | 115 |
| 4.3.2 Transitions..... | 116 |
| 4.3.3 Polarization Ratio..... | 116 |

| | |
|--|------------|
| 4.3.4 M^2 Factor | 117 |
| 4.4 Optical Elements..... | 117 |
| 4.4.1 Optical Lenses..... | 118 |
| 4.4.2 Optical Diffuser | 121 |
| 4.5 Etching Mechanism | 123 |
| 4.5.1 Metal Thin Film Selection..... | 124 |
| 4.6 Modeling of Laser Assisted Process..... | 129 |
| 4.6.1 Laser Heating Modeling Theory..... | 130 |
| 4.6.2 Comsol Simulation Setup..... | 132 |
| 4.7 Etch Results and Discussions | 143 |
| 4.7.1 Etching with Gaussian LASER Profile | 143 |
| 4.7.2 Etching with Top-Hat LASER Profile | 150 |
| 4.8 Conclusion and Discussions..... | 156 |
| APPENDIX A CREATION OF QUARTZ CRYSTAL RESONATOR..... | 158 |
| A.1. Types of Devices Possible with Quartz Crystals..... | 159 |
| A.2. Quartz Crystal Resonators Created By Laser Assisted Wet Etching Technology | 160 |
| APPENDIX B INCOHERENT LIGHT SOURCES..... | 174 |
| B.1. Quartz Resonator Fabrication using LEDs..... | 175 |
| B.2. Incandescent Light Bulbs w/o IR Filter | 179 |

BIBLIOGRAPHY 181

LIST OF TABLES

| | |
|--|-----|
| Table 1.1 Quartz Crystal Oscillators [3]..... | 7 |
| Table 1.2 Atomic Clock [3] | 11 |
| Table 1.3 Quartz Crystals and It's Competitors [4] | 13 |
| Table 1.4 Elements that Limit Quality Factor [3]..... | 21 |
| Table 1.5 Current Industrial Fabrication Processes [40]..... | 35 |
| Table 2.1 PID Control Parameters [42]..... | 48 |
| Table 3.1 Properties of Quartz Alkali Ion Impurities..... | 90 |
| Table 3.2 X-Ray Assisted Etching Results..... | 99 |
| Table 4.1 808nm Laser Properties..... | 113 |
| Table 4.2 Absorption of Materials..... | 126 |
| Table 4.3 Film Thickness Measurements..... | 141 |
| Table 4.4 Laser Standard Deviation Measurements..... | 146 |
| Table 4.5 Heating and Cooling Measurements..... | 147 |
| Table A1. Quality Factor Versus Size..... | 161 |
| Table A2. Figure of Merit for Electrode Materials..... | 162 |
| Table B1 Properties of LED..... | 176 |
| Table B2. Etch Results From Various Sources..... | 180 |

LIST OF FIGURES

| | |
|---|----|
| Figure 1.1 Total Revenue of Quartz Crystal Market [1]. | 3 |
| Figure 1.2 Pie Chart of 2010 Quartz Crystal Market Share [1]. | 5 |
| Figure 1.3 TCF of Diamond, Silicon and AT-Cut Quartz [6, 7]. | 14 |
| Figure 1.4 Tetrahedron Structure of Alpha Quartz [3]. | 17 |
| Figure 1.5 Piezoelectric Effect in Quartz [3]. | 19 |
| Figure 1.6 Modes of Vibration Created in Quartz Crystals [14]. | 20 |
| Figure 1.7 Frequency Shift versus Temperature for AT-Cut Quartz Crystal | 26 |
| Figure 1.8 Arrhenius Plot for AT-Cut Quartz Etched In Ammonium Bifluoride [15]. | 33 |
| Figure 2.1 Open Loop Control System. | 39 |
| Figure 2.2 Closed Loop Control. | 40 |
| Figure 2.3 PID Control Flow Diagram for Laser Diode System | 41 |
| Figure 2.4 Proportional Controller Output | 43 |
| Figure 2.5 PI Controller Output | 45 |
| Figure 2.6 PD Controller Output. | 46 |
| Figure 2.7 PID Controller Output | 48 |
| Figure 2.8 PID Control Interface Created In LABVIEW | 51 |
| Figure 2.9 Experimental Setup of Multiple Resonators Etched with Lasers. | 52 |
| Figure 2.10 Results For Two Resonators Etched On The Same Die | 54 |
| Figure 2.11 Frequencies of Two Resonators Staying Together. | 56 |
| Figure 3.1 DC Bias Voltage Versus Etch Rate of Silicon [48]. | 60 |

| | |
|---|-----|
| Figure 3.2 I-V Graph Of Electrochemical Etching of Silicon While Being Irradiated With White Light [52]..... | 62 |
| Figure 3.3 Band Gap Comparisons | 64 |
| Figure 3.4 Etch Rate of Silica Glass versus Electric Field [54]..... | 66 |
| Figure 3.5 Change in Voltage Versus Radiation Dose [55] | 68 |
| Figure 3.6 Schematic of X-Ray Assisted Electrochemical Etching Setup | 71 |
| Figure 3.7 Experimental Setup of Electrochemical Etching of Quartz Assisted By X- Rays..... | 73 |
| Figure 3.8 X-Ray Tube From Oxford Instruments [61]..... | 74 |
| Figure 3.9 The Relative Intensity of Each Wavelength Output For 50 keV X-Ray Source..... | 78 |
| Figure 3.10 Variation of X-Ray Intensity for Varying Levels of X-Ray Tube Current.... | 79 |
| Figure 3.11 Effects of Varying Potential Applied to X-Ray Tube | 80 |
| Figure 3.12 Types of Defects Present In Crystalline Quartz [82]..... | 82 |
| Figure 3.13 Radiation Induced Current In Quartz Crystals [3] | 89 |
| Figure 3.14 Current Measured From Reference Sample Being Etched. | 95 |
| Figure 3.15 Voltage Versus Current For Quartz Crystals During Irradiation By X- Rays..... | 96 |
| Figure 3.16 Current Induced Through Quartz 5kV to -5kV..... | 97 |
| Figure 3.17 Frequency Measurement During Etching of Reference And Sample Irradiated By X-Rays | 98 |
| Figure 3.18 Four Hour Etch..... | 100 |
| Figure 3.19 Radiation Induced Ionic Current | 102 |

| | |
|--|------|
| Figure 4.1 Laser Assisted Wet Etching of Quartz with Cr Thin Film..... | 107 |
| Figure 4.2 Etch Profile of Laser Assisted Wet Etching of Quartz..... | 107 |
| Figure 4.3 LIBWE(Laser Ablation) Etching Setup [98]..... | 110 |
| Figure 4.4 Laser Assisted Etching Setup with Fresnel Lens..... | 112 |
| Figure 4.5 Gaussian Profile with a Maximum Power Density of 12.5 W/mm^2 | 120 |
| Figure 4.6 Top-Hat Profile with Maximum Power Density of 6.5 W/mm^2 | 121 |
| Figure 4.7 Schematic for Creating Top-Hat Beam Profile [106]..... | 122 |
| Figure 4.8 Etch Mechanism of the Laser assisted Process..... | 123 |
| Figure 4.9 Amount of 808nm Laser Radiation Absorbed By Common Metals..... | 125 |
| Figure 4.10 Etch Rate Vs Thickness of Cr Thin Film..... | 128 |
| Figure 4.11 Gaussian Profile of Laser Modeled In Comsol..... | 133 |
| Figure 4.12 Top-Hat Profile of Laser Created Diffuser Optics Modeled in Comsol..... | 134 |
| Figure 4.13 FEM Mesh of Quartz Crystal..... | 135 |
| Figure 4.14 Experimental Results versus Model Created in Comsol Multiphysics™..... | 140 |
| Figure 4.15 Etch Rate Data From Gaussian LASER Profile..... | 1444 |
| Figure 4.16 Gaussian Etch Profile with Power Density of 4 W/mm^2 | 148 |
| Figure 4.17 SEM Image of Quartz Sample Etched with Gaussian Beam..... | 149 |
| Figure 4.18. Top-Hat Profile, Cr Thickness of 15nm..... | 150 |
| Figure 4.19. Top-Hat Profile with Cr Thin Film Thickness of 20nm..... | 151 |
| Figure 4.20 Side Image of Top-Hat Etch Profile..... | 153 |
| Figure 4.21 SEM Image of Top-Hat Profile with Etch Depth Larger than $100 \mu\text{m}$ | 154 |
| Figure 4.22 SEM Image of Top-Hat Profile Side View..... | 155 |
| Figure 4.23 SEM of Sidewalls..... | 156 |

| | |
|---|-----|
| Figure 4.24 Wafer Level Laser Etching System..... | 157 |
| Figure A.1 Frequency Response of Resonator Etched by 30 μ m..... | 163 |
| Figure A.2 Same Sample From Figure A.1 But with Added Electrode Mass..... | 164 |
| Figure A.3 The 3.5MHz Sample Compared Before and After Adding Addition Mass.. | 165 |
| Figure A.4 Inverted Mesa Resonator at 4.4MHz..... | 166 |
| Figure A.5 Inverted Mesa Crystal Resonator..... | 167 |
| Figure A.6 5.57MHz Resonator with a Q factor of 29,077..... | 168 |
| Figure A.7 8MHz Inverted Mesa Resonator..... | 169 |
| Figure A.8 10 MHz Resonator..... | 170 |
| Figure A.9 11.2 MHz Resonator Before Added Mass..... | 171 |
| Figure A.10 11MHz Resonator with Added Mass..... | 172 |
| Figure B.1 Spectrum of LED Using OceanOptics Spectrometer..... | 176 |
| Figure B.2 Optical Power Output versus LED Current..... | 177 |
| Figure B.3 Two Resonators Wet Etched One With LED and One as Reference..... | 178 |
| Figure B.4 Transmission Spectrum for IR Bandpass Filter..... | 179 |

ACKNOWLEDGEMENTS

I would like to thank my advisor, Dr. Chester Wilson, for financial support and guidance during my journey to obtain my PhD. Thanks to Dr. Ville Kaajakari for starting me out on this topic of research and for his guidance during the start of my degree. Also, I would like to thank Dr. Long Que, Dr. Randal Null, and Dr. Bala Ramachandran for taking time out of their schedules to serve as members on my dissertation committee.

CHAPTER 1

INTRODUCTION TO QUARTZ CRYSTAL INDUSTRY

This dissertation will focus on improving the processing methods of quartz crystals, however, these processes are not limited to quartz and can be applied to any piezoelectric material. Almost all of today's electronic devices require a quartz crystal resonator. Quartz crystals are used as timing devices in the form of tuning forks, or as frequency references typically with a frequency in the MHz range. Tuning forks typically have a frequency of 32 kHz, this frequency signal is then converted into one second pulses to be used in timing devices. Frequency references are used to derive the frequency that is used for communication. An example of a frequency reference is the oscillator used in a global positioning system (GPS), typically an oscillator with a frequency in the range of 8 to 20 MHz is used. The frequency from the oscillator is multiplied to the signal frequency, which for GPS is 1.57542 GHz (L1) and 1.2276 GHz (L2).

There are other timing devices and materials on the market other than quartz crystals. The three main alternatives are atomic clocks, LC-CMOS circuits, and Silicon Microelectromechanical Systems (Si-MEMS) resonators. Atomic clocks are the most accurate time keeping devices, however, most are bulky and very expensive compared to quartz crystals. LC-CMOS circuits are created using CMOS technology, which allows for a small form factor (device size). Si-MEMS are resonators created as a resonating

beam or a resonating plate made out of silicon. Both the LC-CMOS circuits and Si-MEMS resonators are created out of silicon which is a very temperature sensitive material. These three types of devices will be discussed in more detail later in this chapter.

Quartz is the preferred material for resonators (clock crystals and frequency references) because of its piezoelectric nature, high mechanical quality factor, and excellent thermal stability. Unfortunately, the quartz crystal processing technology faces serious challenges in further miniaturizing the packaged resonator size.

Traditionally, the quartz crystal resonators have been etched in hydrofluoric acid based etchants with the etch rate controlled by etchant concentration, temperature, and time. Local variations in the etch rate or initial sample thickness of wafers cannot be controlled in etching but require individual trimming by metal deposition.

Currently, the quartz crystals are individually trimmed and packaged. It takes considerable amount of time and it complicates further miniaturization of high frequency resonators. Typically quartz crystals have lead times between 6 to 8 weeks. This research shows that it is possible to allow for wafer level integration of the quartz resonators by tuning the frequency while it is being wet etched, which eliminates the need for multiple tuning steps.

1.1 Quartz Crystal Industry

This section will cover the current industry leaders of manufacturing quartz crystals, the various applications and devices that quartz is currently being used in and finally the current competitors to quartz crystals. Quartz crystal resonators are a billion dollar industry. Data was obtained from yearly reports from TXC, one of the largest

quartz crystal manufacturers in the world [1]. Figure 1.1 shows the total revenue of quartz crystal and quartz crystal devices from 2005 to 2010 taken from the TXC reports [1].

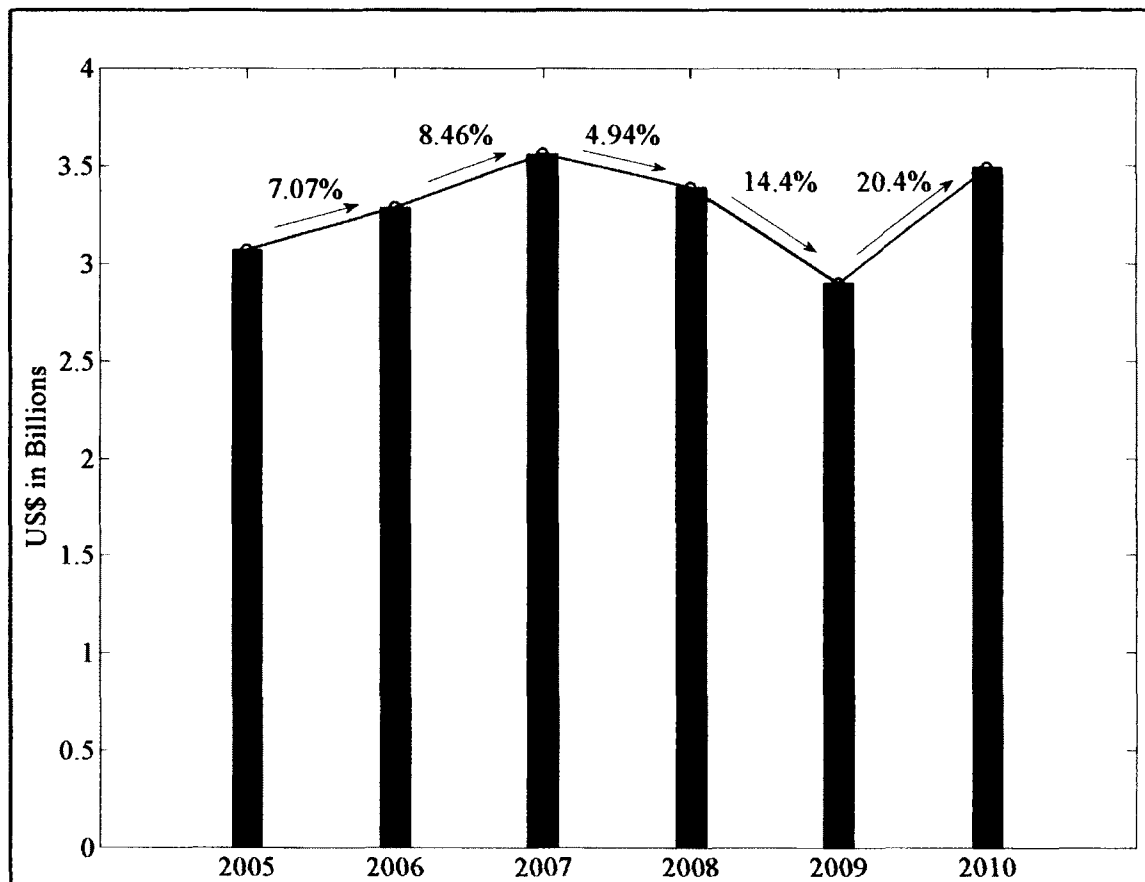


Figure 1.1 Total Revenue of Quartz Crystal Market [1].

Until the market crisis in 2008, the quartz crystal industry experienced steady growth. This was due in large part to wireless communications. More consumers were buying cellular phones and telecommunication companies also needed to increase their ability to handle more customers. Even though the market dropped off in 2008 it bounced back in 2010 with an increase in total revenue of 20.4%. This large increase in

revenue of quartz crystals is due to the fact that smart phones have emerged as must have electronics. Current smart phones typically have around five quartz crystals in the circuit. The quartz crystals in smart phones are utilized as the following: cellular radio, radio sleep mode, application processor, power management, and GPS. All of these quartz crystals operate at various frequencies from the kHz to MHz range. Due to quartz crystals great performance (quality factor ranging from 10,000 to 100,000 and its thermal stability), has allowed it to remain the dominant material in the resonator market. However, due to cellular phones and other portable electronics shrinking, quartz crystals must keep up. The problem is that quartz crystals are starting to reach a bottleneck in the manufacturing process. This bottleneck has allowed silicon based resonators to start gaining ground in the resonator market. However, the current sales of MEMs silicon resonators are less than 1% of the current quartz crystal resonator market. Currently there are only a few companies that have ventured into creating MEMs silicon resonators to compete with quartz. Figure 1.2 shows the quartz crystal market share by company [1].

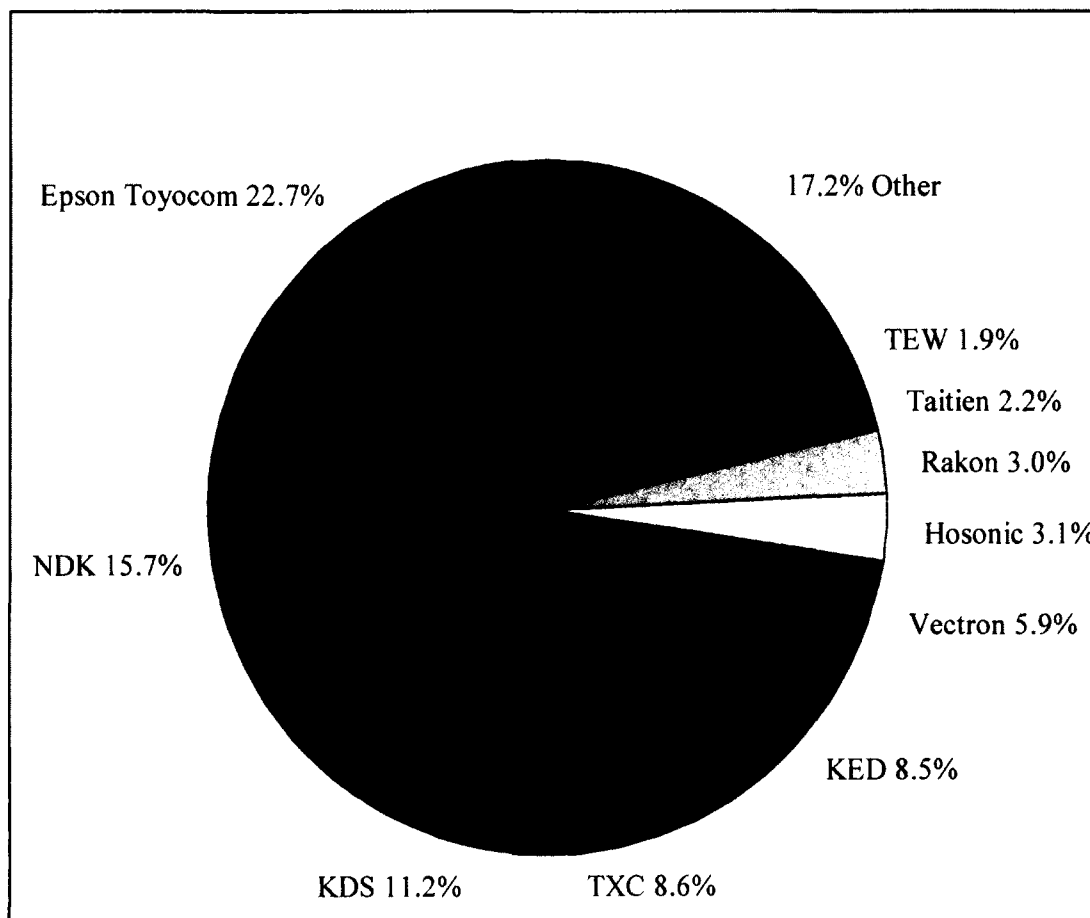


Figure 1. 2 Pie Chart of 2010 Quartz Crystal Market Share [1].

The top company in the quartz industry is Epson Toyocom. The reason for this is that they started using photolithography to create smaller quartz crystals. Epson Toyocom coined the trademark “QMEMS™” signifying the emergence of quartz and MEMS processing [2]. The photolithography process allows for tighter control of the frequency and produces higher frequency resonators by creating thinner samples. The photolithography process has allowed the quartz industry to continue to lead the market. However, this process is reaching its limit on keeping the accuracy of the quartz crystals at its current state and rising costs. This is due to the fact that resonators must be individually measured and etched. If the resonators do not have the required frequency

accuracy they must be individually frequency trimmed after fabrication. This dissertation work was started to find and develop ways to eliminate the need for individual frequency trimming as well as speed up the etch rate compared to current processes.

1.1.1 Applications of Quartz Crystals

Quartz resonators are integrated in almost all electronic devices and especially the wireless transmission systems such as GPS, which requires exceptional stability and ultra low noise performance. The quartz crystal market is extremely large, due to the need to have either a frequency reference or a timing device in almost every type of electronic system. The areas that require a quartz crystal resonator are as follows: Automotive Industry, Consumer Market (ex. Cellular phones and Computers), Medical Applications (ex. Pacemakers), Military Applications, and Navigation systems (ex. GPS and Radar).

With the methods discussed within this dissertation it is possible to create various structures in quartz crystals, thus allowing for fabrication of Quartz-MEMS devices. Various types of devices can be created with the different cuts of quartz from gyroscopes to sensors. However, for this dissertation only the creation of AT-cut quartz crystal resonators will be discussed. AT-cut quartz crystals are the most common type of resonator found due to its cheap processing costs (versus SC-cut) and its excellent thermal stability. However, each process can be applied to any cut of quartz crystal. This body of work's main focus is on the improvement of the processing of the quartz crystals in industry.

1.1.2 Current Quartz Crystal Devices on Market

This section will summarize the current quartz crystal resonator devices that are currently on the market. The importance of this section is to show that there is a quartz crystal resonator device for any application. Table 1.1 summarizes the abilities of the various types of quartz crystal oscillators [3].

Table 1.1 Quartz Crystal Oscillators [3].

| Parameter: | XO | VCXO | TCXO | OCXO | DOCXO | EMXO | MCXO |
|---|-----------|-------------|-------------|-------------|--------------|-------------|-------------|
| Accuracy (Hz) | 10^{-5} | 10^{-6} | 10^{-7} | 10^{-8} | 10^{-9} | 10^{-7} | 10^{-8} |
| Long Term Stability Aging/Year | 10^{-6} | 10^{-6} | 10^{-7} | 10^{-8} | 10^{-10} | 10^{-7} | 10^{-8} |
| Short Term Stability ($\tau=1\text{sec}$) | 10^{-9} | 10^{-9} | 10^{-10} | 10^{-12} | 10^{-12} | 10^{-10} | 10^{-10} |
| Temperature Stability (-55 to 85 °C) | 10^{-6} | 10^{-6} | 10^{-7} | 10^{-9} | 10^{-10} | 10^{-8} | 10^{-8} |
| Size (cm³) | 1 | 1 | 10 | 20-200 | 20-200 | 2 | 30 |
| Warm-up Time(secs) | 0.002 | 0.01 | 1.8 | 240 | 300 | 60 | 1.8 |
| Power Consumption (W) | 0.01 | 0.04 | 0.1 | 0.6 | 1 | 0.35 | 0.04 |
| Price (\$) | 1 | 4 | 10 | 200 | 500 | 200 | <1000 |

The types of resonators typically used are shown in Table 1.1, and a brief description of each follows. The first oscillator to be discussed is the crystal oscillator (XO) and is the most basic design. The XO consists of an amplifier and a quartz crystal resonator. The voltage controlled crystal oscillator (VCXO) is similar to the XO, except that the frequency output is maintained by varying the voltage to the oscillator circuit.

The Oven Controlled Crystal Oscillator (OCXO) and the Temperature Compensated Crystal Oscillator (TCXO) are the most commonly used quartz oscillators for high temperature stability. The OCXO has the crystal in an actual oven that maintains a constant temperature. The TCXO measures the temperature of the crystal and then varies the voltage to maintain the correct frequency. The Double Oven Controlled Crystal Oscillator (DOCXO) was designed to increase the frequency stability, however it consumes more power and is pricey compared to the OCXO. The Evacuated Miniature Crystal Oscillator (EMXO) and Microcomputer Compensated Crystal Oscillator (MCXO) are relatively new designs that maintain good temperature stability while lowering the size of the compensated oscillators.

In the quartz crystal resonator industry, the important terms are defined as the following: Accuracy, Long Term Stability, Short Term Stability, Temperature Stability, Size, Warm-up Time, Power Consumption and Price. Accuracy is the measure of the overall frequency stability of the oscillator. Long term stability of the oscillator is the rate of aging in the device. This parameter is especially important for space applications because of the long duration of these missions. Aging in quartz crystals is influenced mainly by internal defects and stresses present throughout the crystal. Initially quartz crystal resonators were created out of naturally occurring crystals, however natural crystals have a larger amount of defects compared to synthetic crystals. The more defects present in a quartz crystal resonators the more aging that will occur. Space radiation will cause rapid aging effects in quartz crystal resonators. Space radiation causes frequency shifts by energizing the defects present in the crystals. Defect ions that are present in the crystal will become energized and then the ions migrate through the crystal causing the

frequency shifts. This can be mitigated through creating synthetic quartz crystals with as few defects as possible or it can be made radiation hard. This is done by subjecting the crystals to large amounts of radiation or by the electrodiffusion process, which eliminates the amount of defects. Chapter 3 will discuss a process that takes advantage of the defect ions present in the quartz crystals that will increase the etch rate of the crystals during wet etching.

The short term stability is the Allan deviation of the oscillator usually measured at one second. The Allan deviation can be expressed as the following:

$$\sigma_y(\tau) = \sqrt{\frac{1}{2(M-1)} \sum_{i=1}^{M-1} (y_{i+1} - y_i)^2} \quad (1.1)$$

where y_i is the data set (resonator measurements in hertz) and M represents the amount of samples. The Allan deviation shows how much the frequency will fluctuate in one second. All of the oscillators shown here are very stable according to their Allan deviations (short term stability). Temperature stability is the measure of how stable the frequency is over the specified temperature range. The temperature stability is one of the most important parameters especially for military applications. Military applications require very tight tolerances for temperature ranges of -55°C to 85°C . Other parameters used to gauge the performance of these devices are the size, warm-up time, power consumption and price. As stated previously, the size of the quartz crystal oscillators must be decreased in order to meet the demand for smaller mobile devices. The warm-up time is the amount of time required for the frequency to become stabilized once the quartz crystal oscillator is turned on. Power consumption is one of the most important parameters for systems, the smaller power consumption the longer the device can last.

The ultimate goal is to have the smallest device possible consuming a small amount of power in the overall system with a very high frequency accuracy for the lowest price. Quartz crystals have been the dominant oscillator on the market and until recently no competitor has been even close to it. The following section will discuss the current competitors to quartz crystal resonators.

1.1.3 Competitors to Quartz Crystal Resonators

Since the 1920s, quartz crystals have dominated the market being used in the various applications discussed previously. Because of its great properties it has until recently been the only option in most devices. Atomic clocks are currently the only option that has better performance than quartz crystals, however they are large in size and are costly to produce. Due to these restrictions atomic clocks are typically only used in satellites and other space applications, where most missions last longer than a few years. The other competitors coming into the market are Si-MEMS and LC-CMOS resonators. A few MEMS and CMOS resonator startup companies are working their way into the quartz crystal market due to their small sizes (form factor). Hence, the problems with quartz have nothing to do with its performance. These problems are size and long lead times for the quartz components. Currently the quartz crystal is the largest component required in most mobile devices. With the current size of the quartz crystals and the time it takes for individually trimming of the resonant frequency, it makes it impossible to integrate it with current CMOS technology.

The type of clocks to be discussed here are not the typical clocks on the wall. Atomic clocks are used as either a timing device or frequency reference. The frequency for most clocks is 32.768 kHz, which allows for simple math to create 1 pulse-per-second

(pps). However, clocks can use any frequency for creating a 1pps. For instance the GPS satellites in space use 10.23 MHz as the base frequency from an atomic clock. GPS satellites use atomic clocks as a frequency reference, allowing for other devices to communicate with it in order to locate latitude and longitude coordinates on Earth. The atomic clocks are more accurate than quartz crystals; however, they are massive and expensive in comparison. Because of the price and size of the atomic clocks their applications are limited. The atomic clocks to be discussed in this section are summarized in Table 1.2.

Table 1.2 Atomic Clock [3]

| Parameters | Rubidium | RbXO | Cesium | Hydrogen Maser | CSAC | CPT |
|---|-----------------------------------|---------------------------------|---------------------------------|-------------------------------|---------------------------------|--------------------------------|
| Accuracy (Hz) | 10^{-10} | 10^{-10} | 10^{-11} | 10^{-13} | 10^{-11} | 10^{-11} |
| Long Term Stability Aging/Year | 10^{-10} | 10^{-10} | 0 | 10^{-14} | 10^{-9} | 10^{-10} |
| Short Term Stability ($\tau=1\text{sec}$) | 10^{-12} | 10^{-12} | 10^{-11} | 10^{-13} | 10^{-10} | 10^{-11} |
| Temperature Stability | 10^{-10} (-55 to 68) (°C) | 10^{-10} -55 to 85 (°C) | 10^{-11} -28 to 65 (°C) | 10^{-14} 5 to 40 (°C) | 10^{-10} -10 to 70 (°C) | 10^{-12} 15 to 35 (°C) |
| Size (cm ³) | 200-800 | 1000 | 6000 | >30000 | 16 | 220 |
| Warm-up Time (minutes) | 3 | 3 | 3 | 8hr | 2-3 | 6 |
| Power Consumption (W) | 20 | 0.65 | 30 | 100 | 0.12 | 3.4 |
| Price (\$) | 2000 | <10,000 | 50,000 | 250,000 | 1500 | >1000 |

There are a few options for atomic clocks to choose. Atomic clocks are typically used in space satellites or other military applications where accuracy is of utmost

importance. The chip scaled atomic clocks (CSACs) have extremely small size with volumes around 16 cm^3 , however, the price of \$1500 will keep it from the consumer market. Currently there is no cheap atomic clock on the market. Due to the high cost of atomic clocks, quartz crystals are the best alternative for most applications. As shown in Table 1.1 there are quartz crystal oscillators on the market that come close to atomic clock stability at a fraction of the cost.

Atomic clocks are also limited by other problems besides their price. Atomic clocks consume large amounts of power. With the invention of the CSACs the power consumption has been reduced down to that of quartz oscillators. Atomic clocks that use cesium and rubidium will cease to work once the cesium and rubidium elements have become depleted. The typically lifetime of a cesium and rubidium atomic clock is around 10 years. Another problem with most atomic clocks is that they have a lower operational temperature range than quartz crystal oscillators.

Devices that have been created to have a smaller form factor than quartz crystals will now be discussed. Frequency references are predominately used in cell phones or other portable electronics. The goal of consumer electronics is to decrease the size of the devices while lowering the cost and keeping the current performance of quartz crystals. The main technologies in competition with quartz crystals are Si-MEMS, and LC-CMOS. Silicon MEMS resonators are either beams or plates designed to resonant at a specific frequency. LC-CMOS is an LC circuit (composed of an inductor and capacitor) which will resonate at a specific frequency defined by the LC values. Capacitors have negative reactance, while inductors have positive reactance. Due to their 180° phase shift once the

capacitors and inductors have equal magnitude they cancel each other out producing a resonant frequency. Table 1.3 shows the ability comparison of various resonators [4].

Table 1.3 Quartz Crystals and It's Competitors [4]

| | Quartz | Si-MEMS | CMOS LC |
|---------------------------------------|---------------|----------------|----------------|
| Size | | √ | √ |
| TCF | √ | | |
| Q-Factor | √ | | |
| Phase Noise/ Period Jitter | √ | | |
| Power Consumption | √ | | |
| Lead Time | | √ | √ |

The reason that quartz has been the leader in the resonator technology is self-explanatory from Table 1.3, because the parameters shown are the most crucial for resonators. The smaller size (form factor) allows for mobile devices to be reduced in size. Currently quartz crystals competitors are able to decrease the form factor; however, these devices do not measure up to the performance of quartz. A lot of research has been conducted on Si-MEMS resonators, which has allowed it to start to move into the quartz resonator market. However, it represents less than 1% of the current resonator market with only a smaller form factor and better lead times than quartz [5]. Also, the CMOS LC resonators fall into the same categories as Si-MEMS.

The following paragraphs will describe the parameters outlined in Table 1.3. The temperature coefficient of frequency (TCF) is the frequency shift that takes place with a

change in temperature. The TCF measures how stable a material's frequency will be over a specified temperature range. Figure 1.3 shows the TCF of AT-cut quartz, diamond, and silicon [6, 7].

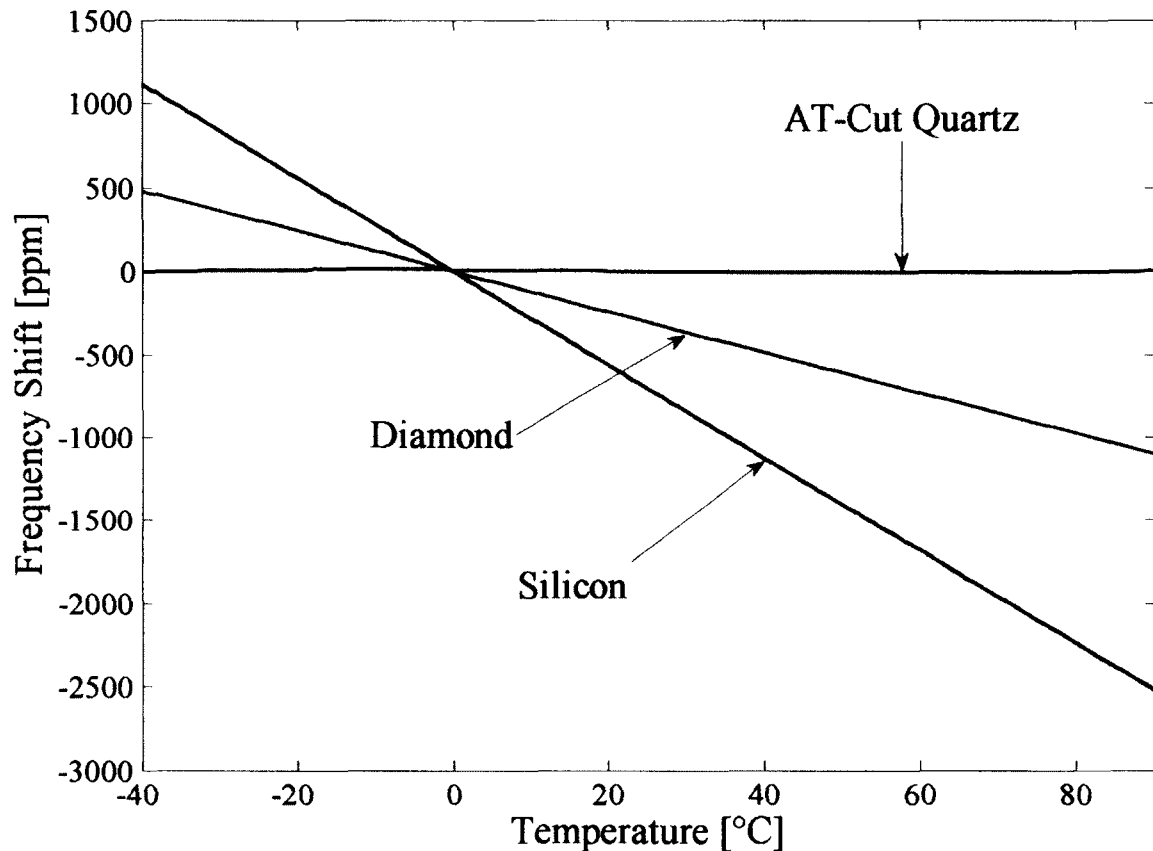


Figure 1.3 TCF of Diamond, Silicon and AT-Cut Quartz [6, 7].

Figure 1.3 shows that AT-cut quartz has the best TCF when compared to diamond and silicon. The next parameter to be discussed is the quality factor of the resonators.

The quality factor (Q factor) represents the accuracy of the resonator. It has been shown that a 5MHz quartz crystal resonator can be created with a Q-factor of 800,000 [8]. Also, at World Technology Instrument Co. they created a 10MHz convex resonator with a Q-factor of 1.3 million [9]. In comparison a 5.1MHz Si-MEMS resonator was created by

SiTime, which only had a Q-factor of 80,000 [10]. Just comparing Q-factor performance, the quartz resonators at the same frequency are at least 10X that of Si-MEMS devices. The LC-CMOS resonator operates around 900 to 960MHz with a Q- factor of 10 and in order to get lower frequencies a frequency divider must be implemented [11, 12].

The next parameter to compare between the resonators is their phase noise/jitter performance. Phase noise and period jitter both represent the resonator's stability, the differences between these, however, is that phase noise represents the stability in the frequency domain and the period jitter is the representation in the time domain. For resonator applications the lower the phase noise in the resonator the easier it is to find the desired frequency signal.

Currently, all of the competitors consume more power than the quartz crystal resonators of the XO and VCXO designs. The reason for their large power consumption is due to the other components needed to help maintain the frequency stability over various environments. The XO and VCXO do not require any compensating circuitry in order to be a stable resonator over a large temperature span.

The final parameter that is important for resonators is the lead time. The lead time is the amount of time required to get the resonators ready for shipping. Si-MEMS and LC-CMOS devices can be processed at the wafer level creating faster lead times compared to quartz resonators. This is due to the fact that quartz resonators require individual frequency trimming in order to have a tight frequency tolerance. Quartz manufacturers offset this by only having a select few of frequencies available to customers. The benefit of the research done in this dissertation by various methods is the fact that lead times can possibly be decreased, by speeding up the processing time. The

following sections will discuss the properties of quartz crystals and how these properties contribute to quartz's excellent resonator performance.

1.2 Properties of Alpha Quartz

There are various forms of quartz that can be found in nature. The main forms of quartz used are alpha quartz and fused quartz. Fused quartz is created by heating quartz above its melting point. This allows for fused quartz to become less brittle, however, by heating quartz past its melting point it degrades or loses all of its piezoelectric properties. Alpha quartz is naturally found in the Earth's crust. The problem with natural alpha quartz is the impurities that are formed randomly in the crystal. These impurities can cause premature aging in quartz crystal resonators. Synthetic quartz crystals are grown to limit the amount of defects present.

Alpha quartz is naturally piezoelectric (even synthetic quartz), it has a low internal loss (high quality factor), can be cut to have zero temperature coefficient (stable frequency over large range of temperature), and low solubility in most chemicals (which is the reason it is difficult to process). These four properties of quartz are the main reasons for it being the best material to use as a resonator.

1.2.1 Piezoelectric Nature

One of the reasons why alpha quartz is sought after as a resonator is its piezoelectric properties. Its piezoelectric properties allow for it to operate without any DC excitation voltage. Alpha quartz has a trigonal crystal structure and it does not have a plane or center of symmetry, this latter part allows quartz to be piezoelectric [13]. The trigonal crystal structure can also be referred to as the crystals unit cell classification.

The trigonal unit cell of quartz has a equaling 4.913 angstrom, c equals 5.405 angstrom and Z is three (Z presents the number of formula units present in the unit cell). There are three silicon atoms and six oxygen atoms present in the unit cell. It has a tetrahedron structure, which means that there will be a silicon atom in the middle and it will be bonded to four oxygen atoms [13]. Another important parameter of a crystal is its unit cell. Figure 1.4 shows the structure of the tetrahedron structure with the additional silicon atoms attached to the oxygen atoms.

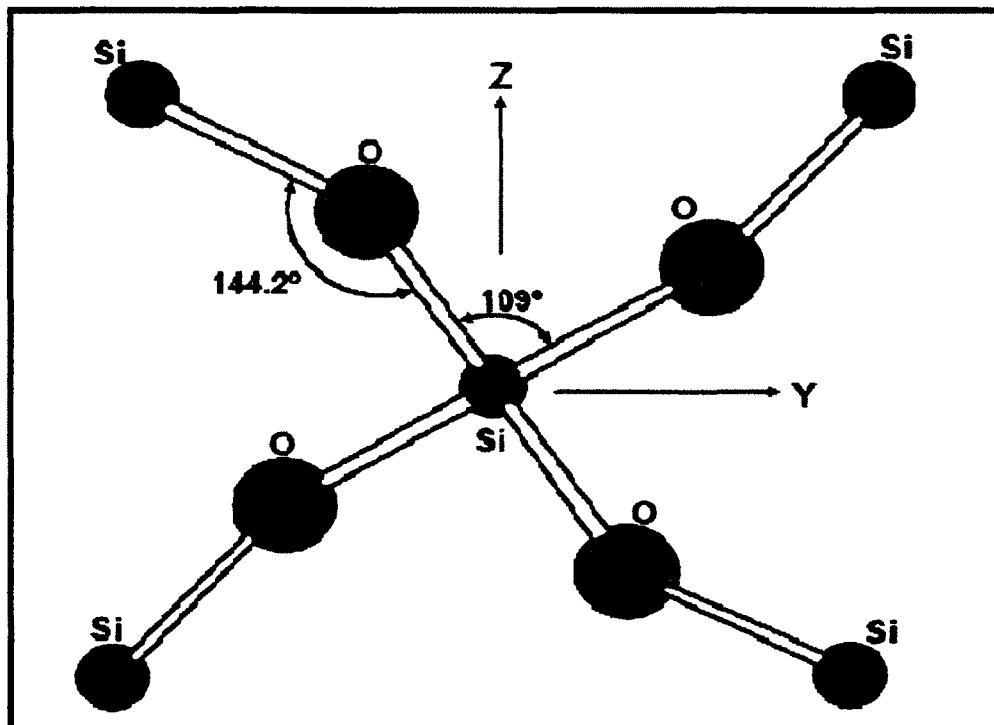


Figure 1.4 Tetrahedron Structure of Alpha Quartz [3].

Piezoelectricity can be divided into two effects which are called the piezoelectric effect and the converse piezoelectric effect. The piezoelectric effect is defined by force applied to the quartz crystal to create a potential between the positive silicon atoms and

the negative oxygen atoms. The strain throughout the quartz crystal causes the atoms to be deformed, more specifically the strain on the lattice creates a charge mismatch. The piezoelectric effect is governed by the stress and the electric displacement equations. The mechanical stress (T) in piezoelectric materials is shown in Equation 1.2:

$$T = YS - eE \quad (1.2)$$

where Y is the Young's modulus of the material (units of MPa or GPa), S is the strain (dimensionless), e is the piezoelectric stress coefficient (C/m^2) and E is the electric field applied to the material (units of N/C or V/m). The piezoelectric stress coefficient is different for every material and it relates how much of an electric field is produced when a mechanical stress is applied to the material. Equation 1.3 shows the electric displacement (D) for a piezoelectric material under strain:

$$D = \epsilon E + eS \quad (1.3)$$

where ϵ is the permittivity of the material, which is found by multiplying the vacuum permittivity ($8.854e-12$ F/m) with the relative permittivity (defined by the material) and D the electric displacement will have units of C/m^2 . The piezoelectric stress coefficient couples the electric displacement and stress equations. For non-piezoelectric materials the electric displacement is affected only by the permittivity and the electric field. The same goes for the stress equation, which only requires the strain and Young's modulus for non-piezoelectric materials. Figure 1.5 shows the structure of alpha quartz and how the piezoelectric effect works.

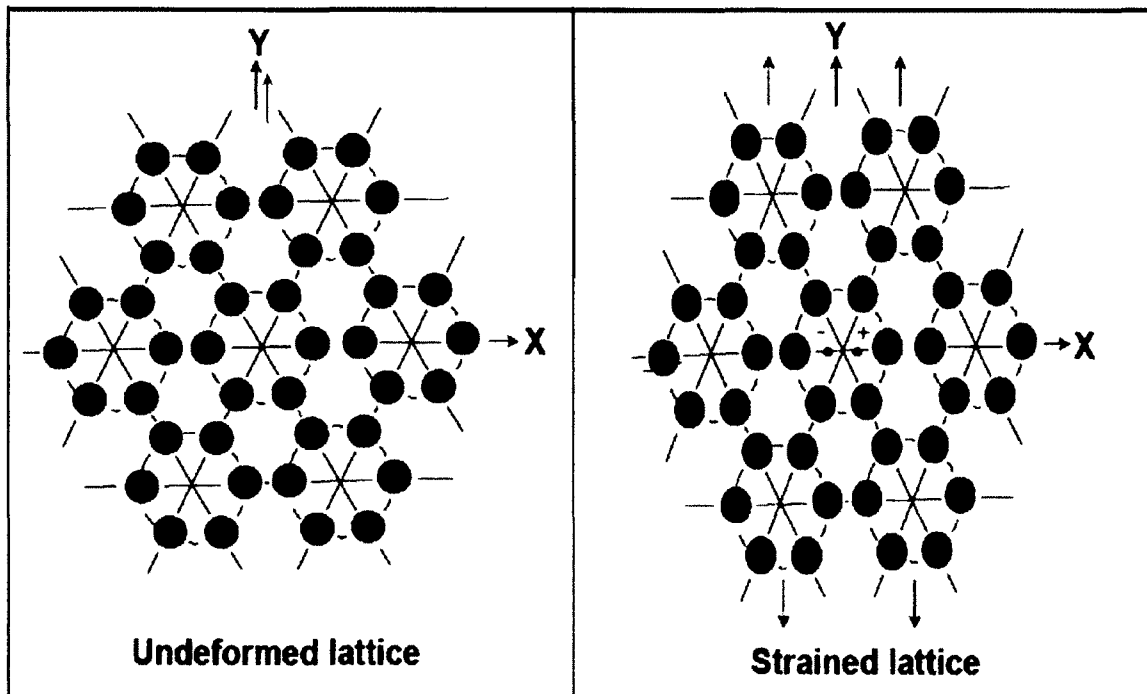


Figure 1.5 Piezoelectric Effect in Quartz [3].

Figure 1.5 shows the piezoelectric effect however, for resonators, the converse piezoelectric effect is used. The converse piezoelectric effect occurs when a voltage is applied to the crystal and the lattice becomes strained. This strain creates acoustic waves that travel through the quartz crystal. These acoustic waves control the resonator's vibration frequency, which is determined by the geometry of the quartz crystal. The converse piezoelectric effect is shown in Figure 1.6 for various types of vibration modes that can occur in quartz crystals [14].

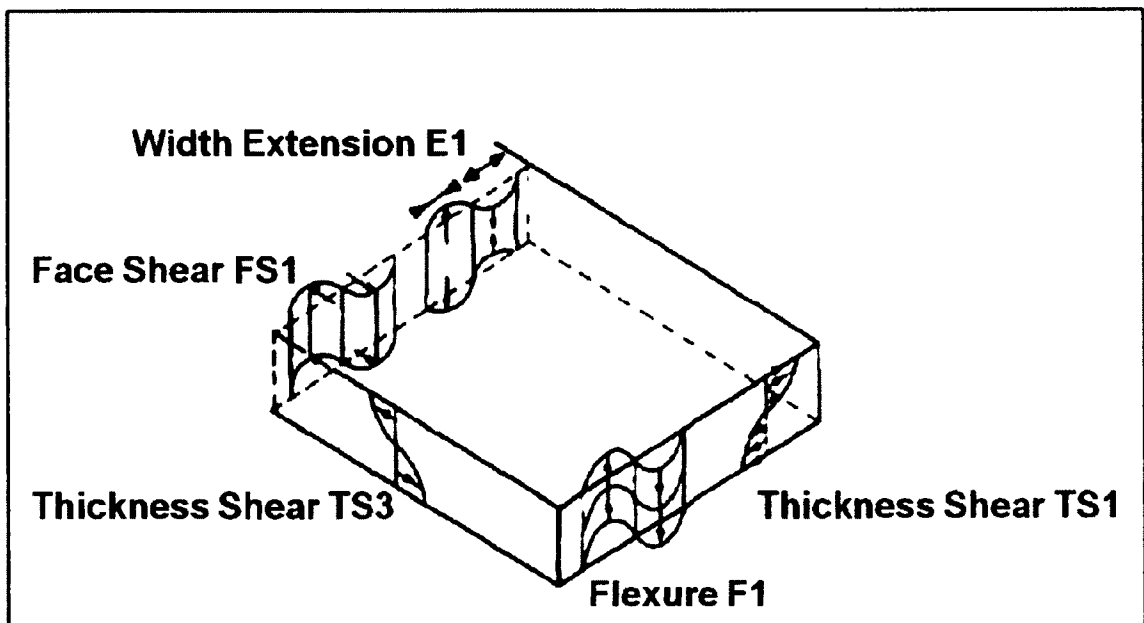


Figure 1.6 Modes of Vibration Created in Quartz Crystals [14].

These acoustic waves are due to the voltage applied to the crystal via electrodes, which allow the quartz crystals to resonate at a specific frequency. The resonant frequency of the quartz crystal varies with the geometry of the quartz crystals and also will vary with the type of cut of the crystal. Figure 1.6 shows the flexure, width extensional, face shear, and thickness shear modes. The thickness shear mode is the mode that is important for AT-cut quartz crystal resonators. The other modes are considered spurious modes, and are to be avoided for AT-cut quartz. Since the AT-cut crystals main mode is the thickness shear mode its frequency is proportional to its thickness and is related by Equation 1.4:

$$\text{Frequency (MHz)} = \frac{1667 \text{ (MHz} \cdot \mu\text{m)}}{\text{thickness } (\mu\text{m})} \quad (1.4)$$

the frequency is calculated in MHz, since most applications involving AT-cut quartz crystals involves the MHz region. The 1667 value is a constant specific to AT-cut quartz crystals. Each specific type of quartz cut has its own constant value. For thickness shear

mode cuts, the higher the constant value the thinner the resonator for a specific frequency. The next important property of quartz to discuss is its large internal mechanical quality factor.

1.2.2 Quality Factor

The quality factor (Q factor) of a resonator is one of the most important parameters to look at in the overall performance of a resonator. The higher the Q factor, the more stable the frequency will be and the more accurate the frequency of the quartz resonator. The intrinsic mechanical Q factor of quartz is extremely high. For AT-cut quartz the frequency and Q factor product equals 1.6×10^{13} Hz. This means at a frequency of 1 MHz the highest possible Q factor would be 16 million. Of course this is not possible due to the losses that come from the various circumstances outlined in Table 1.4 [3].

Table 1.4 Elements that Limit Quality Factor [3]

| Factors Limiting Quality Factor of Quartz Resonators | |
|--|--|
| <ul style="list-style-type: none"> • Quality of Resonator Surface • Mounting Losses • Temperature | <ul style="list-style-type: none"> • Quartz and Electrode Geometry • Drive Level • Spurious Modes |

Table 1.4 lists the various factors that can affect the Q factor of all quartz crystal resonators regardless of cut type. These factors will have an extreme deterioration on the quality factor of the quartz resonators. Therefore, great effort must be taken to ensure that none of these issues will greatly decrease the intrinsic quality factor. The total

quality factor is the sum of the inverse of the various factors shown in Table 1.4 and is determined by Equation 1.5 [15].

$$\frac{1}{Q_{\text{Total}}} = \frac{1}{Q_1} + \frac{1}{Q_2} + \dots + \frac{1}{Q_N} \quad (1.5)$$

By this equation, it should be easy to see how one parameter can degrade the total quality of the resonator. If the smallest Q factor of the entire loss mechanism is ten thousand, then the Q factor of the resonator will not be greater than ten thousand. However, if the loss mechanisms are limited the quartz resonator can have a very large quality factor. The loss mechanisms listed in Table 1.4 will be discussed in more detail now.

The surface of the quartz resonator will greatly influence the Q factor of the quartz resonators. Also, rough or pitted surfaces will make it more difficult to deposit electrodes on the quartz resonator. If the etched pits are numerous or very large it could cause spurious modes in the resonator. And as shown in Equation 1.4 any loss can cause the Q factor to degrade significantly. This problem is easily fixed by polishing the quartz resonator during etching using saturated ammonium bifluoride with details of this process discussed later [15].

Mounting losses are very difficult to control property of quartz resonators. Most of the losses for quartz resonators are from mounting losses. If wires are bonded onto the quartz resonator it will significantly damp the resonator's signal. Commercial resonators today are either mounted on the sides by aluminum that is bonded with conductive epoxy or they are enclosed in ceramic cases. Most of today's applications require surface mount resonators which use the ceramic cases. If the mounting is effective it will eliminate most of the flexure modes that are present in all quartz crystals. However if it is not effective the flexure modes can cause interference with the main thickness-shear

mode. For this research the losses occurring to improper mounting was the most difficult to handle of all of the parameters that effect the Q factor.

Every quartz crystal cut has its own unique frequency versus temperature behavior. For instance, Z-cut quartz resonators have a frequency shift over 200 parts per million (ppm) from -50°C to 80°C . Whereas the AT-cut quartz crystals have frequency shifts of only 15 ppm for -50°C to 100°C . Frequency stability at a wide range of temperatures is the reason that quartz has been the dominate material in the resonator industry. The problem that occurs for quartz resonators is when the temperature change forces the frequency to shift to a spurious mode frequency. This will decay the quality factor and could possibly cause the oscillator to stop working. This can be avoided if the quartz resonator is designed properly by limiting the spurious modes produced during oscillation.

Another important parameter for the quality factor of quartz resonators is the geometry of the crystal and electrode. The quartz blank must be of proper dimensions for a specific frequency in order to obtain the maximum quality factor and eliminate spurious modes. As the AC signal is applied to the electrodes (which are deposited on both sides of the crystal) a vibration wave is created that travels through the crystal. Energy trapping involves trapping these waves in order to keep the wave's signal amplitude as large as possible. The energy will be trapped more effectively where the electrodes are deposited on the crystal. For the best results the electrodes must be patterned on the quartz crystal to trap as much energy in the central part of the quartz crystal resonator.

The drive level represents the amount of power applied to the quartz crystal. As the drive level is increased there is a point when the quartz crystal will be pushed to its

nonlinear region [8]. At this point the frequency will have a shift in the positive direction. Therefore if the quartz resonator's drive level is increased into the nonlinear region the frequency will shift, which can also cause the quality factor to decrease. If the frequency shift is larger than the oscillator's required tolerance the entire system could cease to function. Typically 10 μ W or 0 dBm is the maximum power applied to the crystals for this research unless otherwise noted.

Behind mounting losses, spurious modes are the second most likely cause for the quality factor becoming degraded. Spurious modes occur when different waves are excited in the quartz crystals. AT-cut quartz crystals main mode is the thickness shear, when the resonator is not properly designed the flexure mode can become excited at the same time. This flexure (spurious or unwanted mode) will take away some of the energy that should be going to the main thickness shear mode. Spurious modes can easily be eliminated with special care during the design of the quartz crystal resonators. The design depends on the quartz blank, electrode geometry and also the type of mounting that is used for the resonator [16].

1.2.3 Zero Temperature Coefficient Cuts

Alpha quartz can be cut into many different types of angles. There are single rotated temperature compensated cuts like the AT and BT cuts and then the double rotated cuts like SC, which is the stress compensated cut. The type of cut that is used throughout this research is the AT-cut. AT-cut quartz has a very small amount of frequency change due to the change in temperature making it the most common type of cut used for quartz resonators. Even though the SC-cut has better performance than AT-cut crystals, it is more difficult to create the SC-cut crystals.

The AT-cut wafers used were cut from Y-bar quartz at an angle of $35^{\circ}15'$ with respect to the Z-axis. From previous sections discussed earlier the frequency shift in ppm from the temperature range of -50°C to 100°C is only ± 15 ppm. The temperature compensated crystal oscillator (TXCO) and the oven controlled crystal oscillator (OCXO) allows for only a frequency variation of 2 ppm and less than 1 ppm respectively. The AT-cut quartz crystal frequency versus temperature graph follows the cubic function, which is shown in Equation 1.6:

$$\frac{\Delta f}{f_0} = a_0(T - T_0) + b_0(T - T_0)^2 + c_0(T - T_0)^3 \quad (1.6)$$

where a_0 , b_0 , c_0 are coefficients, which change for the various angles cut in the quartz crystal. For AT-cut quartz with $35^{\circ}15'$ the coefficients are as follows: a_0 is 0, b_0 is $0.4\text{e-}9$, and c_0 is $109.5\text{e-}12$. The units for the temperature coefficients are as follows $1/^{\circ}\text{C}$ for a_0 , b_0 has units of $1/^{\circ}\text{C}^2$ and c_0 has units of $1/^{\circ}\text{C}^3$. Also, for AT-cut quartz the T_0 , which is the inflection temperature, has a value of 25°C . Figure 1.7 shows the change in frequency for every change in temperature for an AT-cut quartz crystal at the $35^{\circ}15'$ angle.

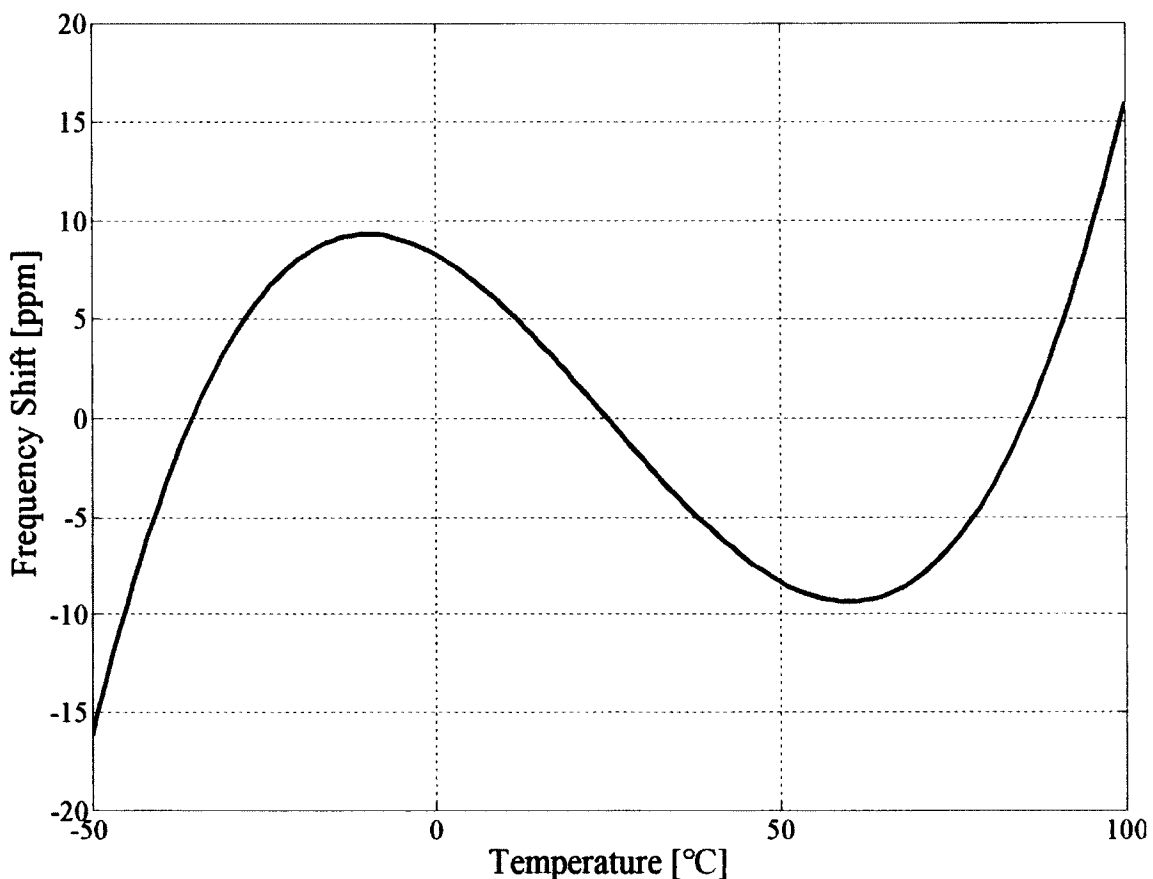


Figure 1.7 Frequency Shift versus Temperature for AT-Cut Quartz Crystal

The zero temperature coefficient cut crystals still have frequency variations with the change of temperature. However, when compared to other materials in Figure 1.3 it can be seen clearly that the zero temperature coefficient AT-cut quartz has the best temperature performance of most materials. The final reason quartz is an important material is the fact that it has a low solubility in most chemicals allowing it to be used in extreme chemical environments.

1.2.4 Low Solubility of Quartz Crystals

Quartz crystals have a low solubility in most chemicals. The exceptions are the fluoride and the hydroxide family of chemicals. The reason why quartz crystals have

such a low solubility in most acids is due to the fact that it is formed by an acid. It is formed by the silicic acid family and can be described by the following chemical formula:



For quartz crystals orthosilicic acid is present in the reaction and is represented by H_4SiO_4 . The ability for quartz crystals to be immune to most chemicals allows for it to be used as a sensor in harsh environments. The only problem with quartz having a low solubility is that it makes it difficult to process with wet etching techniques. For instance the fluoride based etchants require temperatures in the 70 to 85°C range to have a significant etch rate. While the hydroxide based etchants require temperatures up to 200°C [17, 18]. The next section will discuss the different processing methods that have been attempted for quartz crystals.

1.3 Current Processing Methods

Currently there are only two types of quartz processing methods that are dominant in the commercialization of quartz crystals and they are mechanical lapping and wet etching. There are other quartz processing methods; however, they are not best for mass producing quartz crystal resonators. The two other processes to be discussed are the deep reactive ion etching (DRIE) and the micromachining by ion track etching (MITE) [19, 20]. Currently between these two new approaches that have created working resonators the most used process is the DRIE process. Whereas MITE processing can etch quartz it causes some damage to the crystal. Since the start of the quartz resonator industry mechanical lapping has been used and is typically used for AT-cut resonators with a maximum resonant frequency of 50MHz. At 50MHz resonant frequency correlates to a

thickness of $33.5\mu\text{m}$. For thicknesses smaller than $33.5\mu\text{m}$ it is not practical for commercial applications due to the fragile nature of the crystals it is quite easy to break with the mechanical lapping process. The other type of commercial process for quartz is wet etching and the etchant used in this process is typically some form of hydrofluoric acid (HF). It has been reported on the creation of a 2GHz AT-cut fundamental frequency quartz crystal resonator produced by wet etching [21]. At this point in time the wet etching process seems to be the best technique for the creation of quartz crystal resonators on an industrial scale.

1.3.1 Deep Reactive Ion Etching (DRIE)

Deep reactive ion etching (DRIE) has been studied recently to improve the etch quality (polishing) of quartz crystal resonators. However, even though DRIE produces slightly better structures, it takes a considerably longer time. Takashi Abe *et al* have reported a DRIE process for AT-cut quartz that has an etch rate of $0.2\mu\text{m}/\text{min}$ ($12\mu\text{m}/\text{hr}$) [19]. Another problem with DRIE is the expensive equipment required for processing. For DRIE processes high vacuum equipment is needed, as well as large RF power sources around 500W. Even though it can create better structures in quartz crystals, the price and time required to do so limits its use on the industrial scale.

1.3.2 Micromachining Ion Track Etching (MITE)

Micromachining by ion track etching (MITE) processed used by Klas Hjort *et al* uses Xe ions with an energy of 11.4MeV and a dose range of $2.6e8$ to $2.6e10$ ions/cm² [20]. These Xe ions bombard the surface of the quartz crystal, and in the process damage the surface. The surface damage as discussed previously will cause the Q factor of the

quartz resonators to degrade. After the quartz crystals go through the MITE process, they are placed in a KOH solution at 143°C for at least 12 hours [20]. Currently there have been no quartz resonators fabricated commercially with this process due to the expensive equipment required, the damage created through the ion bombardment and long processing times.

1.3.3 Mechanical Lapping

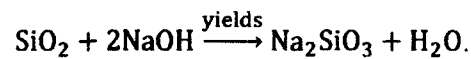
The mechanical lapping process involves placing the quartz die in a shaker with abrasive materials [22]. Multiple lapping attempts must be done to meet the specific dimensions of the resonators increasing the processing time. These multiple lapping attempts increase the cost of the resonators. Other problems with mechanical processing of quartz are the surface defects and the limit of thicknesses that can physically be created [23]. The defects of the surface layer degrade the quality factor of the quartz resonators and also make depositing electrodes more difficult [23-26]. From Vondeling, it was found that the crystal structure had strain layers one quarter the diameter of the abrasive material deep within the quartz crystal from mechanical lapping [23]. Due to the damage from lapping it is not possible to make small geometries and ultra-high frequency (UHF) resonators. This is because for 300MHz AT-cut quartz crystal for example has a thickness of only 5 μ m. At 5 μ m any material becomes brittle and difficult to handle.

1.3.4 Wet Etching of Quartz Resonators

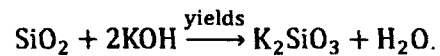
The next and more commonly used process to create quartz resonators is wet etching [20-38]. There are two types of chemical groups that can be used to etch quartz

and they are hydroxides and fluoride based etchants [24-38]. For both of these types of solutions safety measures must be put in place before use. By varying different factors both solutions are able to etch quartz crystal resonators.

The hydroxide group of etchants are rarely used in commercial etching of quartz crystals due to the high pressures and temperatures needed for significant etch rates. For wet etching of quartz crystals sodium hydroxide (NaOH) and potassium hydroxide (KOH) are the most commonly used hydroxide etchants. The chemical reaction of sodium hydroxide (NaOH) with quartz crystals is as follows:



The chemical reaction of quartz and potassium hydroxide (KOH) is shown by:

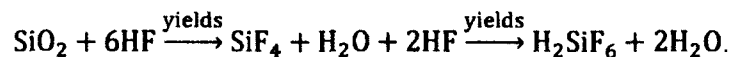


For the hydroxide etchants it takes temperatures up to 200°C to get any significant increase in the etch rate [17, 18]. For example, the etch rate for AT-cut quartz at 190°C using potassium hydroxide (KOH) is only 5µm/hr [17]. Another problem with using hydroxide etchants on AT-cut quartz is that they do not polish the surface, but leave it with a rough finish [17, 18]. The low etch rate for the extremely high temperature of 190°C and rough surface finish has made hydroxide based etchants not a viable option for commercially processed quartz crystals.

Fluoride based etchants are the most commonly used etchants for fabricating quartz resonators commercially. Fluoride based etchants allow for the fastest etch rates and it can polish the quartz crystals. Fluoride based etchants can produce these results at lower temperatures than the hydroxide etchants previously discussed. Concentrated

hydrofluoric acid (HF) is used in order to obtain the highest etch rate for quartz crystals.

The reaction for concentrated HF acid and quartz crystals is as follows:



It has been found that the etch rate depends on the concentration of HF_2^- and HF, however, F^- has been found not to effect the etch rate of crystalline quartz [19, 28].

Hydrofluoric acid (HF) can be used at various concentrations for wet etching quartz, with the highest concentration of HF typically used is around 60%. Any concentration beyond 60% will cause too much pitting in the crystal. Another type of fluoride based etchant used is saturated ammonium bifluoride (NH_4HF_2) [15, 23, 28, 32]. At temperatures below 40°C a saturated ammonium bifluoride solution will polish the quartz crystals.

The reaction between saturated ammonium bifluoride and quartz crystals is as follows:



When ammonium bifluoride becomes saturated with water, hydrofluoric acid will be produced. This reaction allows for the solution to always have a constant amount of HF acid present in the reaction. The saturated ammonium bifluoride creates a HF acid concentration of about 13%. This lower concentration of HF allows for the ability to polish the crystals while keeping the etch rate at reasonable commercial etch rate.

Temperature is a very important parameter for the etching of quartz crystals with fluoride based etchants. This is due to the fluoride etchant's etch rate varying exponentially with temperature for quartz crystals. The relationship between fluoride etchants and quartz crystals can be expressed using the rate equation:

$$\text{rate} = k[\text{A}]^a[\text{B}]^b \quad (1.7)$$

where k is the rate constant, A and B are the concentrations of the reactants, and a and b are the orders of reaction. The fluoride and quartz reaction being discussed has an order of reaction of one, which then allows the rate to be expressed as:

$$k = Ae^{-E/k_B T} \quad (1.8)$$

where k is the rate constant, A is the pre-exponential factor (takes into account frequency of collisions and the orientation), E is the activation energy, k_B is Boltzmann's constant and T is the temperature measured in Kelvin [15]. By taking the natural logarithm the rate equation can be expressed as:

$$\ln k = \ln A - \frac{E}{k_B T} \quad (1.9)$$

which allows for the activation energy and pre-exponential factor to be determined by plotting $\ln(k)$ versus the temperature inverse. Extensive work has been done involving the temperature effects and the etch rate of various cuts of quartz crystals [15, 23, 25, 27]. It is well known that Z-Cut quartz crystals have the fastest etch rates of all the quartz cuts, but it has a poor TCF compared to AT-cut quartz. Since AT-cut quartz has a zero temperature coefficient it is the preferred material for resonators, however, it is one of the most difficult cuts of quartz to etch. Usually commercial processes use bulk solutions of saturated ammonium bifluoride at 80°C to 85°C and then use the same solution with a lower temperature, usually around room temperature in order to polish the crystals. Figure 1.8 shows the etch rate versus etchant temperature for an AT-cut quartz crystal being etched in a saturated ammonium bifluoride solution based on Vig *et al* [15].

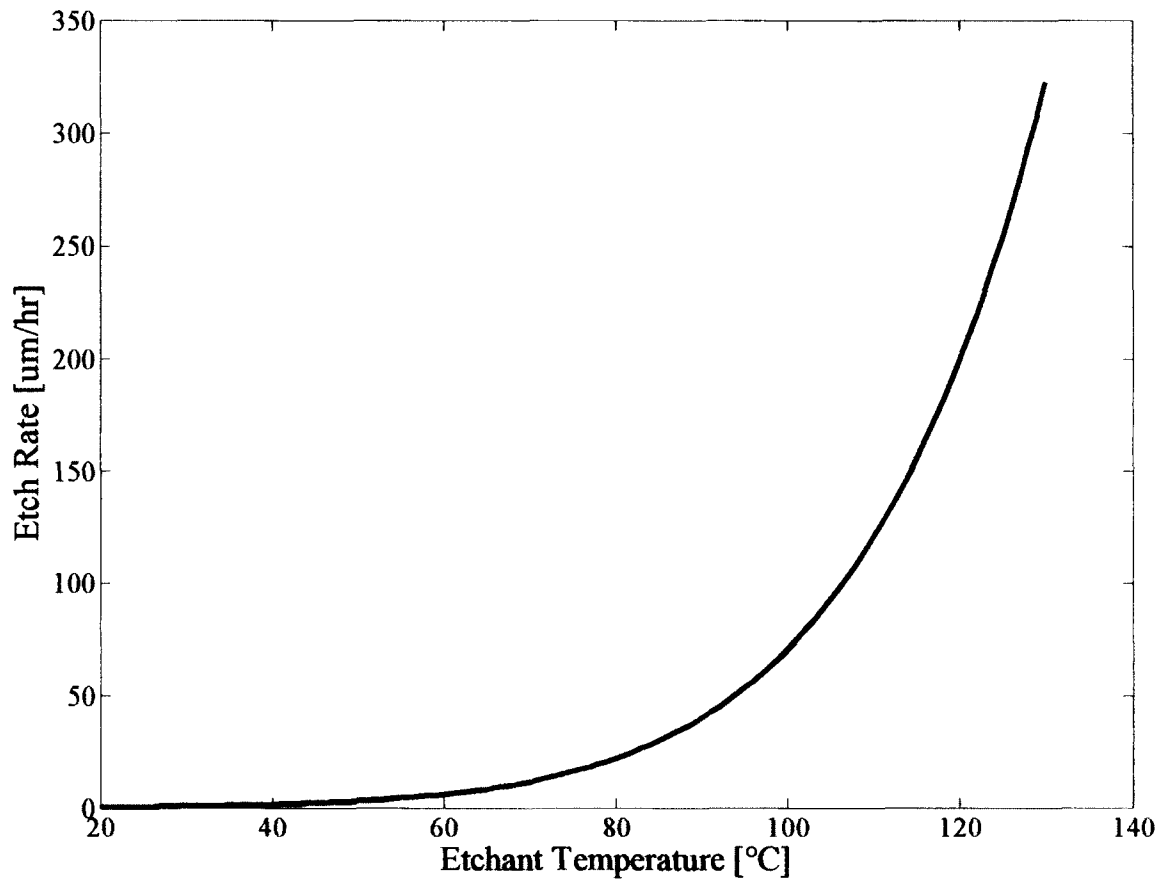


Figure 1.8 Etch Rate Versus Temperature for AT-Cut Quartz Etched In Ammonium Bifluoride [15].

The frequency factor (A) was found by Vig *et al* to be $5.083 \times 10^8 \frac{\Delta f}{f_0 f_{min}}$,

which is expressed in units of frequency [15]. Vig *et al* found the activation energy (E) to be 0.62eV [15]. Other research work done by Tellier found the activation energy to be 0.39eV [38]. Vallin *et al* found that AT-cut quartz crystals could be etched by saturated ammonium bifluoride up to 130°C to obtain an etch rate of 324um/hr [27]. After reviewing Suda *et al* and Vallin *et al* the activation energy that corresponds to both of these works is around 0.65eV [25, 27]. The problem with Vig *et al* research was the fact that they only used temperatures up to 90°C, which did not take into account any of the higher temperatures. Therefore Figure 1.8 is calculated by using the activation energy of

0.65eV [25, 27]. It is possible to increase the etch rate of AT-cut quartz crystals beyond what is shown in Figure 1.8 by increasing the concentration of HF. At higher etch rates the surface will become rough, which has the chance to lower the quality factor of the resonators.

The quality of the quartz surface was discussed briefly in Section 1.1.2 about how the quality factor increases as the surface is more polished. Discussed previously the higher concentration of HF has an etch rate significantly higher than the saturated ammonium bifluoride at the same temperature. However, HF solutions that allow for an increase in the etch rate beyond saturated ammonium bifluoride cause the quartz surface to become rough and it creates etch pits during etching. Saturated ammonium bifluoride will polish quartz crystals during etching at temperatures of 40°C and lower. Also, to limit the roughness of the quartz crystals during etching, the quartz crystals are put through a process called “sweeping” [31, 39]. The sweeping process removes impurities that are present after growing the quartz crystals. It does this by applying a large electric field on the order of 2000V/cm and temperatures up to 500°C, which removes impurities present in the quartz crystals [39]. Hunt found that the sweeping of AT-cut quartz before etching reduced the surface defects by 81.2% [31]. The sweeping process will be discussed in more detail in Chapter 3.

1.3.5 Commercial Wet Etching Process

This section will discuss the current wet etching procedures that are commercially used to produce quartz crystal resonators. The etch rate for a typical solution of saturated ammonium bifluoride for AT-cut quartz wafers at 81°C is 12µm/hr on a single side etch [25]. As discussed before, the etch rate of saturated ammonium bifluoride at 130°C was

found to be $324\mu\text{m/hr}$ [27]. The problem is the fact that it is not safe to heat up bulk solutions of saturated ammonium bifluoride to 130°C and it is difficult to control the etch rate to get the resonator's specified frequency. Therefore 81°C is typically the highest temperature companies will use to process quartz crystals. The problem with the quartz crystal industry processes is that multiple etching steps are needed to get the correct frequency [40]. Table 1.5 shows the multiple steps needed for wet etching quartz resonators in a batch process [40].

Table 1.5 Current Industrial Fabrication Processes [40]

| |
|---|
| Wafer Sawing, Lapping and Polishing |
| Double-sided Cr/Au Metallization |
| Patterning of Cr/Au |
| Wet Chemical Etching of Outer Shape |
| Removal of Cr/Au Over the Area to Be Thinned |
| Thinning Down to $30\mu\text{m}$ |
| First Thickness Adjustment |
| Thinning Down to the Final Thickness |
| Second Thickness Adjustment |
| Deposition of Electrodes and Contacts |
| Final Tuning by Plating on the Wafer |

In this process layout for batch etching of quartz resonators it takes six different etching steps to reach the correct frequency [40]. As can be seen in the table, there are

three thickness adjustments that are needed in order to meet a specific frequency. Each resonator must be individually trimmed to get the correct frequency. Initial variations in the wafer thickness and local variations in the etch rate due to bulk heating are the reason that resonators must be individually trimmed. The research conducted for this dissertation eliminates the need for final frequency trimming by being able to monitor and control the etch rate of the individual resonators.

1.4 Research Objective

The main objective of this research was to find a way to increase the etch rate of quartz crystals beyond the current industrial methods. The new processing methods were incorporated with a control system that allowed for the fine tuning of the etch rate of the quartz crystals. The control system along with the ability to increase the etch rate will allow two things to happen. First, the control system will allow for the ability to eliminate the multiple levels of frequency trimming, while creating the opportunity to have wafer level encapsulation and on chip integration of the quartz crystal resonators on an industrial scale. Second, the fast etch rate will allow for the processing time of quartz crystal resonators to be decreased significantly. The following will discuss information that can be found in each additional chapter:

Chapter 2: This chapter deals with the PID (proportional integral derivative) control system that is implemented in this dissertation work. The basic control theory will be discussed as a review. Also, the implementation of the PID controller in LABVIEW will be discussed in detail. Finally this chapter will show the results of resonators in parallel being etched simultaneously to a similar frequency.

Chapter 3: This chapter discusses the photon induced electrochemical etching of the quartz crystals. We have now augmented the electrochemical etching assisted by X-rays with a closed loop measurement and control of the resonant frequency of individual resonators [41].

Chapter 4: The rapid etching of the quartz resonators will be done with a near infrared (NIR) laser that is focused with a lens. Using this setup allows for the ability to etch the resonators at an extremely high etch rate and also gives the option to create microstructures. This will allow for the processing time of the quartz crystal resonator to be decreased significantly. Also, the modeling of this process in COMSOL will be shown.

CHAPTER 2

ETCHING CONTROL SYSTEM

In order to obtain wafer level encapsulation and integration for quartz crystal resonators a control system must be implemented with the etching process. Another important aspect is to eliminate the current requirement in industry, which is to have multiple processing steps to reach a specified frequency. Due to these multiple processing steps most companies have a selective amount of frequencies they produce. With a control system incorporated with a process that can vary the etch rate there is no need to have only a select number of frequencies. This control system must be able to monitor the resonant frequency of multiple resonators. It must be able to compensate for initial wafer thickness variation and local variations in the etch rate. A PID (Proportional-Integral-Derivative) controller was designed and optimized in LABVIEW to measure the resonant frequency of multiple resonators and control the output that is applied to the resonator. To demonstrate the PID control system, two IIIB class 635nm lasers, with the power supply connected to the computer through GPIB were used to etch two different resonators. This chapter will also discuss the basic theory of PID control systems along with experimental results from the previously outlined demonstration.

2.1 PID Control Theory

PID controllers have been used in many industrial applications and have been perfected over the years. PID stands for Proportional Integral Derivative control, and can be used in parallel or in series. These three types of control can be combined up in different ways to get varying degrees of control. Before going into the details of PID control, a quick overview of two types of control systems will be discussed. These two types of control systems are open loop and closed loop. The open loop system is the most basic of the two. Figure 2.1 shows an open loop system, it consists of a set point, controller, actuator and process to be activated.



Figure 2.1 Open Loop Control System

The set point is the value that the control system is trying to obtain. The controller can be considered the brains of the control system as it sends the information to the actuator. The actuator actually does the action in the control system. The process is the action that is needed to be completed in the control system. In an open loop system, the controller has no knowledge of what is happening in the system. A washing machine is an example of an open loop system. The set point is the cycle option on the washing machine which is decided by the operator, this cycle can have varying operating times, amount of water in the machine, and the temperature of water. The controller initiates the actuator, which lets in the water and changes the water's temperature. The controller

never knows if the right amount of water is in the system, it has no way of measuring the temperature to see if it is correct, and it does not know if the timer in the washing machine is working properly. For systems like a washing machine, a lot of control is not needed to complete the process.

The closed loop system was designed to be able to monitor the process variable and then be able to respond to any changes in the overall system. The closed loop system is shown in Figure 2.2, which adds a feedback line in the system and a comparator to calculate the amount of error in the system.

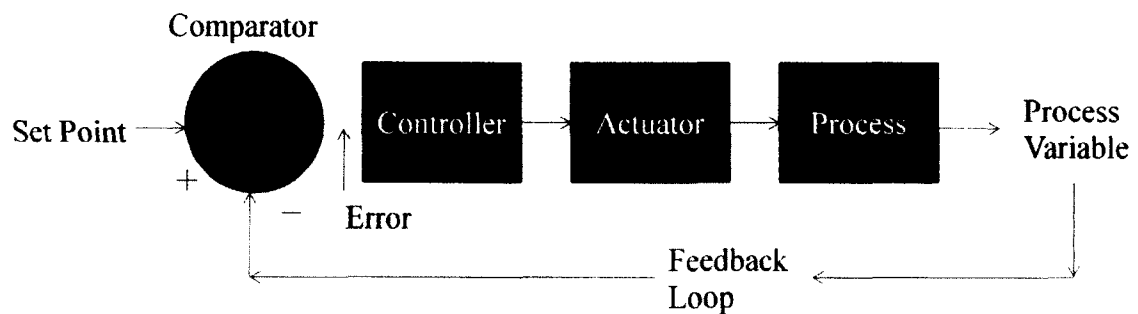


Figure 2.2 Closed Loop Control

The feedback path has a sensor that measures the process variable produced. The process variable passes through the feedback loop to the comparator. The comparator then compares the set point to the process variable and produces the error signal. The controller will compensate the actuator based on the error signal. The closed loop system will allow for complete control over the output of the system. An example of a closed loop control system is a vehicles cruise control system. Where the control system's feedback will measure the speed of the car and keep it constant whether going up or down hill.

The next part of this section will describe the PID control system incorporated with two laser diodes. The two diodes were controlled by a PID controller built using Labview software, and had their voltages varied to in order to manipulate the laser diodes' power output. Figure 2.3 shows the PID control system flow diagram utilized for two resonators being etched on the same die with two laser diodes.

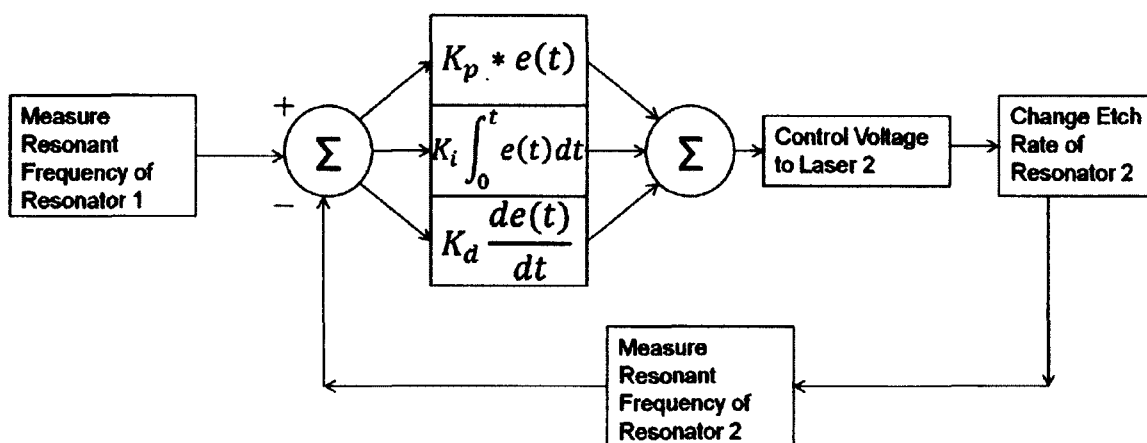


Figure 2.3. PID Control Flow Diagram for Laser Diode System

By incorporating the PID controller, it is possible to control the etch rates of multiple resonators on the same die. Due to the piezoelectric effect of quartz crystal resonators, the resonant frequency can be measured during wet etching with a network analyzer. This can be done due to the electrical conductivity of HF, which is in contact on the backside of the quartz crystal. The resonant frequency is the process variable of the closed loop system and the etch rate would be considered the actuator of the system. The various parts of the PID controller will be discussed in the next sections.

2.1.1 Proportional Control

Proportional control is the first part of the PID controller. The proportional control does as its name implies it tells the actuator to apply an output that is proportional to the error in the system. The proportional control makes up the main part of the control system. The proportional control part of the PID system is calculated using the following equation:

$$\text{Proportional Output} = K_p * E, \quad (2.1)$$

where K_p is the gain of the proportional constant, and E is the error, which is the difference between the set point value and the process variable [42]. What happens when the K_p is changed? As K_p is increased it will speed up the response of the system. Using only a proportional controller will cause the system to have a large steady-state error [42]. The proportional gain must be very large to correct the large steady-state error. Figure 2.4 shows a simulation of a proportional controller, which was programmed in MATLAB.

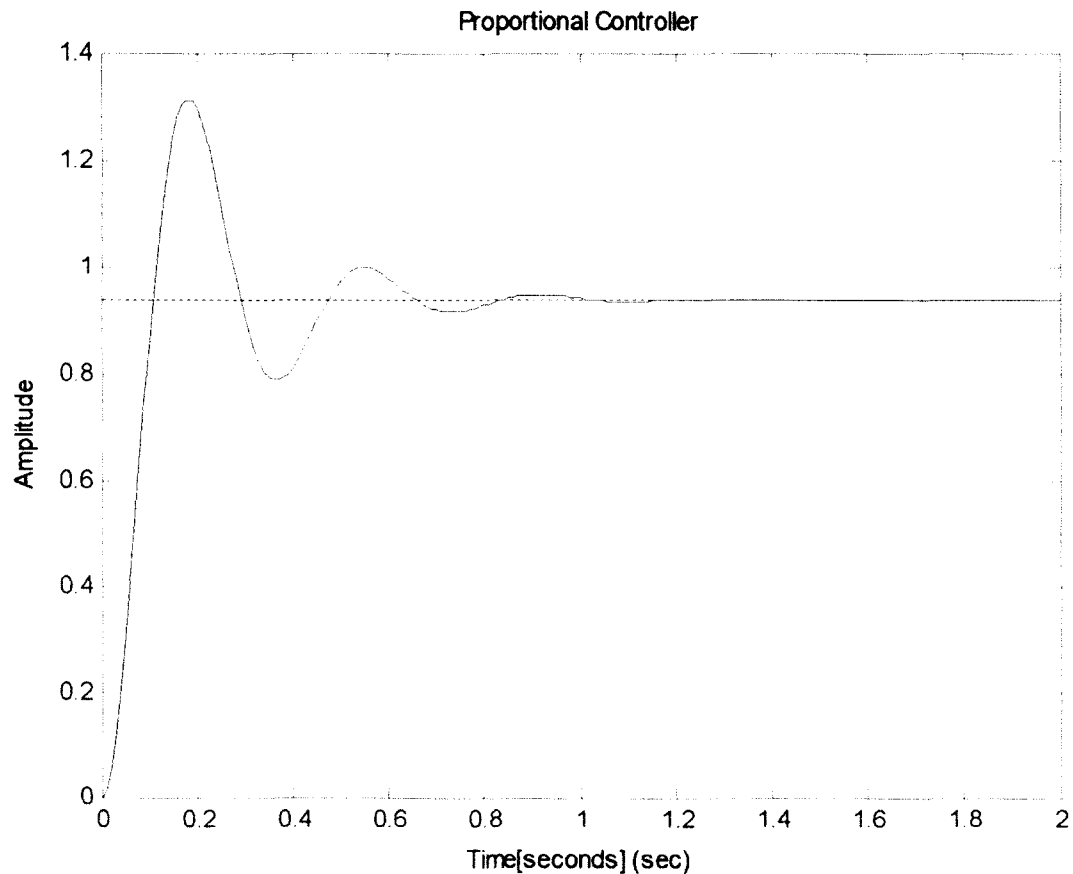


Figure 2.4 Proportional Controller Output

It can be seen from Figure 2.4 that the proportional controller can reach the set point in about 0.1 seconds. The problem with Figure 2.4 is the ringing effect that takes place initially before the output makes it to the steady-state value at the set point. Since the process variable reaches the set point value at steady-state in less than two seconds, the proportional control can be used in a lot of noncritical systems. For systems that cannot afford to have the control system to overshoot, then the proportional controller needs to be added with the two other control mechanisms. The next part of the control system to be discussed is the integral controller.

2.1.2 Integral Control

Integral control is the second part of the PID control system. Integral control is used to eliminate the steady-state error that is caused by the proportional part of the control system. The output of the integral control is proportional to the sum of all past errors multiplied by the amount of time the errors have taken place [42]. The integral control output can be calculated by the following equation:

$$\text{Integral Output} = K_I \sum (E * \Delta t) \quad (2.2)$$

where K_I is the integral gain that can be control in the integral control system, and the error multiplied by the change in time is summed together [42]. Normally integral control does not start working until a certain amount of time has passed. This is due to the fact that integral control waits until the error of the system builds up with time and then once the error is large enough its starts to correct the process variable. The problem with integral control is that it will increase the overshoot of the system and the overall system stability is lowered. This is why integral control cannot stand alone and must be accompanied with proportional control to maintain the balance in the system. Figure 2.5 shows the output of a proportional and integral controller (PI controller).

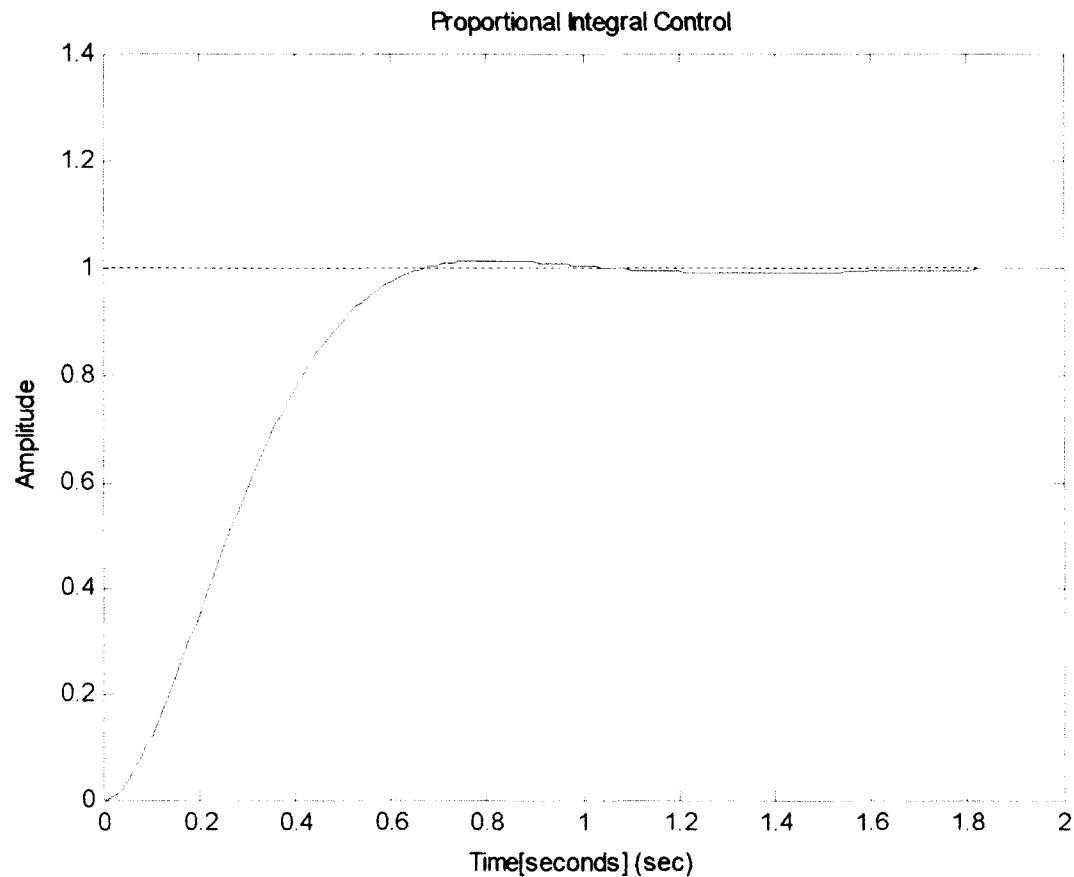


Figure 2.5 PI Controller Output

The integral as stated previously helps eliminate the ringing effect caused by the proportional controller, however, by adding the integral control it increases the time it takes for the process variable to reach the set point value. Therefore some tradeoffs must be made in order to get a stable control system. Still even with the tradeoffs the output is not accurate and quick enough to control a system that needs the highest degree of control for instance an experiment that needs temperature controlled down to the 0.01°C . In order to get this kind of control the PID controller is needed.

2.1.3 Derivative Control

To reduce the overshoot problem that is caused by the PI control a derivative part must be added to the controller. The derivative control is the rate of change of the error in the system. This can be calculated by the following equation:

$$\text{Derivative Output} = K_D \frac{\Delta E}{\Delta t}, \quad (2.3)$$

where K_D is the derivative gain. The derivative control of the system is proportional to the error slope [42]. The derivative control is designed to speed up or slow down the response of the control system. However, if the derivative gain is too high it will cause noise already present in the system to be magnified to the point of disrupting the control system. Figure 2.6 shows the proportional and derivative controller output.

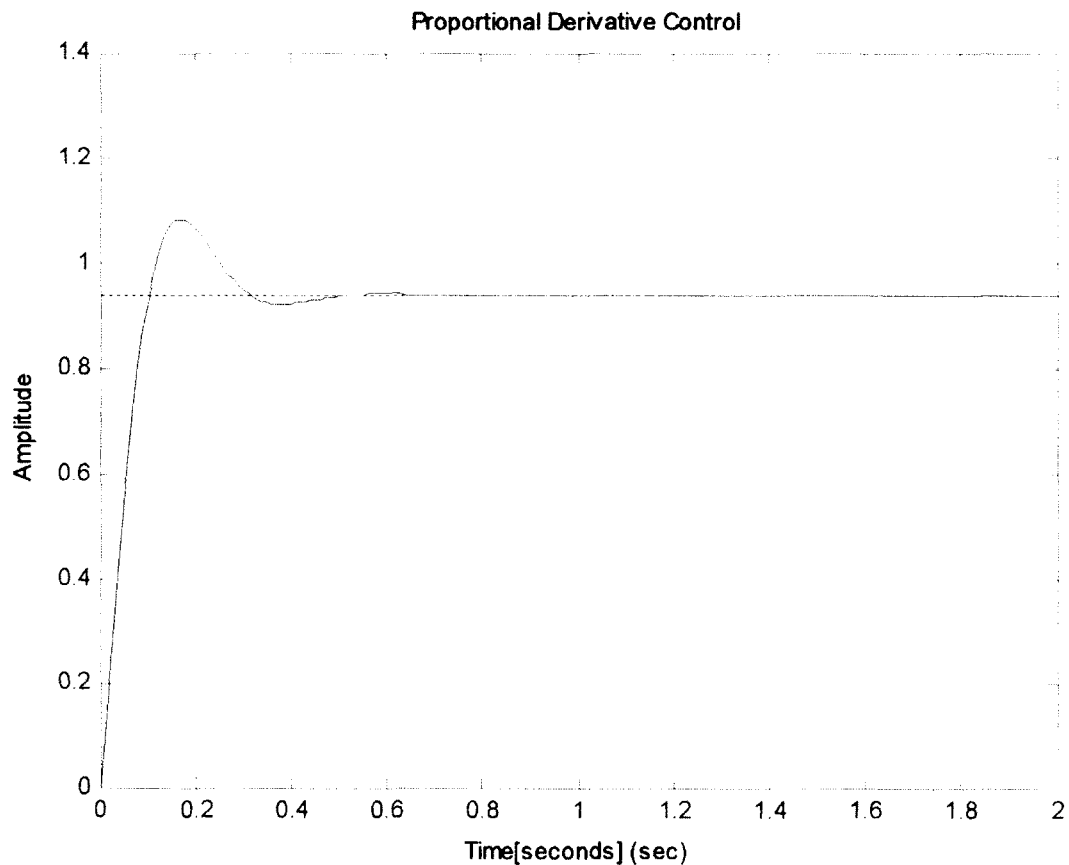


Figure 2.6 PD Controller Output

The output of a proportional and derivative control (PD control) has ringing from the proportional control but it has a faster response than the PI controller. However, for more sensitive applications ringing will not be suitable. This requires the use of a PID controller and the best ratio of the gains of each parameter must be adjusted properly.

2.1.4 PID Controller

The best type of controller utilizes all three components combined. If the gain values for each part of the controller are set correctly then the PID controller will function without any of the problems mentioned previously. The PID controller output can be characterized by the following equation:

$$u_c(t) = K_p e(t) + K_I \int e(\tau) d\tau + K_D \frac{de}{dt}, \quad (2.4)$$

where the $e(t)$ is the error in the system, which is taken by subtracting the set point from the process variable, K_p is proportional gain, K_I is the integral gain, and K_D is the derivative gain [42]. Figure 2.7 shows the output of PID controller simulated in MATLAB.

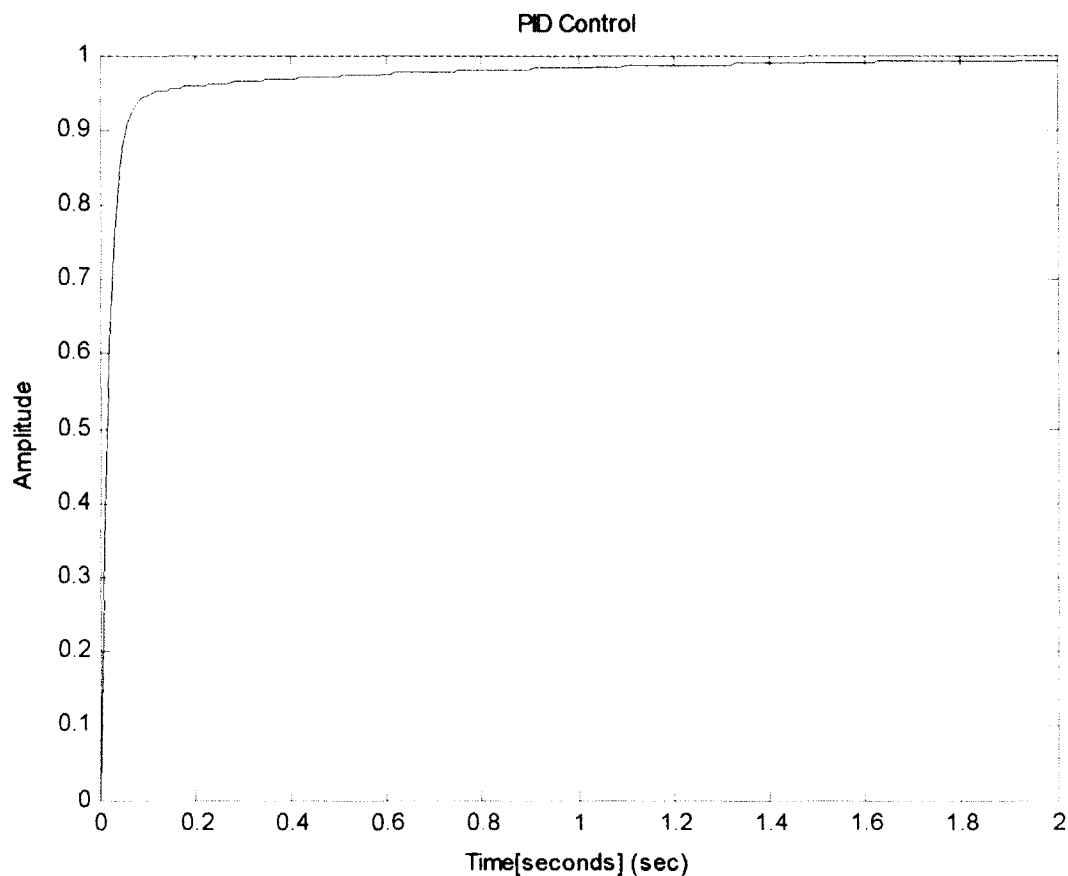


Figure 2.7 PID Controller Output

This figure shows that the response of PID controller eliminates the overshoot. Figure 2.7 shows why the PID controller has become one of the most used electronic systems for various industrial fields. Table 2.1 shows a summary of the effects that each part of the PID controller will change when the gain is adjusted [42].

Table 2.1 PID Control Parameters [42]

| Controller Type | Rise Time | Overshoot | Settling Time | Steady-State Error |
|-----------------|---------------|-----------|---------------|--------------------|
| Kp | Decrease | Increase | Slight Change | Decrease |
| Ki | Decrease | Increase | Increase | Eliminate |
| Kd | Slight Change | Decrease | Decrease | Slight Change |

The PID controller can be fine tuned to allow for fast rise times, while eliminating overshoot in the system. The parameters must be balanced in order to get the best results. The important parameters in a control system are shown in Table 2.1, which are rise time, overshoot, settling time, and steady-state error. Rise time is the amount of time it takes for the process variable to reach the set point value. The control system will increase the output so much that it overcompensates causing the process variable to overshoot the set point value. The overshoot can occur with various outcomes; usually causing the process variable to oscillate above and below the set point. The settling time is how long it takes the process variable to reach its steady-state value. The steady-state error in the control system is the difference between the process variable and the set point after the process variable reaches steady-state. The P controller has a fast rise time but it introduces ringing (overshoot) in the system. Since the integral control cannot stand alone it must be incorporated with the P controller. The integral control eliminates the steady-state error, but decreases the rise time and increases the time for the system to reach steady-state.

2.2 Implementation of PID Control In LABVIEW

The final PID controller used in this research was created entirely in LABVIEW. There were however previous iterations that were created using LABVIEW and Matlab in conjunction. LABVIEW allows for the creation of an interface for data acquisition and instrumentation control. The LABVIEW control system allows for real time measurement of the etch rate during fabrication of quartz crystal resonators. This control interface creates the opportunity of measuring the resonant frequency of multiple resonators and processing the data in a PID controller. The resonant frequency can be

measured down to an accuracy of +/- 10ppm. The next section will cover the interface created in LABVIEW.

2.2.1 Control Interface

The creation of the control interface is a very straightforward process due to the fact that LABVIEW is a graphical programming language. The control interface allows for easy access to all of the program's data on one screen. The important parameters on the control interface are the following: Level, Receiver Bandwidth, Measured Frequency, and Target Frequency. The Level option represents the amount of power applied, which could be varied from -22 dBm to 13dBm (2 μ W to 19mW) during measurement. Receiver Bandwidth represents how fast data is taken from the resonator. The measured frequency is found by applying curve fitting techniques to measure the frequency signals. The target frequency is determined before the etching process; however, this can be changed after the system has already started. Figure 2.8 shows the control interface created in LABVIEW.

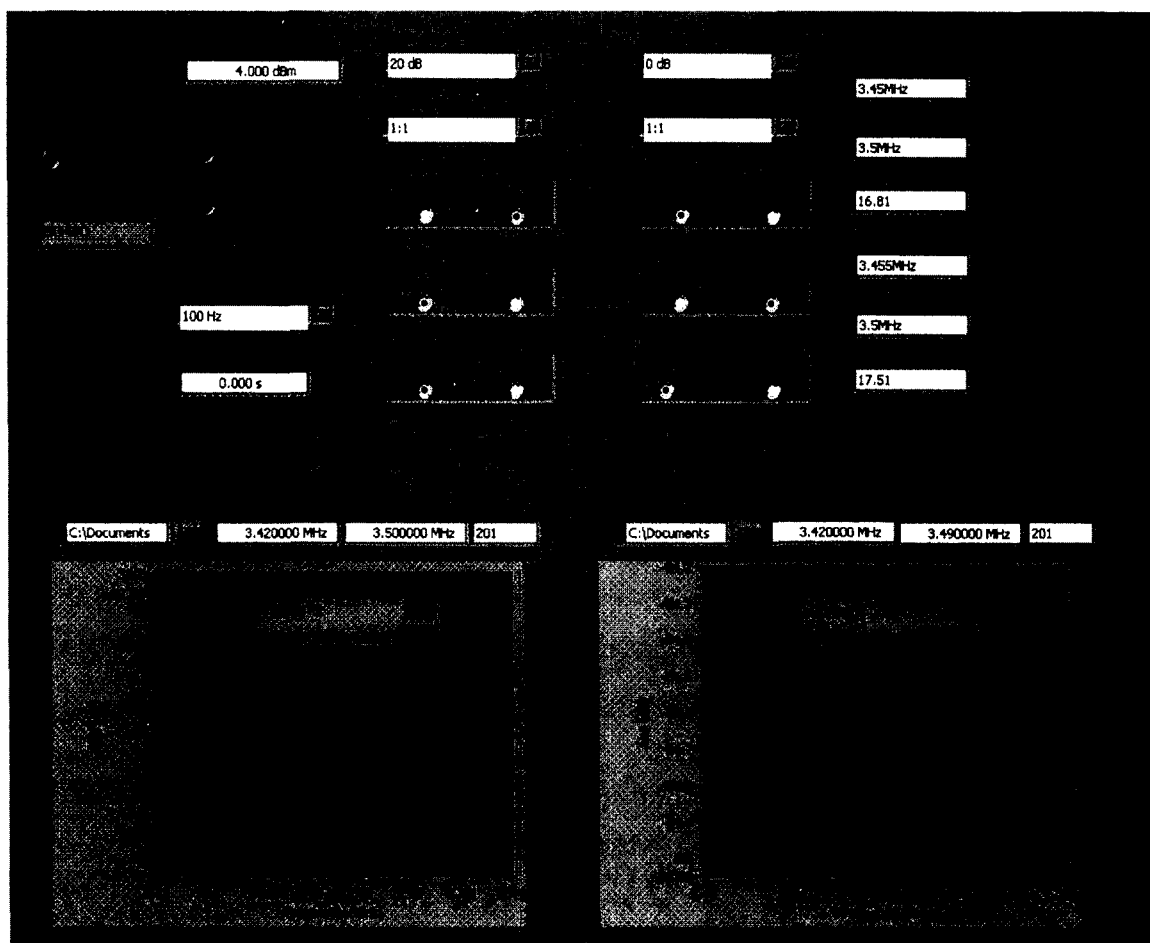


Figure 2.8 PID Control Interface Created In LABVIEW

The initialization of the control interface and how the system works will now be discussed. The program reads the source level and the receiver bandwidth and sets the network analyzer. The source level is the amount of power that is applied to the crystal resonator. The dB level of the power applied to the resonator is set at 0dBm, which corresponds to a power of 1mW and a peak voltage of 0.316V. The receiver bandwidth is set at 100Hz and records data every 10 milliseconds.

2.3 Resonators On Same Die Simultaneously Etched

The PID controller was tested using two small class IIIB class lasers to etch two resonators on the same die. The quartz crystal blank used for these experiments has an area of 12.5mm^2 . The crystal blank can be created smaller, all that is needed is for is each laser beam focused down to a smaller spotsize.

2.3.1 Experiment Setup

The equipment used in these experiments are as follows: network analyzer, control switch, programmable power supply, two class IIIB class 635nm lasers, and the control interface designed in LABVIEW. Figure 2.9 shows the experimental setup of the two lasers etching two resonators.

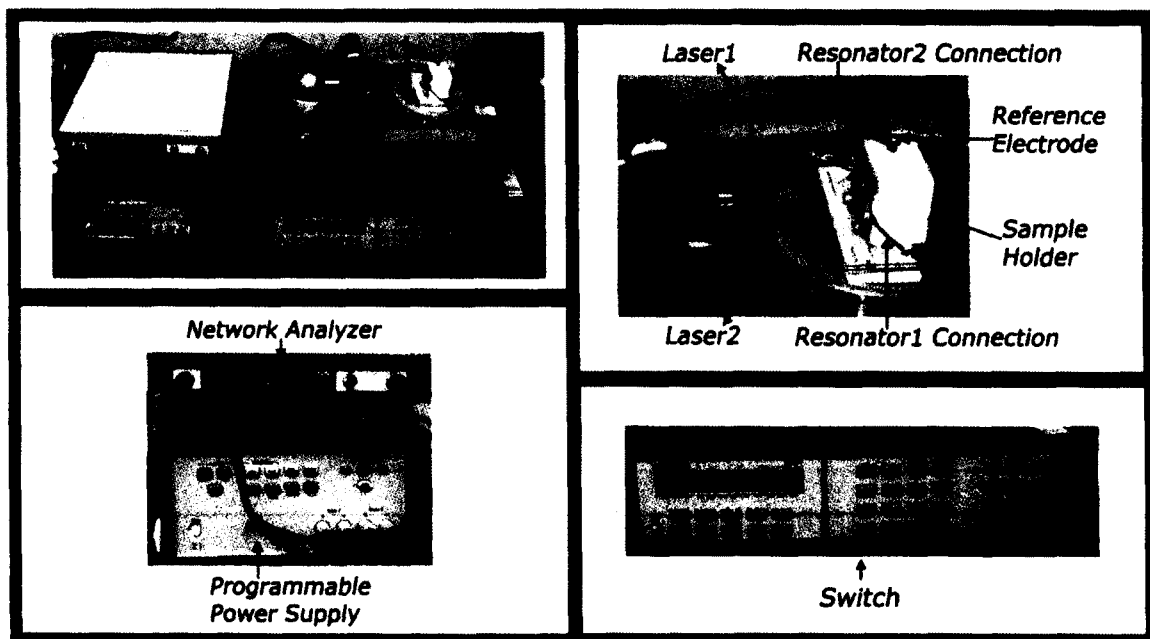


Figure 2.9 Experimental Setup of Multiple Resonators Etched with Lasers

The network analyzer allows for the measuring of each resonator's frequency. This is done using the control switch unit that allows the network analyzer to switch back and forth between resonators. The lasers specifications are as follows: wavelength is 635nm, and they are semiconductor based (rectangular beam output). The laser's power is controlled by the programmable power supply that is connected with the PID control system. The PID control system works as follows: one is turned on at low power output, while the second is varied using the PID controller.

2.3.2 Results and Discussions

The first experiment dealt with allowing both resonators to have frequencies that were separated by over 10,000ppm. Two resonators on the same die, where one of the resonators was etched with a laser in order to get its frequency higher than the other. Then the control flow discussed in Figure 2.3 was used in order to have the frequencies merge together. Figure 2.10 shows the results for this experiment.

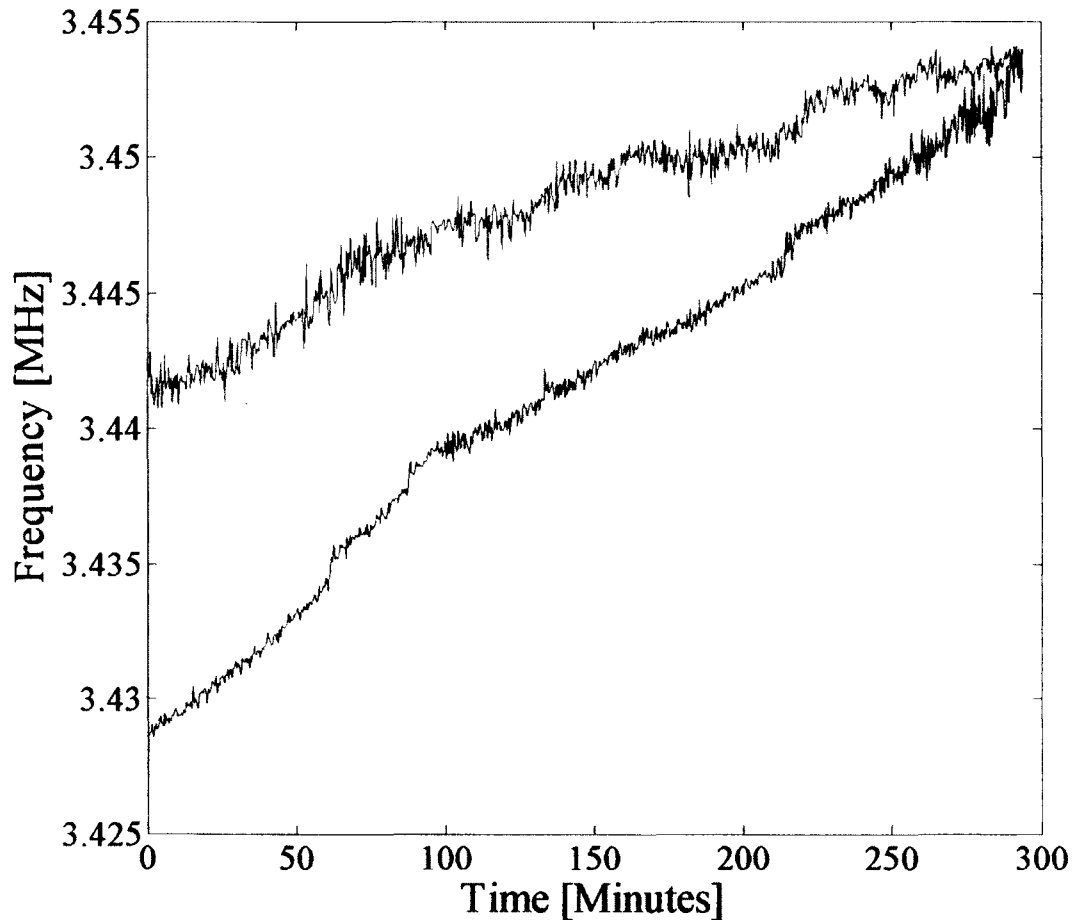


Figure 2.10 Results For Two Resonators Etched On The Same Die

For this experiment it took 280 minutes for the frequencies of the two resonators to match each other. The reason for this is due to the fact that the lasers used are of low power and the etchant was at room temperature. The LABVIEW control interface has a frequency measurement accuracy of ± 10 ppm. The measurement frequency accuracy is how well the system will measure the frequency for each set of recorded data. This means that each time the frequency is measured it will have an accuracy of ± 10 ppm. The second accuracy to be discussed is that of the PID controller. The PID controller accuracy is how close it can bring the two resonator's frequencies together. The initial

resonators had frequency differences over 10,000ppm from each other and the final frequencies were measured to be within 28ppm. The 28ppm is how well the PID controller can get the two resonators frequencies to be identical. This can be improved upon by using a commercial grade PID controller instead of one created in LABVIEW. The accuracy of the PID control of the laser etching system falls within the +/- 50 ppm range, which can be used for low-end applications. High-end applications require frequency accuracies in the +/- 5ppm range, for example crystal resonators used for GPS systems.

It was shown that the PID control system can take two resonators on the same die that have a large frequency difference and bring the frequencies within +/- 50ppm of each other. The second experiment was to have two resonators at similar frequencies and then allow the PID control system to keep the frequencies together. The results of this experiment are shown in Figure 2.11.

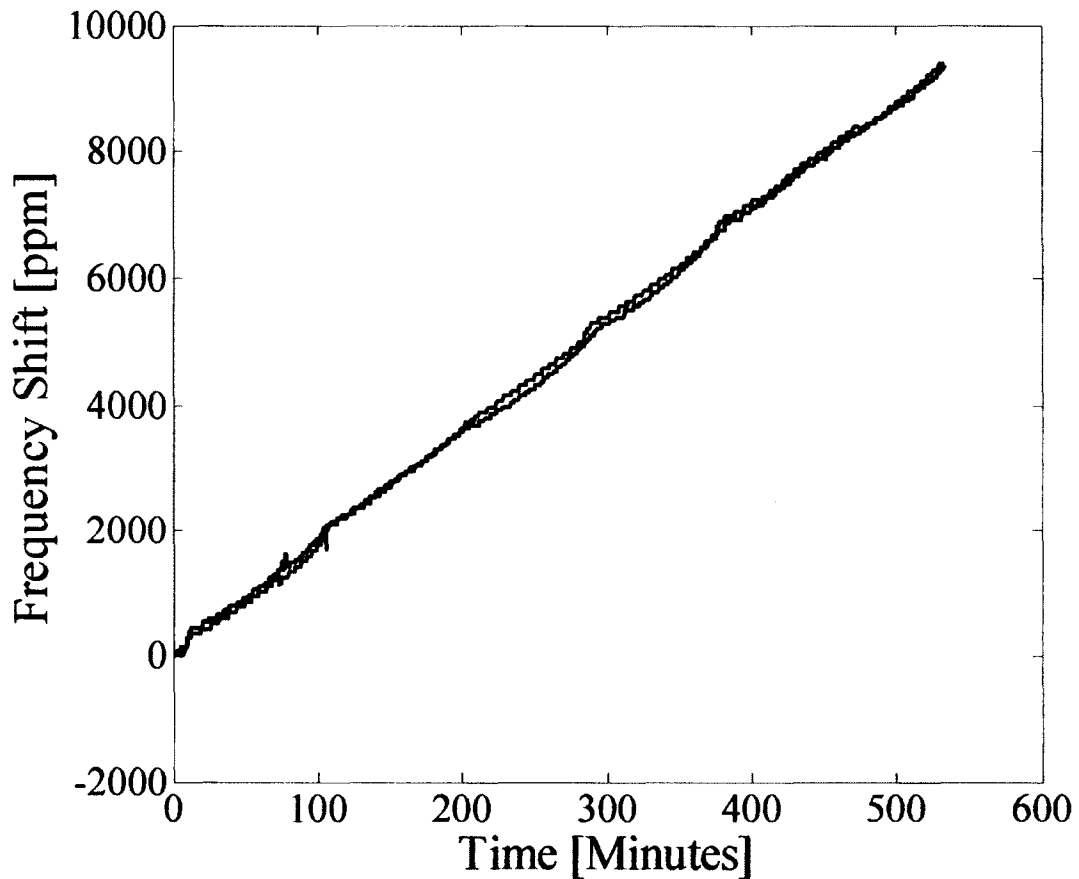


Figure 2.11 Frequencies of Two Resonators Staying Together

The experiment was carried out at room temperature, only the lasers were applying any external heat to the etching setup. One laser was kept at a constant power and the second laser was controlled by the PID controller. The PID controller allowed for the two quartz crystal resonators to remain similar in frequency for over eight hours.

2.4 Conclusion

In this chapter, it was shown that it is possible to control multiple resonators during etching while maintaining a measurement accuracy of ± 10 ppm. Even when initial frequencies on the same die are beyond 10,000 ppm, it is possible to reach a final frequency difference better than ± 50 ppm. Future work will involve increasing the

measurement accuracy of the resonant frequency and the PID controller's accuracy to allow for creating resonators that can be used in high-end applications such as GPS systems. The measurement frequency accuracy can be improved upon by varying the curve fitting algorithms used in LABVIEW. Since the PID controller used was built inside of LABVIEW, it is possible to replace this controller with a commercial grade controller to increase the accuracy of overall control of the etching system. The measurement system has an accuracy of +/-10ppm and the PID controller accuracy is below +/-30ppm (28ppm). Current commercial processes require individual measurement of the resonators after wet etching. Each commercial resonator is metalized and the resonant frequency is measured. This control system presented in this dissertation allows for the measurement of the resonant frequency of each resonator while it is being wet etched.

CHAPTER 3

ELECTROCHEMICAL ETCHING ASSISTED BY X-RAYS

The objective of this chapter is to show that there are other variables that can influence the etch rate of quartz crystals other than the current industry standard. In industry the following effects are varied to influence the etch rate: etchant concentration, temperature, time, and type of etchant. It was found during this research that subjecting the quartz crystals with x-rays and applying a DC bias voltage while being wet etched can vary the etch rate of the crystals. To the author's knowledge this is the first thesis work to show quartz crystals (or any insulating crystal) can be successfully electrochemically etched with assistance from x-ray radiation.

The first section of this chapter will discuss electrochemical etching of silicon, which has been extensively researched through the years [43-49]. The reason for the extensive research on electrochemical etching of silicon is the fact that semiconductor materials do not require large amounts of bias voltage for the electrons to move across the band gap. In comparison insulating materials require large amounts of bias voltage in order to induce a current through the material. However, for insulators such as quartz, large DC bias voltages alone will not induce any significant current that would affect the etch rate of the quartz crystals. Insulators need another mechanism to allow electrons to move across their large band gaps. Quartz has an energy band gap of 9eV compared to silicon which has an energy band gap of 1.1eV. To overcome the quartz crystals band

gap, x-rays were used to energize the electrons in order for them to move across the band gap. The first two sections will cover background literature on the electrochemical process and photon effects on etching silicon. Then background material will be covered on ways other researchers have attempted to find alternative ways to etch quartz crystals. This section will be followed by theory and experimental results of electrochemical etching of quartz crystals assisted by x-rays. To this researcher's knowledge this is the only work that takes all of these aspects and combined them into one process.

3.1 Electrochemical Etching of Silicon

Electrochemical etching has been extensively studied by researchers in order to find ways to vary the etch rate of silicon for MEMS applications [43-49]. Electrochemical etching involves the wet etching process of the material while a current passes through it. The current then interacts with the etchant, thereby affecting the etch rate of the material [43-49]. A reference electrode is immersed in the etchant to complete the circuit. Figure 3.1 shows the effects DC bias voltage has on n-type silicon wafers [48]. It can be seen clearly that from -1V to -3V that the etch rate increased above 10 $\mu\text{m/hr}$, however when the bias voltage is from -0.5V to 0V the etch rate was around 0.2 $\mu\text{m/hr}$ [48].

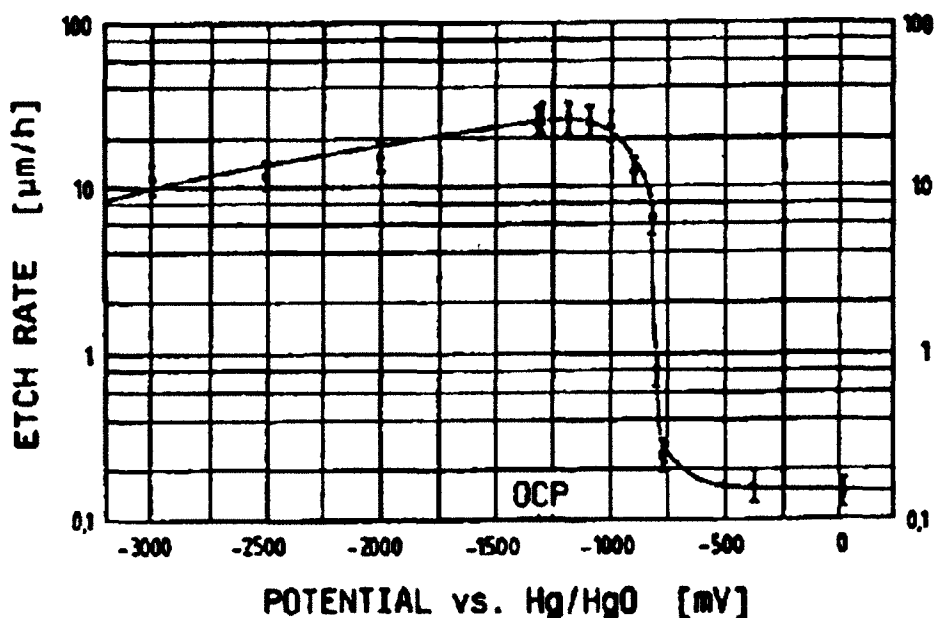


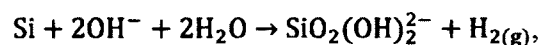
Figure 3.1 DC Bias Voltage Versus Etch Rate of Silicon [48]

Figure 3.1 data is n-type silicon being etched by a 30% KOH solution at 65°C [48]. For n-type silicon being etched in an alkaline solution with a -0.5 voltage bias applied a silicon dioxide layer is formed [48]. The etch stop is created due to the fact that the current being pass through the silicon wafer cancels out the negative surface charge that normally repels the OH⁻ ions [48,52]. Once the OH⁻ ions are allowed to move to the silicon surface freely, the hydroxide ions can form silicon dioxide [48,52]. Silicon dioxide has a much slower etch rate than crystalline silicon in hydroxide and hydrofluoric based etchants allows for the creation of the etch stop [48,52]. With semiconductors it is possible to increase and decrease the etch rate of silicon simply by varying the DC bias voltage applied. In order to electrochemical etch quartz crystals, the etching process must be aided by high energy photons. The effects photons have on etching silicon will be discussed in the next section and photon effects on insulators will be briefly discussed in Section 3.3.

3.2 Photon Effects on Etching Silicon

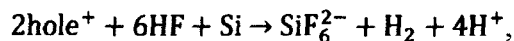
This section will cover background literature on photons and their effects on etching silicon. It was found that when a light was shined on silicon wafers during etching that the etch rate was affected [50-53]. When light with energy greater than silicon's band gap, which is 1.1eV, the current passing through the silicon wafers will increase [52]. The band gap of silicon corresponds to a wavelength of about 1127nm, which is in the near infrared (NIR) region of light.

The first work reviewed involved using a broad wavelength spectrum. The light source they used in their work was a xenon broadband lamp, which contains the entire visible spectrum 390nm to 700nm (3.2eV to 1.6eV) [52]. It was found that light would create an etch stop for n-type silicon wafers and that for a p-type silicon wafer it helped to selectively etch the wafer by increasing the etch rate [52]. Previously discussed was the fact that a small negative bias voltage applied to n-type silicon would create an etch stop [48]. It was later shown that it is possible to shine only light on the n-type silicon to create an etch stop using hydrofluoric acid as the etchant [52]. The light being applied to the silicon substrate allows electron-hole pair generation to take place much faster [52]. The more electrons present the faster the negative surface charge of silicon can be negated allowing silicon dioxide to grow fast enough to slow the etch rate down significantly [52]. The reaction that creates the etch stop for alkaline etchant solutions is as follows:



The alkaline etchant could be CsOH or KOH, the only thing that matters is the OH- ion that creates the silicon dioxide to slow down the etch rate [50,52]. The reaction for

silicon being irradiated by light while being electrochemically etched in hydrofluoric acid (HF) is as follows:



where the holes are created through the silicon wafer being irradiated by the light [53]. Figure 3.2 shows the amount of current produced while a DC bias voltage is applied and the silicon wafers are irradiated by white light of various power densities.

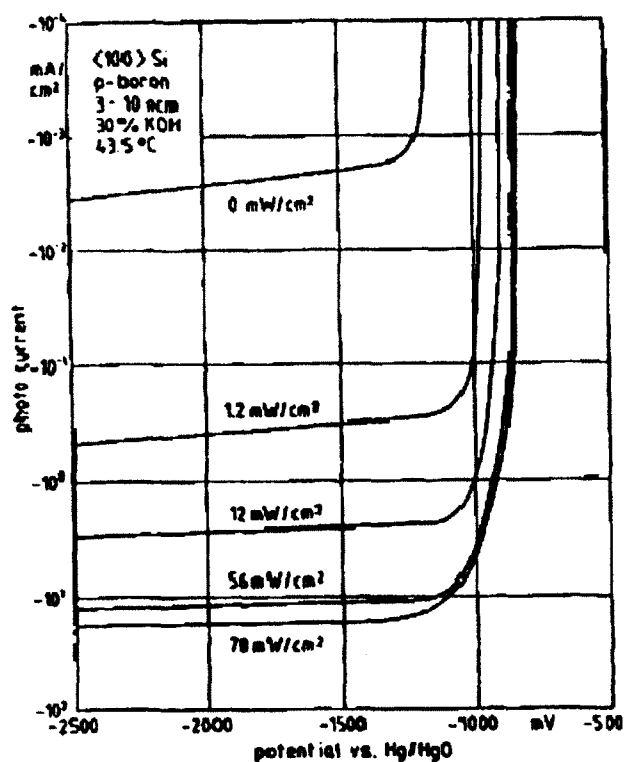


Figure 3.2 I-V Graph Of Electrochemical Etching of Silicon While Being Irradiated With White Light [52]

The maximum power density used in these experiments was 78 mW/cm² [52]. Through Figure 3.2 it can be seen that once the voltage applied is past -1V the photocurrent remains relatively constant no matter how much the bias voltage is

increased [52]. However, it is clearly shown in Figure 3.2 that shining light onto a silicon wafer during electrochemical etching has an effect on the amount of current passing through the silicon wafer.

Other research has been done using a single wavelength of light instead of the broadband lamps used in the research discussed in the previous paragraph [53]. Using a single wavelength of light allowed for the silicon wafers to be etched with an aspect ratio greater than 125:1 [53]. However, they found that the light intensity does not have an effect on the overall etch rate of silicon in 5% HF [53]. This literature review of light photon effects on electrochemical etching silicon has concluded that photons can be used to vary the etch rate of silicon wafers. Section 3.3 will cover how photons interact with insulators and their large energy band gaps.

3.3 Photon Effects on The Energy Band Gap of Insulators

The energy band gap determines the materials ability to allow current to pass through the material. If the energy is equal to or greater than the band gap energy the electrons in the valence band (VB) will have enough energy to move across to the conduction band (CB), allowing electrical current to flow through the material. Figure 3.3 shows the band gap difference between metals, semiconductors and insulators.

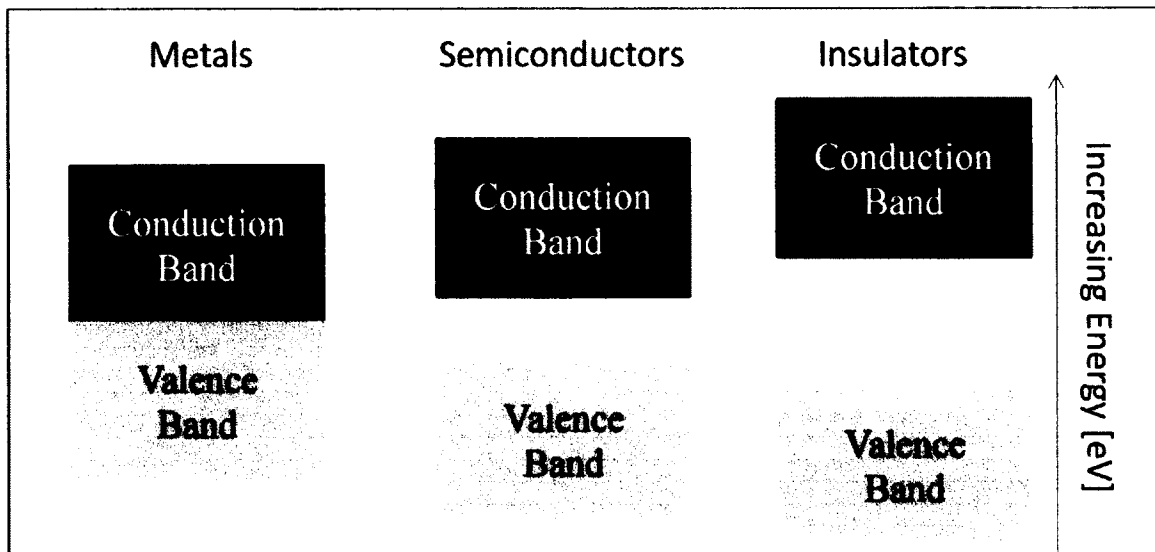


Figure 3.3 Band Gap Comparisons

The band gap for metals actually overlaps, that is why they make excellent electrical conductors. Semiconductors are useful for the fact that they can be doped with different impurities to either have conductive or insulating electrical properties. Even though insulators have large band gaps, it is still possible to make them conductive through either doping them with impurities or applying external energy sources. For this dissertation work doping is out of the question, due to the fact that impurities in quartz crystal resonators will cause aging. This aging will make the resonant frequency drift over time. Therefore this body of work will focus on applying external energy sources. The relationship between the photons wavelength and energy level is given by the following equation:

$$E = \frac{1240}{\lambda(\text{nm})} \text{eV} \quad (3.1)$$

Equation 3.1 gives the energy in electron volts (eV), when the wavelength is given in nanometers. Crystalline quartz has a band gap of 9eV. Using Equation 3.1 to calculate

the wavelength for quartz's 9eV band gap corresponds to a wavelength of 137nm. This wavelength falls into the area called Vacuum Ultra Violet (VUV) light. VUV light is easily absorbed in the atmosphere and requires a vacuum system if it would be used in processing quartz crystals. Due to this constraint the next step was to investigate x-ray radiation. X-ray radiation is perfect for assisting the electrochemical etching of quartz crystals, as it has enough energy to move electrons from the VB to CB in quartz. Also x-ray radiation does not require a vacuum system. However, the main limiting factor of using x-rays is the requirement to build a housing that shields the x-rays from leaking into the environment. The shielding required for the x-ray source used in this research is far cheaper than using a vacuum system for VUV radiation. The next section of this dissertation will review other researchers attempts to find ways to vary the etch rate of amorphous silicon dioxide.

3.4 Review of Electrochemical and UV Radiation Etching of Amorphous Silicon Dioxide

This section will discuss a literature review of works that involved the electrochemical etching of amorphous silicon dioxide and the effects ultraviolet radiation has when it is irradiating silicon dioxide [54, 55]. The first review will be of electrochemical etching of amorphous silicon dioxide with a DC bias voltage and 40% hydrofluoric acid (HF) [54]. The silicon dioxide used here is amorphous, compared to crystalline quartz (which is used in this dissertation's research). Amorphous silicon dioxide has a much faster etch rate in hydrofluoric acid than crystalline quartz. They used voltages in the range of +/-2.7 kV and the sample had a thickness of 170 μ m [54]. The electric field strength (E) was in the range of +/- 20MV/m and the experiments were

carried at room temperature [54]. For 2.7kV applied to 9mm² electrodes, the current passing through the amorphous silicon dioxide sample was less than 1nA (smallest amount of current they could accurately measure) [54]. The etch rate was found to have a linear dependence on the bias voltage applied to the amorphous silicon dioxide samples [54]. Figure 3.4 shows the results they found on the effect of a DC bias voltage being applied to amorphous silicon dioxide during wet etching [54].

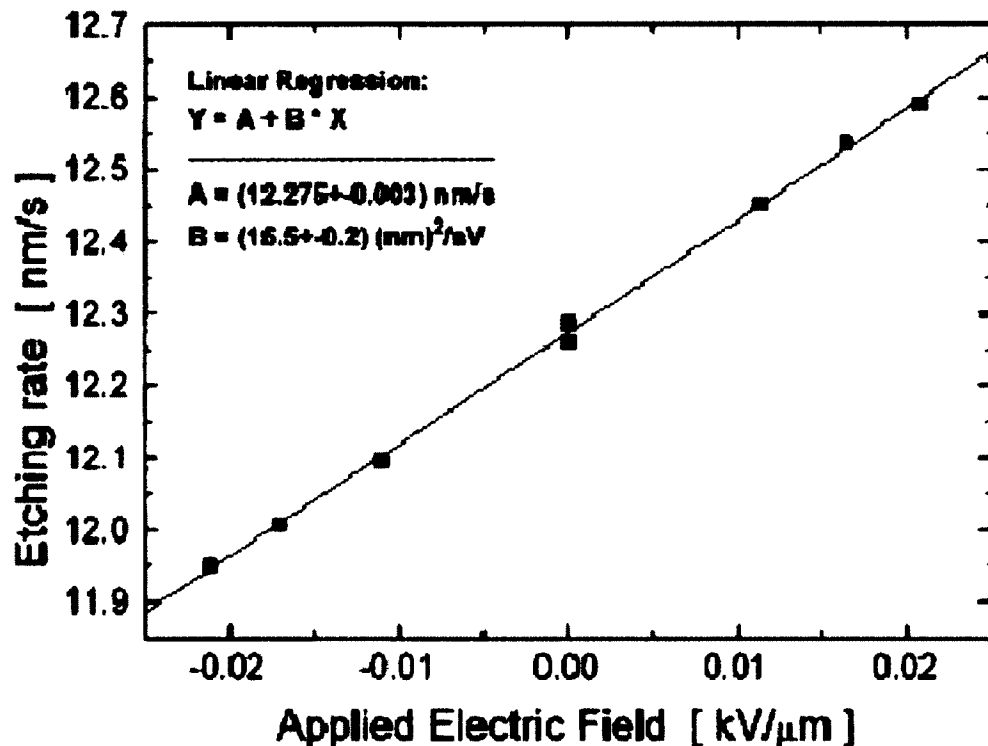


Figure 3.4 Etch Rate of Silica Glass versus Electric Field [54]

The etch rate of amorphous silicon dioxide at room temperature with no external field was 12.25nm/s [54]. Lesche *et al* found that it is possible to vary the etch rate of amorphous silicon dioxide by +/-2.5% with just varying the electric field. They were not able to accurately measure the current, only that the current had to be below 1nA (which

was the lowest current they could measure) [54]. Their research shows it is possible to vary the etch rate of amorphous silicon dioxide by applying an electric field.

The next part of this review is based on exciting electrons in silicon dioxide by irradiating it with photons [55]. The silicon dioxide-MOS structures were irradiated with VUV radiation [55]. The silicon is p-type with 200 nm of thermal oxide grown on top with 10nm thick gold electrodes [55]. The reason for using the VUV radiation was to control the depth at which the radiation would be absorbed. Ionizing radiation with a higher energy level (higher than VUV radiation) would mostly pass through the silicon dioxide. The VUV dosage used was 6.7×10^{14} photons/cm², while a gate bias voltage of 20V was applied [55]. It was found that for electrons with energies of 8.4eV the voltage through the silicon dioxide/silicon interface did not change [55]. However, when the radiation was at 10.2eV the voltage increased to over 30V [55]. In order to excite electronic or ionic current through silicon dioxide the external radiation source's energy must be above 9eV. Figure 3.5 shows the change in voltage versus the change in radiation dose at 10.2eV for different gate bias voltages [55].

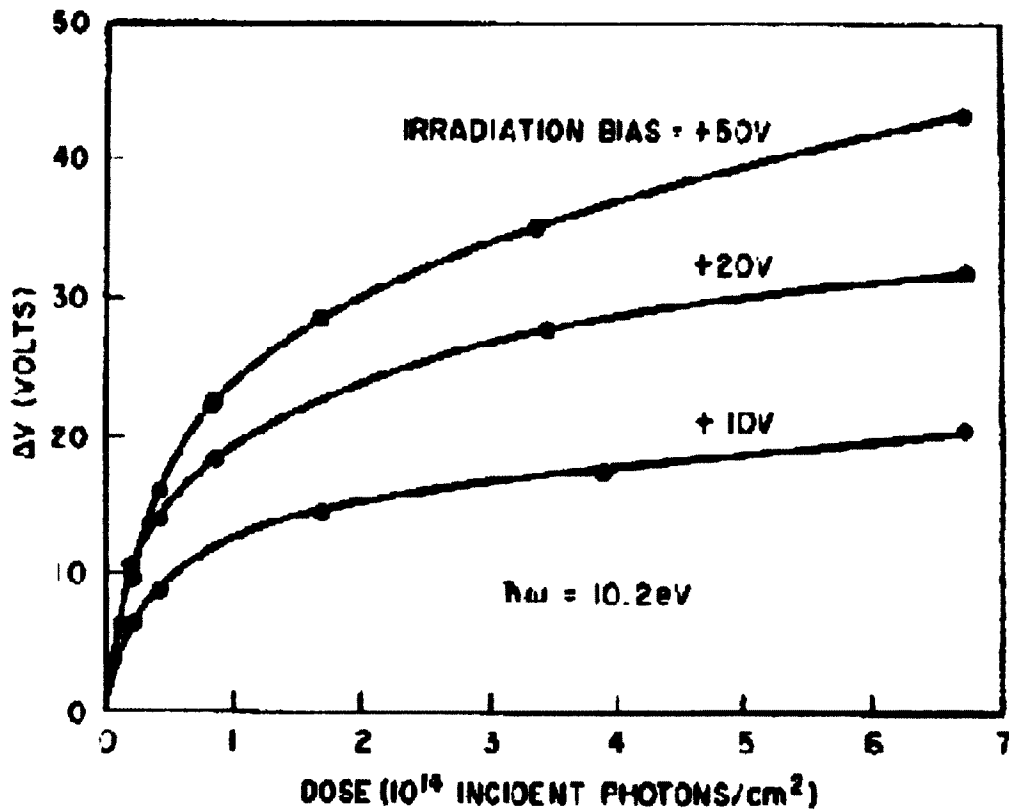


Figure 3.5 Change in Voltage Versus Radiation Dose [55]

From Figure 3.5 the data shows the change in voltage continued to increase as the radiation dose increases. However, there is no experimental data to show if this effect becomes saturated. The literature review has shown experiments that were designed to change the current and voltage in silicon dioxide either through electrochemical etching or by injecting it with photons greater than silicon dioxide's band gap. The next section will review researchers previous attempts to vary the etch rate of crystalline silicon dioxide (quartz).

3.5 Review of Assisted Wet Etching of Quartz Crystals

The previous section covered the ability to enhance the wet etching effect on amorphous silicon dioxide and increase the change in voltage across a silicon dioxide/silicon interface by irradiating it with VUV radiation. This section will review literature on other researcher's attempts to vary the etch rate of quartz crystals through various means.

The processing time is faster for amorphous silicon dioxide than quartz crystals. For silicon dioxide being wet etched by HF acid, the main mechanism is the double bond between silicon and oxygen [56-59]. Ernsberger found that the more double bonds the silicon atom had, the more F or HF species that will be attracted to it [56,57]. Silicon is able to maintain a bond with at least six fluoride atoms. Since fluoride is the most electronegative element, this will remove the silicon atom from the glass or crystal surface [56]. Amorphous silicon dioxide will have double bonds of Si-O randomly on its surface [56]. The more double bonds available the faster the etch rate of silicon dioxide. AT-cut quartz has one of the slowest etch rates due to the angle at which the crystal is cut, the angle of cut limits the number of Si-O double bonds on its surface.

Shin Piaw Choong was the first to experiment with assisting the wet etching process of quartz crystals with various forms of energy back in 1944 [58,59]. He found that a strong AC electric field could produce channels and etch pits in the quartz crystal during wet etching with hydrofluoric acid [58]. Channels and etch pits are defects that occur when wet etching quartz crystals, they are usually formed when the wet etchant temperature is increased above 35°C. He also applied a DC electric field to the crystals during etching and found no effect on the etching process [58]. Another method he

implemented was applying UV radiation to the quartz crystals during wet etching [59]. The UV radiation wavelength used was in the range of 190nm to 280nm wavelengths (6.5eV to 4.4eV). It was found that etch rate would be increased by applying the UV radiation [59]. Another method of assisting the wet etching process of quartz crystals is by applying an AC and DC magnetic field [58]. The DC magnetic field applied was 30,000 Gauss and the AC field was around 8000 Gauss, both of which resulted in no effects on the etch rate [58]. Shin Piaw Choong also experimented on irradiating the quartz crystals with x-rays [58]. The x-ray source was rated at 50kV and 3.5mA [58]. He would apply only x-ray radiation to the quartz crystals during etching for 3 to 5 hours and found that alone x-rays did not have an effect on the etch profile or the etch rate [58]. His results are for applying DC bias voltage and x-rays during etching separately. He never reported that he used these methods in conjunction. In Section 3.6 it will be shown the role that x-rays play in increasing the current through quartz crystals and its ability to increase the etch rate.

3.6 Experimental Setup

The x-ray assisted electrochemical etching setup is comprised of the following: bias voltage (power supply and picoammeter), control switch, network analyzer, Pt reference electrode in conjunction with HF acid, quartz crystal (200nm Au and 5nm Cr) and a x-ray tube (50kV and 2mA). Another important aspect of the experimental setup is the etchant temperature. The etchant temperature was heated to 40°C using a DC ohmic heater attached to the backside of the etchant holder made from polytetrafluoroethylene (PTFE). The temperature is being controlled by a commercial PID controller with an accuracy of +/- 0.1 °C. The temperature must be maintained at this level of accuracy due

to the sensitivity of the etch rate of quartz using HF based solutions, which was previously discussed in Section 1.3.4. Figure 3.6 shows the schematic for the electrochemical etching of quartz crystals assisted by x-ray radiation.

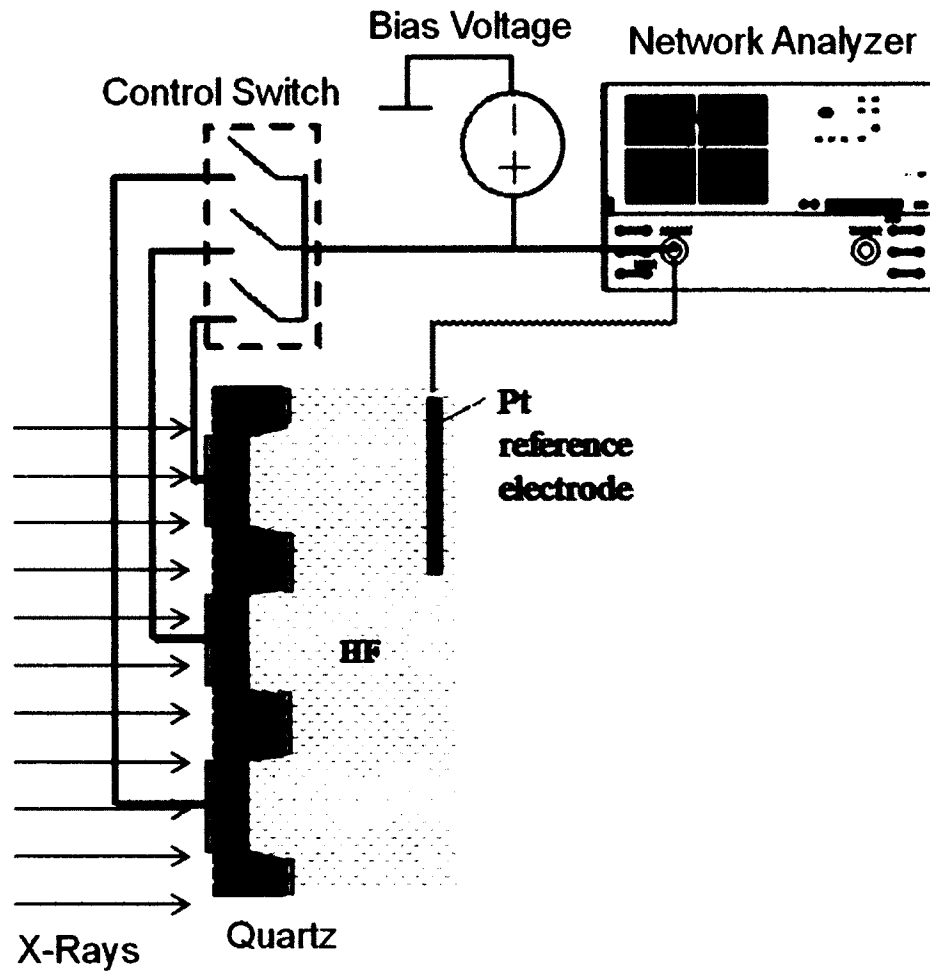


Figure 3.6 Schematic of X-Ray Assisted Electrochemical Etching Setup

The power supply was purchased from Stanford Research Systems, it has a +/- 5kV range with a max wattage of 25W, this allows for a maximum of 5mA at 5kV [60]. The ammeter is a Keithly 486 picoammeter, it has a sensitivity of 10fA. Both the power supply and the ammeter have a GBIP interface to allow for computer control and

recording the data. The control switch is used to vary which resonator's resonant frequency is being measured and it allows for the DC bias voltage to selectively be applied to individual resonators. This allows for the etch rate to be varied to different resonators on the same die/wafer. This effect allows for the compensation of initial wafer thickness variations. The platinum reference electrode is used to complete the circuit for the electrochemical etching setup. Platinum is used as the reference electrode due to its chemical resistance to HF based acids. A network analyzer was used to measure and record the resonant frequency of the quartz crystals during etching. Therefore in order to selectively etch individual resonators on the same wafer the bias voltage is turned on or off in order to vary the etch rate. The x-ray radiation allows for the ions in the quartz crystal to become free and flow through the crystal. The DC bias voltage helps to push these energetic ions through the crystal by creating a current in the crystal. More detail into the radiation and bias voltage effects on the ions in the quartz crystals will be discussed in Section 3.7. The x-ray etching chamber used is shown in Figure 3.7.

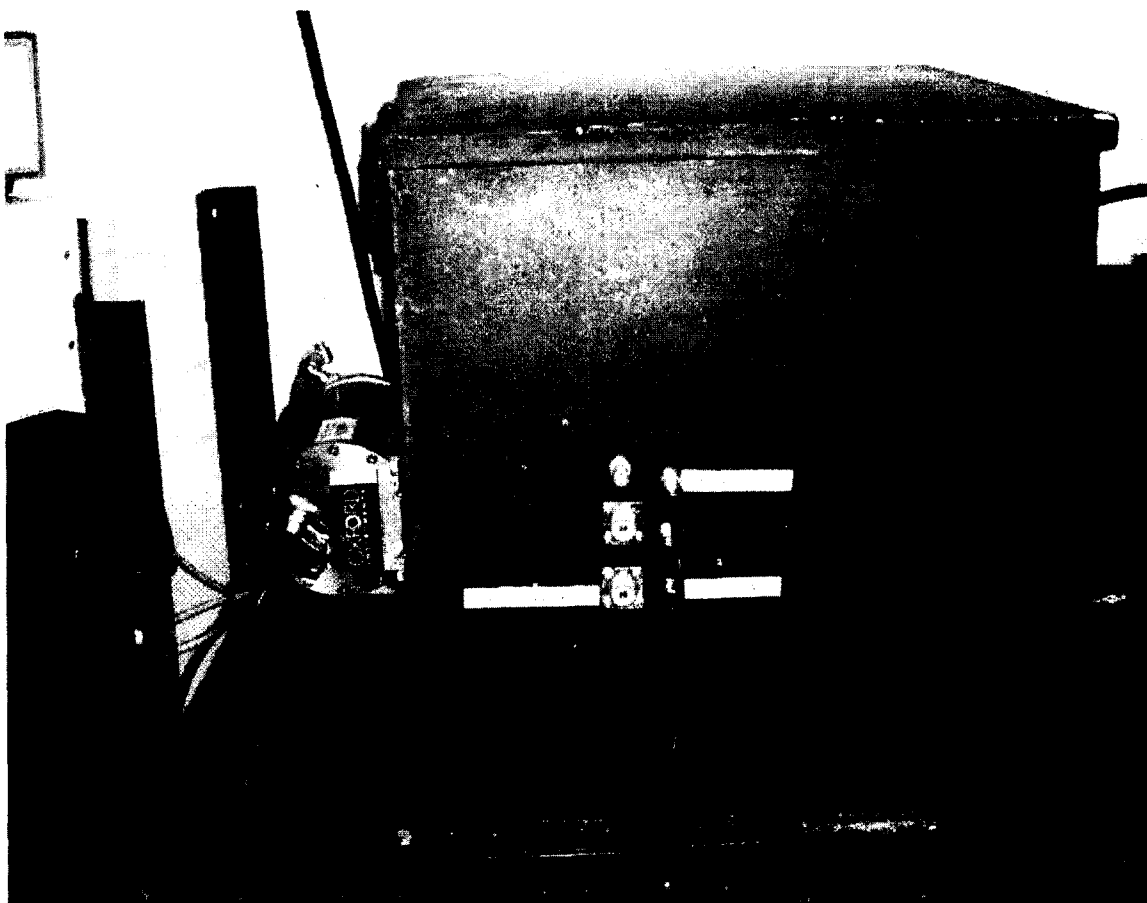


Figure 3.7 Experimental Setup of Electrochemical Etching of Quartz Assisted By X-Rays

The x-ray chamber was created out of steel and has a 6mm thick layer of lead inside of the chamber. The thickness of lead needed for lining the x-ray chamber was calculated by the following equation:

$$\text{Intensity} = \exp(-\mu * t) \quad (3.2)$$

where μ is the linear attenuation coefficient of the material used for blocking, and t is the thickness of the material. For a 6mm thick layer of lead, the intensity of the x-rays passing through the lead layer is essentially zero. The following was calculated for x-rays having energies at 50keV. The 50kV x-ray tube will produce relatively zero x-ray

photons with energies of 50keV, which will be explained in the next section along with a detail overview of the x-ray tube used in this research.

3.6.1 X-Ray Tube and Operational Principles

The x-ray tube used was a 100W, single-pole, continuous duty industrial source from Oxford Instruments with a water cooling system [61]. Figure 3.8 shows a diagram of the packaged x-ray tube.

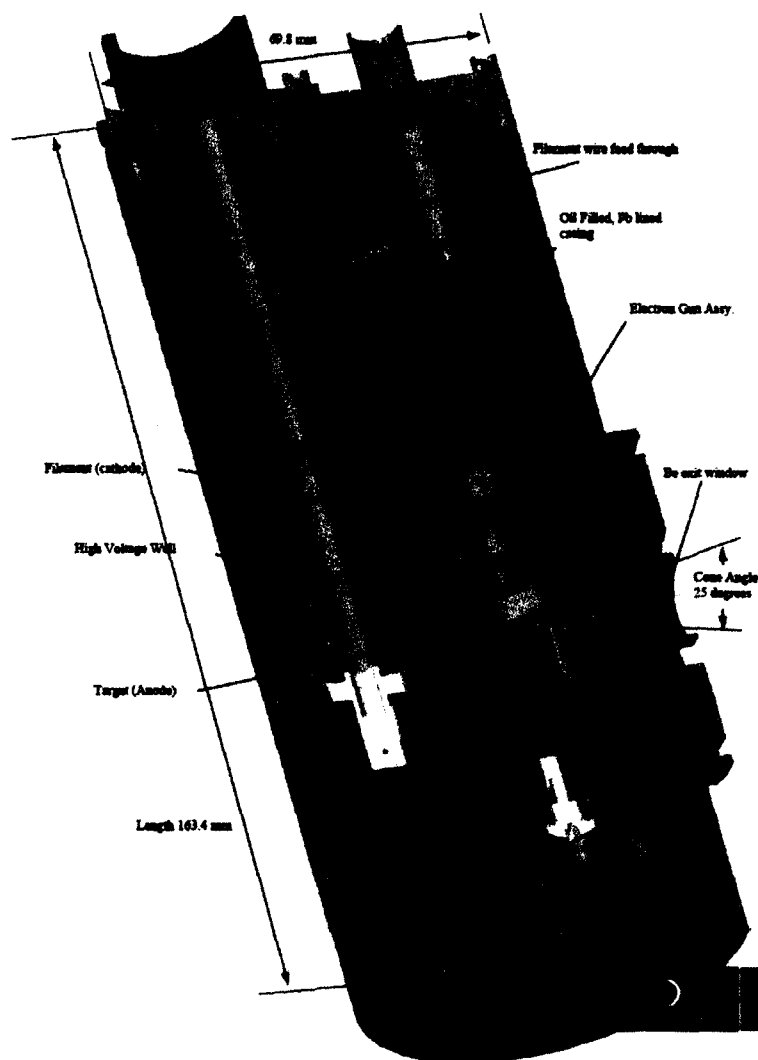


Figure 3.8 X-Ray Tube From Oxford Instruments [61]

The three main components to be discussed of the x-ray tube are as follows: Filament (Cathode), Target (Anode), and a Beryllium exit window. The filament (cathode) produces the electrons that bombard the target material (anode). This interaction of electrons with the target material produces x-rays. The Be exit window allows the x-ray tube to be sealed in vacuum while allowing the x-rays to leave the tube. Beryllium windows are used because they do not absorb much of the x-rays leaving the target material (anode). The x-ray system's operation will be discussed in the next section.

The basic operation principles of x-ray tubes will be discussed briefly. The cathode of the x-ray tube consists of a filament and a focusing cup. The filament has a current passing through it which causes the filament to heat up rapidly. This heating of the filament will create a flow of electrons due to thermionic emission. Thermionic emission is when the heat created by the current flowing through the filament exceeds the work function of the filament. The max filament current for the x-ray tube used in these experiments is 4Amps. In order keep the electrons from having random motion; a focusing cup is placed at end of the filament. The focusing cup is designed to focus the electrons to the anode by having a negative charge placed on it. This makes the electrons squeeze together to create a focused beam to strike the anode target. The anode target of the x-ray system will convert the electrical energy bombarding the target into x-rays. The effects the anode material have on x-ray production will be discussed in the next section.

The majority of energy produced by x-ray systems is in the form of heat. X-rays only represent about one percent of the energy in the total system. The anode material is responsible for converting the electrical energy into x-ray photons and the optimum

results would be to keep the heat production to a minimum. This is done by selecting the right anode material for the specific wavelengths of x-rays needed to be produced. The atomic number of the anode material determines its efficiency of converting electron energy into x-rays. The more efficient the anode material is at converting electron energy into x-rays, the lower amount of heat produced in the system. The higher the atomic number the better the material is at converting electron energy into x-rays. For this research the x-ray system has Tungsten (W) as the anode material, which has the atomic number of 74. Tungsten does not lose its strength at very high temperatures that are associated with producing x-rays. Also, tungsten has the highest melting point and lowest evaporation rate of any metal making it a great material for use as an anode in an x-ray tube. Another key parameter of choosing an anode material is the characteristic x-rays it produces.

X-ray tubes produce two types of x-ray radiation: characteristic and continuum. Continuum x-ray radiation spectrum will be discussed first due to its importance in this dissertation's research. The spectrum of continuum radiation (bremsstrahlung) produce from x-ray tubes is independent of the target material (anode). The target material (anode) only changes the intensity of the continuum x-rays leaving the x-ray tube. The x-ray tube's continuum radiation spectrum can be varied by the potential applied to the tube. The following is Kramer's Law, which describes the wavelength output of the x-ray tube and the intensity of each wavelength:

$$I(\lambda)d\lambda = K \left(\frac{\lambda}{\lambda_{\min}} - 1 \right) \frac{1}{\lambda^2} d\lambda \quad (3.3)$$

where K is a constant relating to the x-ray tube current and the target material's (anode) atomic number, λ is the wavelength output of the x-ray tube, λ_{\min} is the shortest

wavelength that can be produced by the x-ray tube. The λ_{\min} can be calculated by the Duane-Hunt Law which is as follows:

$$\lambda_{\min} = \frac{1239.8}{V} [\text{nm}] \quad (3.4)$$

where V is the voltage being applied to the x-ray tube, and 1239.8 is a constant to produce the wavelength in nanometers. The x-ray intensity is non-linear as described by Kramer's Law. In order to keep in the limits of the conservation of energy, the x-ray tube will not produce any x-rays beyond the potential applied to the x-ray tube. Also, the x-ray tube will only produce very small amount of x-rays at its maximum voltage rating. For example a 50kV source will only produce a single x-ray photon at an energy of 50keV. The 50kV max potential is the cutoff wavelength as shown by the Duane-Hunt Law. Figure 3.9 shows the wavelengths produced from x-ray tube versus the relative intensity for the 50kV source used in this dissertation research.

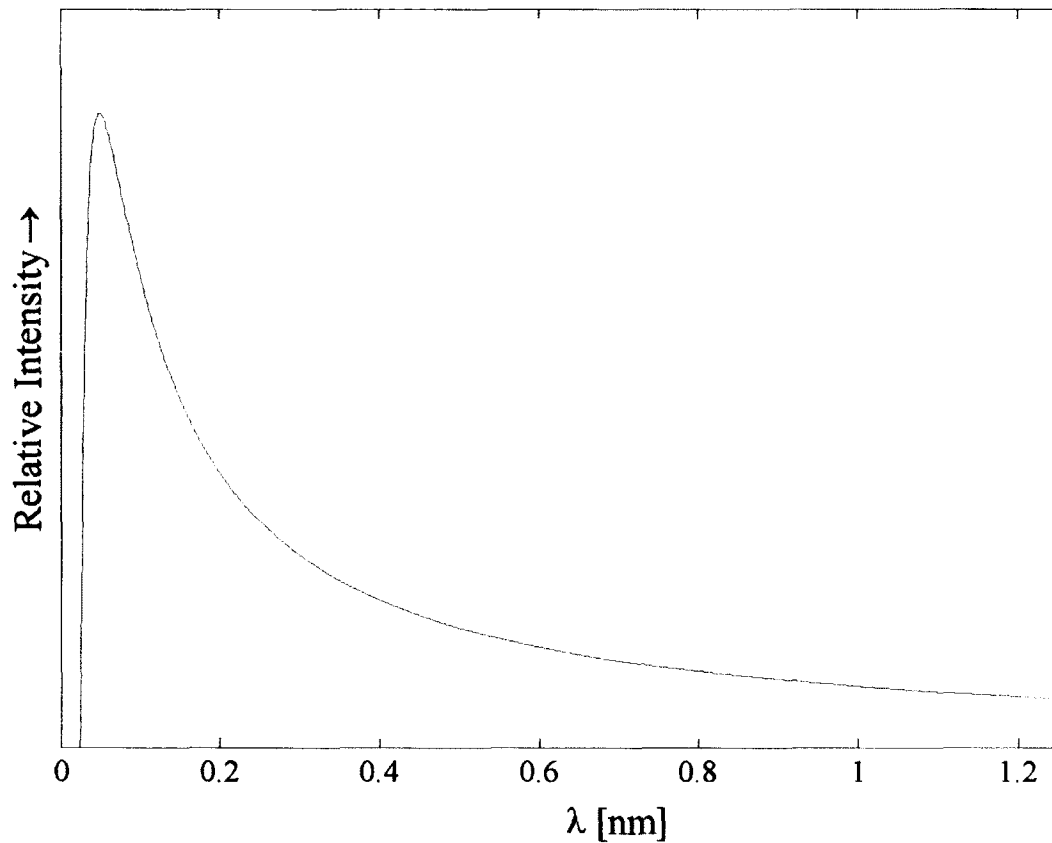


Figure 3.9 The Relative Intensity of Each Wavelength Output For 50 keV X-Ray Source

The characteristic x-rays produced from the x-ray tube is dependent on the anode target material. Characteristic x-rays occur when electrons bombard the K and L shells in the target material. The characteristic x-rays appear as very sharp energy peaks and have the highest intensities leaving the x-ray tube. The following equation shows the calculation of the energy transition from L-Shell to the K-Shell:

$$E_{k\alpha} = \frac{3}{4} * 13.6(Z - 1)^2 \quad (3.5)$$

where Z is the atomic number of the target material, the 13.6eV constant is the ionization energy of a hydrogen atom and the $(3/4)$ represents the transition from the L-Shell to the K-Shell. For tungsten it has a K alpha wavelength around 54keV, since the wavelength

cutoff for the x-ray tube used in this work is 50keV, the characteristic x-rays can be ignored.

The next important parameter to discuss is how the x-ray tube current and voltage can vary the flux intensity of the x-ray tube. The x-ray tube current is different than the filament current (which creates thermionic emission), it controls the radiation flux leaving the x-ray tube. The x-ray tube current varies the radiation flux (x-ray intensity) from the tube output for all wavelengths. Figure 3.10 shows the variation in the x-ray intensity for different levels of tube current.

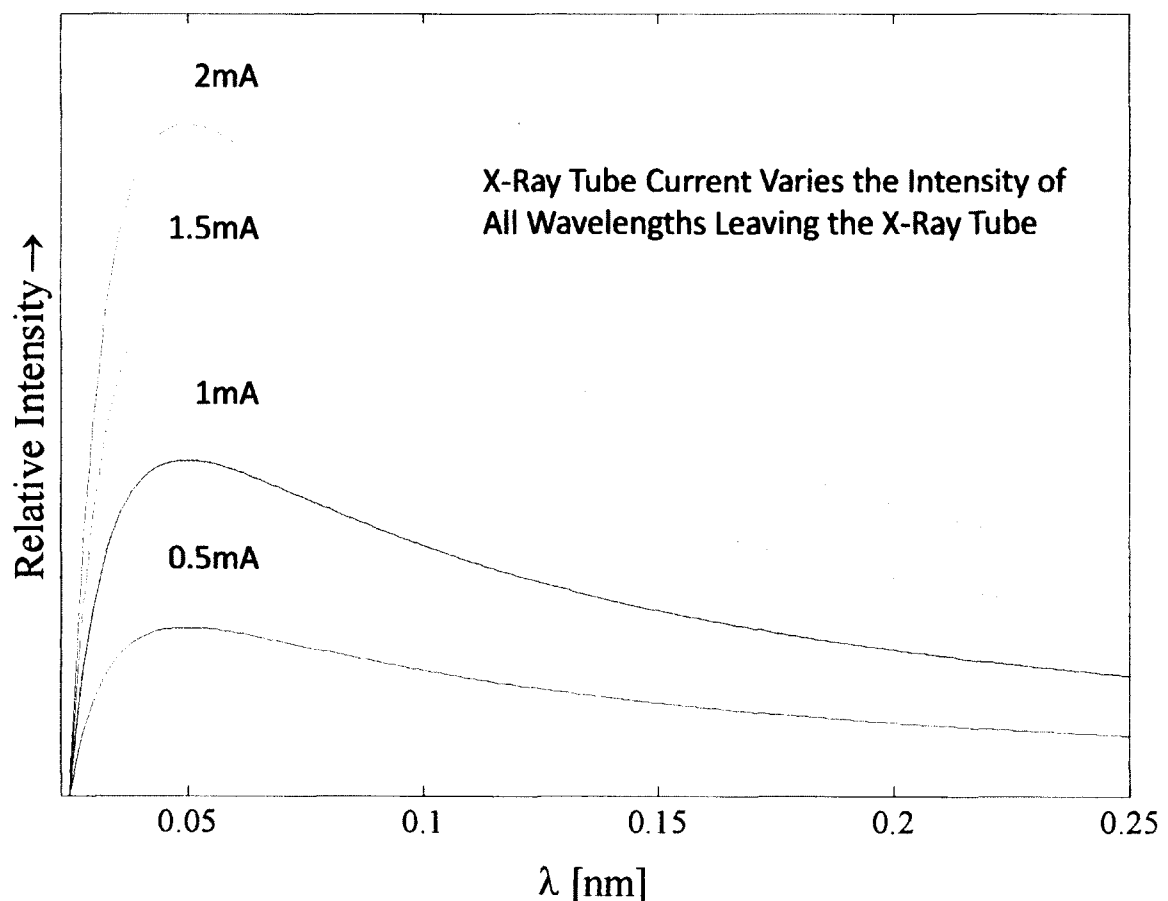


Figure 3.10 Variation of X-Ray Intensity for Varying Levels of X-Ray Tube Current

Figure 3.10 clearly shows that as the x-ray tube current increases so does the intensity for all wavelengths and has no other effects on the output of the x-ray tube. The x-ray tube voltage being applied allows for the x-ray intensity of all wavelengths to increase. Also, x-ray tube voltage increases the energy of the x-rays that are produced by the x-ray tube. Figure 3.11 shows the effect of increasing the x-ray tube voltage.

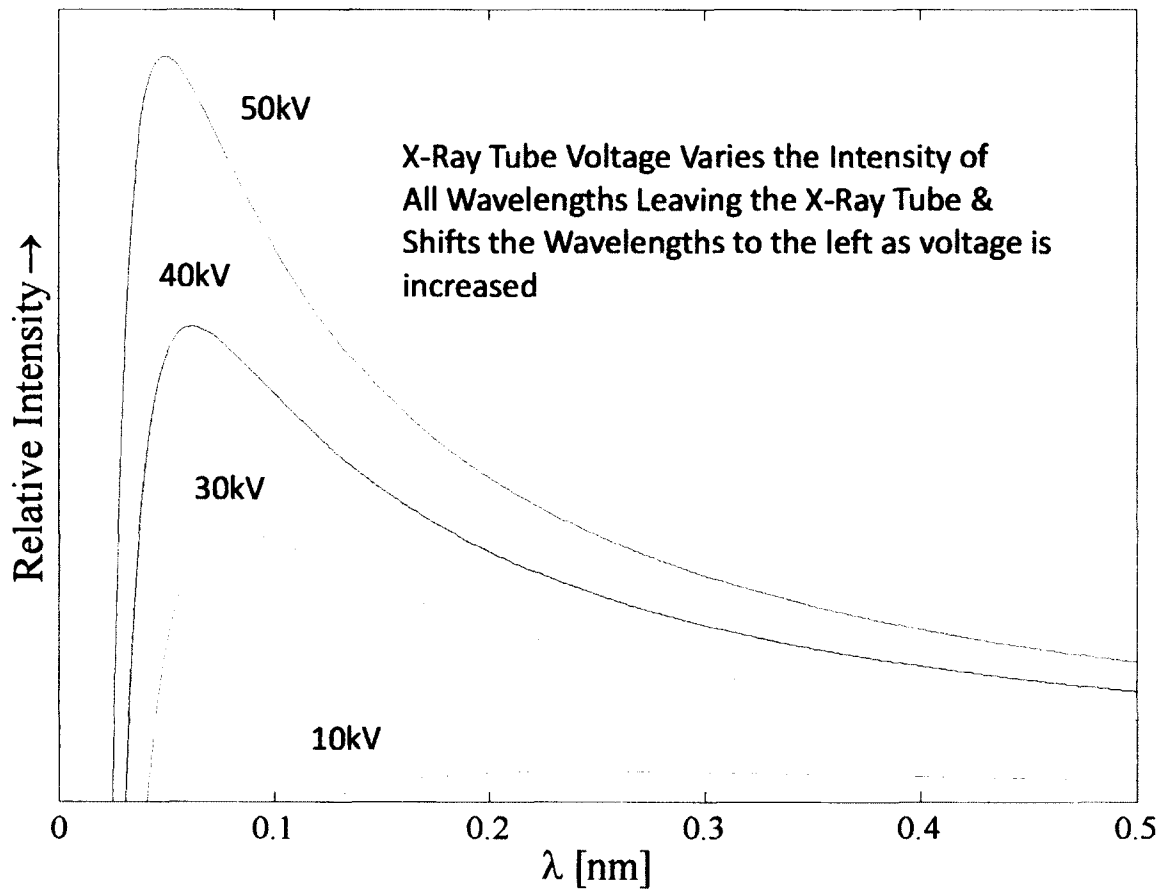


Figure 3.11 Effects of Varying Potential Applied to X-Ray Tube

3.7 Radiation Effects on Quartz

Radiation induced conductivity and other radiological effects on quartz have been studied extensively over the years. Most of the studies were conducted to determine the performance of quartz crystal resonators while being used for space applications [63-69]. Other studies have been conducted on the change in electrical conductivity of quartz crystals when irradiated by continuous and pulsed radiation [70-80]. Both x-rays and γ -rays have been used to test their effects on the electrical conductivity of quartz crystals. However, the experiments conducted for the research presented in this dissertation used only x-ray radiation. Through the calculations using Equation 3.1, only a wavelength of 137 nm is needed, therefore any x-ray wavelength will be sufficient for energizing electrons (or ion species) to move across the band gap of quartz. For pair production to take place in quartz crystals it requires energy per pair of at least 28eV/pair [73]. This value was found by using the following equation:

$$W(\text{eV/pair}) \cong 1\text{eV} + 3X \quad (3.7)$$

where X represents the band gap of the material in units of electron volts and W is the electron volts required to create an electron hole pair in the material [73]. For this work the energies of the x-ray system were 10keV to 50keV, which corresponds to wavelengths of 0.124nm to 0.0248nm.

3.7.1 Defects Present in Quartz Crystals

Quartz filters and resonators in their early history were created out of natural crystals. Natural crystals have a very large amount of defects in the crystalline structure (caused by impurities) due to their random growth process. Synthetic quartz crystals are

hydrothermally grown inside a controlled environment to help limit the amount of impurities deposited in the quartz crystals [81]. However, even synthetic crystals have impurities present in its lattice due to the chemicals (such as NaOH) used during the crystal growing process [81]. The most common types of impurities present in synthetic quartz crystals are as follows: Aluminum, Carbon, Iron, Lithium, Potassium, Sodium, and Titanium. These impurities stem from the chemicals used as additives, mineralizers, and the metals used as baffles and containers [81]. These impurities can cause various types of defects in the quartz crystal lattice as shown in Figure 3.12.

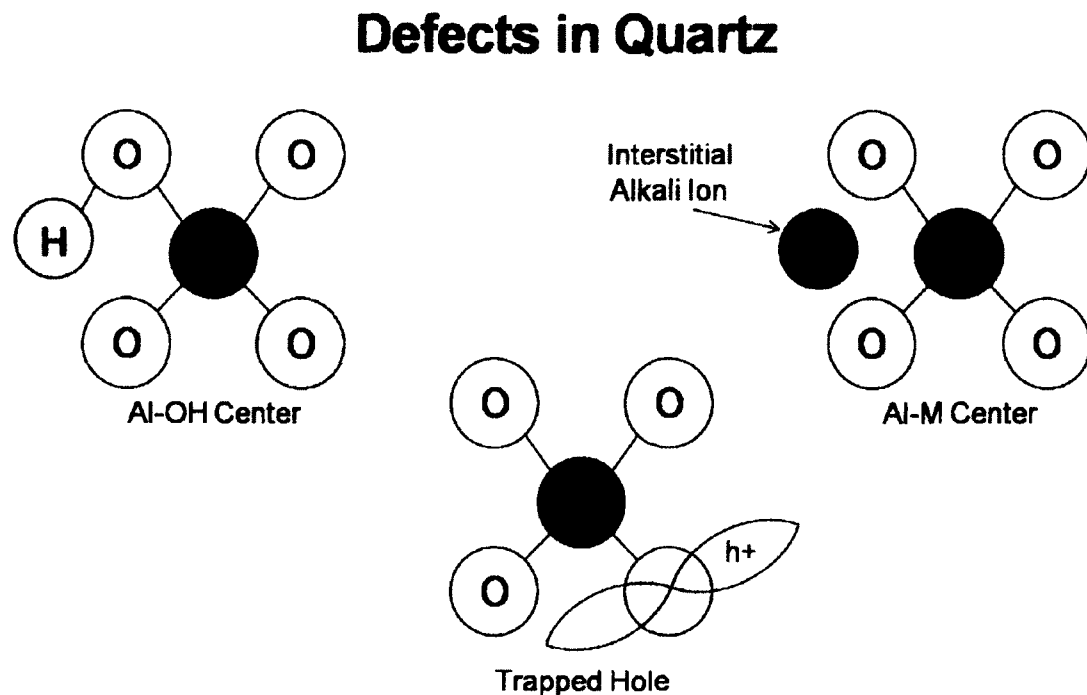


Figure 3.12 Types of Defects Present In Crystalline Quartz [82].

The most common defect present in quartz crystals is due to substitutional impurities. Aluminum is the most occurring substitutional impurity found in synthetic quartz crystals (others are iron, titanium, and in natural crystals germanium). All three of

the defects shown in Figure 3.12 are caused by substitutional impurities, which are represented by aluminum (Al). The three main defects are oxygen associated defects (Al-OH Center), the trapping of electronic holes (AlO_4), and interstitial impurities (Al-M Center) [82]. Each of these defects will be discussed in more detail in the following paragraphs.

The crystalline structure of quartz consists of a silicon atom surrounded by four oxygen atoms. An Al^{3+} will replace the Si^{4+} through substitution and cause very little distortions due to the trivalent aluminum ions being of similar size to silicon atoms. Since the Al^{3+} causes little distortion and is in low concentrations in synthetic quartz therefore it does not affect the piezoelectric properties. The problem with the Al^{3+} and the parameter that the x-ray assisted electrochemical etching of quartz process takes advantage of is that the trivalent aluminum needs to be charge compensated. Typically alkali impurity ions compensate for the trivalent aluminum, this is due to the alkali ions having the second largest concentration (behind aluminum) in synthetic quartz.

Also, there are other impurity ions that can be present in the quartz crystal process that will substitute for silicon in quartz. In the past Fe ions would contribute to the overall impurities and act as a substitute of silicon, however with the improvements of the growth process of quartz Fe ions have been eliminated [83]. Another substitutional ion that can be present in synthetic quartz is the Ti^{4+} ion [83]. The Ti^{4+} ion does not need any charge compensation, as it completely replaces Si^{4+} and since Ti^{4+} ion does not need charge compensation it is not important for this work. The next section will discuss the interstitial impurity defects (alkali ions) present in quartz crystals.

The most common types of alkali ions present in the synthetic quartz crystals are Lithium, Potassium, and Sodium. These alkali ions represent the interstitial defects that occur in quartz crystals. They are typically represented by M^+ . These alkali defects become embedded in the quartz crystals during the growing process. NaOH and Na_2CO_3 are often the main chemicals used as mineralizers in the hydrothermal growth of quartz crystals. Mineralizers are needed for hydrothermal growth of quartz in order to increase the solubility of the seed crystals [81]. During the growth process of quartz, an alkali solution (type of solution based on growth needs) is used to help promote the growth of the quartz crystals. Therefore alkali ions are always going to be present in synthetic quartz crystals but at a much lower concentration than naturally occurring quartz. Lithium is present as a defect in quartz crystals due to its use during the hydrothermal growth process [81]. In most quartz crystals the Li^+ ion is the most common alkali ion [39]. Lithium is added during the hydrothermal growth process in order to increase the growth rate of the quartz crystals [81]. These interstitial alkali ions (other alkali elements can be used as mineralizers) are needed to compensate the net charge in the quartz lattice when the trivalent aluminum replaces the quadrivalent silicon [39]. This creates centers formed by aluminum and the interstitial alkali ions and is represented by $Al-M^+$. In all the studies involving electrodiffusion or in cases where the crystals were irradiated with high energy radiation, the alkali ions are the dominate factor in producing current through quartz crystals. Other defects present in synthetic quartz crystals involve oxygen atoms.

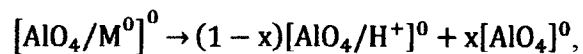
Another type of defect is oxygen related and can take two forms inside a quartz crystal. The first defect is when hydrogen bonds with oxygen in order to compensate for the aluminum defect, this creates an OH^- pair. Hydrogen enters the quartz crystals during

the growth process and also through the electrodiffusion process (with atmospheric conditions) [39]. Due to the strength of the bond of the OH⁻ molecule it is only important for creating current at extremely high temperatures (>100°C) [39]. The experiments conducted for this chapter had etchant temperatures at 40°C, therefore this type of defect is of little importance. The next oxygen associated impurity defect is the creation of Al-Hole centers.

The final defect to be discussed is the creation of an Al-hole center, which is caused by a hole that becomes trapped in a nonbinding oxygen p-orbital. As shown in Section 3.7, electron-hole pairs are formed while the quartz crystal is being irradiated with energy above 28eV, which was calculated from Equation 3.7. Electrons will break away and travel through the quartz crystal, while the holes become trapped creating a positive space charge allowing for compensation of the substitutional Al³⁺ [39,55]. The interstitial impurity defects occur during the growth phase, Al-hole centers can be created two ways:

1. The quartz crystal is irradiated by photons with an energy of at least 28eV,
2. The quartz crystals are put through the electrodiffusion process in vacuum [39].

The following expression shows the creation of Al-hole centers and Al-OH centers from interstitial impurity defect centers:



x represents the fraction of Al-hole centers present [39]. This reaction occurs when the quartz crystals are saturated by radiation at temperatures above -73.15°C [39]. Another important process that has been used to remove impurity ions from quartz crystals is electrodiffusion. Electrodiffusion will remove the ions from the crystal and replace it with Al-OH centers and will not create Al-hole centers [39]. The next section will discuss

in more detail the electrodiffusion process and the benefits of this dissertation's work on removing impurity ions.

3.7.2 Electrodiffusion of Impurity Ions in Quartz Crystals

Extensive research has been conducted on the electrodiffusion of impurity ions out of quartz crystals [39, 84, 85, 86]. Alkali ions are known to cause a decrease in the mechanical quality factor of quartz crystal resonators [87]. Also, for space applications the impurity ions cause frequency shifts as they are bombarded by solar radiation [88, 89]. Therefore research went into finding out ways to remove the impurity ions that were still present in synthetic crystals.

Electrodiffusion (sweeping) of quartz is when a bias voltage is applied to the crystal while it is being subjected to a heating cycle [39, 84, 85, 86]. The maximum temperature of this process is typically around 500°C this temperature is determined by the fact that quartz has a Curie temperature of 573°C. To avoid the alpha-beta phase transition that occurs in quartz crystals the temperature of the electrodiffusion process must remain below the Curie temperature. The electrodiffusion process requires high temperatures in order for large amounts of current to pass through the quartz crystals. Using only bias voltage this dissertation found that only current in the picoamps range could flow through the quartz crystals. The typical bias voltage used to sweep out impurity ions is typically in the 1000 V/cm² range [39]. Most published works found that biasing quartz crystals at 1000 V/cm² while the temperature was constant around 500°C produced currents ranging from μA to mA [39, 84, 85, 86].

All of the electrodiffusion studies show that the current through quartz decays with time. The current decay is due to the impurity ions being swept out of the crystal.

Charge compensation must occur as the impurity ions are swept out of the crystal. The contents that replace the impurity ions in the quartz crystal during the sweeping process will depend on the environment the sweeping takes place. Typically the sweeping process occurs in atmospheric conditions, however, research has been conducted on the sweeping process being performed in vacuum. The sweeping of quartz in atmospheric conditions will remove the interstitial alkali ions and replace them with hydrogen ions that will form the OH^- molecule [39]. The vacuum swept process will remove the alkali ions as well as eliminate the hydrogen ions from entering the quartz crystals [39]. By removing the alkali ions and hydrogen ions the vacuum sweeping process allows for holes to become trapped along the nonbinding oxygen p-orbital shown in Figure 3.12 [81]. The next section will show that there is another means to create current through quartz without the need of temperatures around the Curie temperature of quartz.

3.7.3 Radiation Induced Current Through Quartz

This section will discuss the ability to create current through quartz crystals without the need of high temperatures near the Curie temperature. This is done by applying an external radiation source that will bombard the front-side of the crystals. Shin Piaw Choong found that x-rays irradiating the front-side of the quartz crystals have no effect on the etch rate of quartz crystals during wet etching [58]. The x-ray tube used by Choong was a Hilger Y.25microns that produced x-rays at 50keV with a tube current of 3.5mA and the quartz samples being wet etched were irradiated to the x-ray radiation from 3 to 5 hours [58]. His x-ray tube has very similar output to the one used in this dissertation, which has a voltage potential of 50keV and a tube current of 2mA.

The research conducted for this dissertation has verified that x-rays alone do not have any effect on the etching process. The x-ray radiation excites the impurity ions present in the quartz crystal structure, however, no current is produced because more is needed instead of just exciting the ions. A bias voltage is applied to the crystals to force the impurity ions through the crystal, this is similar to the electrodiffusion process. It has been shown that the F^- and HF^- species (hydrofluoric acid) are affected by the amount of potential being applied [90, 91]. Current created through the quartz crystals will allow for the crystals etch rate to be varied by influencing the HF based etchant. Since quartz is a great insulator it requires large electric fields to get extremely small amounts of DC current to flow through it. Experiments conducted during this dissertation's research found that only current in the picoamp range will flow through the crystal when a bias voltage was only applied. This small amount of current had no effect on the etch rate of the quartz crystals. Therefore it is not one single mechanism affecting the etch rate of quartz crystals but the combined effort of bias voltage and x-ray radiation. The combination of these two mechanisms will now be discussed.

When the alkali ions are irradiated by x-rays they will have enough energy to break the Coulombic attraction to the Al^{3+} centers (28eV). The bias voltage applied to the crystal will then push the ions through, creating current in the nanoamp range. Figure 3.13 shows the mechanism that creates current through quartz.

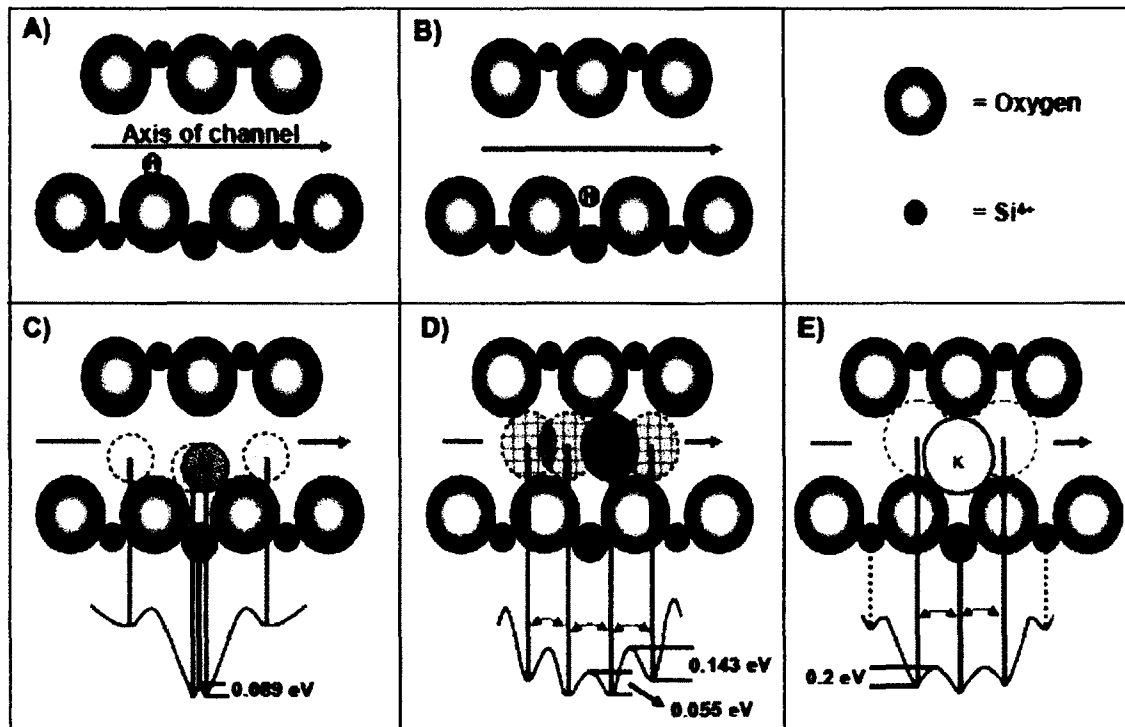


Figure 3.13 Radiation Induced Current In Quartz Crystals [3]

Figure 3.13a shows the Al^{3+} center substituting for the silicon center, with hydrogen being the compensating ion. The axis channel is in the thickness direction of the quartz crystals. Figure 3.13b shows the hydrogen given enough energy to break its bond. However, the OH bond is strong enough to not be broken at normal temperatures. Therefore, higher temperatures are needed in order to have hydrogen move through the axis channel, typically during the electrodiffusion process when temperatures are around 500°C . Figure 3.13c,d,e shows the alkali ions compensating for the Al^{3+} center, once the alkali ions have enough energy (from x-ray radiation) they are moved through the axis channel due to the applied bias voltage. As it is shown in Figure 3.13, the larger the ion the more energy is required to move it through the axis channel in the thickness direction. The channel created in the optical axis (thickness direction) will have a width of 160 pm

for the Si-O bond length [3]. For Al-O bond the length is longer than Si-O with a length of 177 pm. This shows that the small alkali ions have plenty of room to move through the quartz crystal channels in the optical axis direction. It was found by White that it is even possible to move the larger Cesium and Rubidium ions through quartz [92]. White noted that the quartz lattice will shift in most cases but still allows the larger alkali ions to be present [92]. Table 3.1 shows the atomic radii, diffusion coefficient (cm^2/sec), and the activation energy for the common alkali ions present in quartz crystal resonators.

Table 3.1 [93, 94] Properties of Quartz Alkali Ion Impurities

| | Atomic Radii [pm] | Diffusion Coefficient [cm^2/sec]@RT | Activation Energy [eV] |
|-----------|-------------------|--|------------------------|
| Hydrogen | 25 | 8×10^{-23} | 0.829 to 2.176 |
| Lithium | 68 | 4×10^{-15} | 0.781 |
| Sodium | 98 | 5×10^{-17} | 0.911 |
| Potassium | 133 | 2×10^{-20} | 1.21 |
| Rubidium | 148 | 5×10^{-22} | 1.3 |
| Cesium | 167 | 8×10^{-24} | 1.43 |

The diffusion coefficient and activation energy of the interstitials is for diffusion through the optical axis. Through Table 3.1 it can be seen that as the atomic radius increases the mobility through quartz decreases and the activation energy increases. However, the hydrogen interstitial does not follow this path and it has a much slower mobility and higher activation energy even though it has the smallest radius of all atoms [94]. Typically the substitutional aluminum will form ionic bonds with the interstitial alkali ions. The hydrogen interstitials will form bonds to the oxygen present in the quartz crystals. These bonds form hydroxyl molecules which are more difficult to break. Since the hydroxyl molecules are stronger the activation energy is much higher. The diffusion

coefficient of hydrogen is much lower (than alkali ions) due to the fact that the hydrogen will easily bond to the oxygen atoms. Therefore for most experiments the alkali ions will be depleted and will be replaced by hydrogen (obtained from the atmosphere). Now that the mechanisms that create the current flowing through the quartz crystal when irradiated by x-rays while a bias voltage is applied have been discussed, the next section will cover modeling the radiation induced current.

3.7.4 Modeling of Radiation Induced Current Through Quartz

This section will review modeling work done by previous researchers and the results will be compared to the experiments conducted in this dissertation. The works of D.R.Koehler and R.C. Hughes will first be discussed in detail in this section [73, 95]. The work by Hughes was focused on irradiating quartz crystals with pulsed x-rays [73]. Hughes concluded that the current produced through the quartz crystals is not a thermal phenomenon but the ionic impurities being excited by the external radiation [73]. He found the relationship of current density through the quartz crystals by the following equation:

$$i = n_0 e \mu E \left[1 - \left(\frac{\mu E}{d} \right) t \right] e^{-t/\tau} [\text{amps/cm}^2] \quad (3.8)$$

where n_0 is the carrier concentration (in our case it is alkali ions), e is the electric charge (q), μ is the mobility of the ionic carriers (units of $\text{cm}^2/\text{V-sec}$), E is the applied electric field (V/cm), d is the thickness of the quartz crystal, t is the pulse width of the x-ray radiation, and τ is the lifetime of the ionic carriers [73]. Through various types of experiments conducted Hughes found that the mobility of the lithium ion through quartz

was on the order of $7e-4 \text{ cm}^2/\text{V-sec}$ [73]. The mobility of ions present can be modeled by the following Arrhenius expression:

$$\mu_i = 17 * \exp(-0.27\text{eV}/kT) \quad (3.9)$$

where k is Boltzmann's constant, T is the temperature, and 0.27eV is the activation energy for lithium in quartz used by Hughes [73]. The diffusion coefficients found by previous researchers that are detailed in Table 3.1 are orders of magnitude lower than the results produced by Hughes [73]. Hughes is taking into account not only the initial energy to excite the impurity ions in the quartz crystals but also the energy required to move through the crystal as the total activation energy [73]. Koehler found the relationship of current and a constant dose of x-rays [95]. The following equation shows this relationship:

$$I(\text{amps})=a e f_1 f_2 A \phi d \quad (3.10)$$

where a is the concentration of carriers per rad, e is the electric charge (q), f_1 is the number of impurity ions being released per carrier, f_2 is the effect that the electric field has on the movement of the ions through quartz, A is the area of the electrodes (cm^2), ϕ is the radiation rate (rads/sec), d is the thickness of the quartz crystal (cm) [95]. The electric field effect on the movement of ions through quartz f_2 is found by the following equation:

$$f_2 = \frac{\mu\tau E}{d} \left[1 + \frac{\mu\tau E}{d} e^{-d/\mu\tau E} - \frac{\mu\tau E}{d} \right] \quad (3.11)$$

where μ is the carrier mobility ($\text{cm}^2/\text{V-sec}$), τ is the carrier lifetime in quartz (seconds), and E is the electric field being applied to the electrodes (V/cm) [95]. The concentration of carriers per rad was found to be in the range of 1 to $4e12$ carriers/ cm^3/rad , this means that for one rad/sec of radiation 1 to $4E12$ ions/ cm^3 are being freed every second

according to Kohelor [95]. The f_i is the number of ions released per carrier and Kohelor has it equal to one, this however, could change depending on the amount of impurities present in the quartz crystal [95]. To produce current in the nanoamp range requires a large dose of radiation according to Kohelor's equations. For a current of 10 nA, the radiation dose must be at least $1.5E6$ R/sec. Discussed previously the radiation dose was calculated using Equation 3.6 in Section 3.6.1, with a radiation dose of 5.75 mR/hr. Also, with the Rad Pro Calculator developed by R. McGinnis, the radiation dose was calculated to be $2.68E7$ R/hr [96]. Even using the values obtained from the Rad Pro Calculator, there is not enough radiation to reach a current through quartz in the nA range according to Equation 3.10. For this dissertation the radiation dose was not varied, however, for future work this will be explored. Another area that will be looked into is a more detailed simulation of radiation induced current. The next section will display and discuss the first successful results from electrochemical etching quartz crystals assisted by x-rays.

3.7.5 Results and Discussions

The first goal is to etch multiple resonators at one time to a specific resonant frequency in order to eliminate final frequency tuning to each individual resonator. Chapter 2 showed results that prove it is possible to etch multiple resonators in parallel to within a final frequency accuracy of ± 50 ppm by using off the shelf laser diodes. The second goal of this dissertation research is to find new ways to increase the etch rate of quartz crystals. It will be shown in this section that it is possible to increase the etch rate of quartz crystal resonators using the x-ray assisted electrochemical etching process. By using this electrochemical setup it allows for another degree of freedom in the etching of quartz crystal resonators. In industry they only use temperature and etchant

concentration to vary the etch rate of the resonators. The etch rate is strongly related to temperature, so an increase from 40°C to 80°C in the etchant temperature will increase the etch rate for AT-cut quartz crystals by 11 times. Saturated ammonium bifluoride is used as the etchant due to its chemical polishing properties discussed in Chapter 1. With the x-ray assisted electrochemical etching system the experiments were carried out at 40°C. However, it is possible to use this system at higher temperatures due to the fact that the x-rays are inducing current in the quartz crystal through the movement of ions and not through heating the crystal. Experiments were carried out at room temperature that verified that the x-rays irradiating the crystals did not heat the substrate or etchant to affect the etch rate. Another set of experiments were done using just the x-rays alone and the DC bias voltage only. Neither one of the processes alone would cause the etch rate to change at all. This verified the work of Shin Piaw Choong, who did not find an etch rate increase due to x-rays or bias voltage being applied separately to the quartz crystals [58,59]. The current through the quartz crystals with only the bias voltage applied was measured in the picoamps range. Figure 3.14 shows the current measured for a sample without x-rays during the etching process.

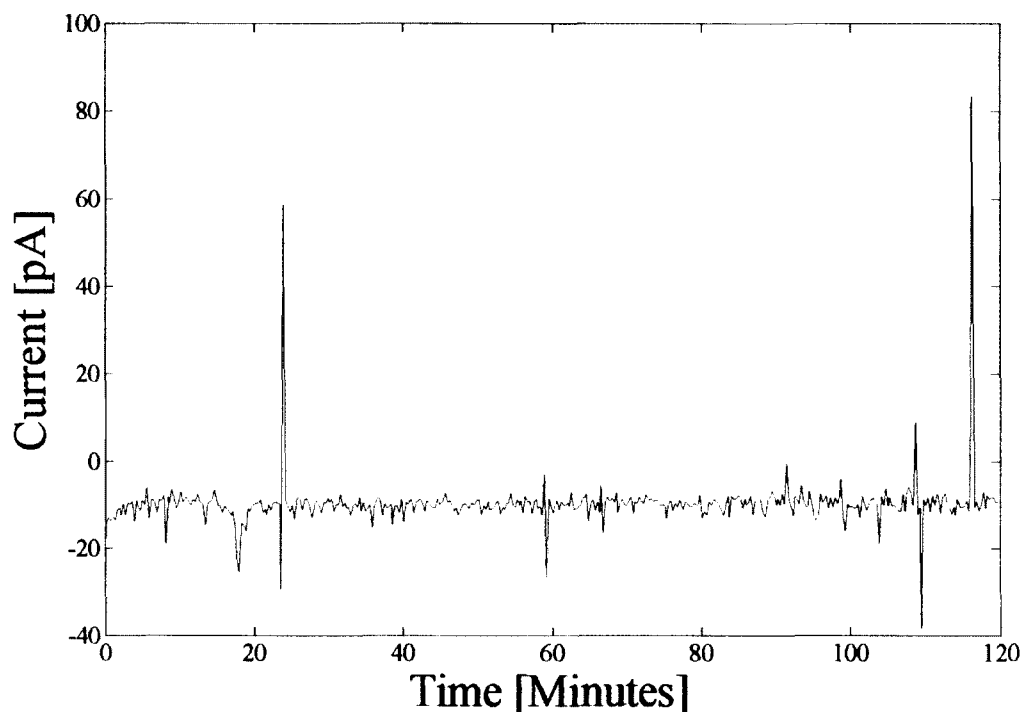


Figure 3.14. Current Measured From Reference Sample Being Etched.

The current being measured is in picoamps, which is orders of magnitude smaller than the current being measured while the electrochemical process is being used. The large spikes are only noise in the system, which can be from typical heating in the ammeter. The current that is created during the electrochemical process will be shown later. One of the key things to take from Figure 3.14 is the consistent and steady current flow measurement with a few random spikes. The next few figures will show the current measured at various bias voltages and x-ray potential. Figure 3.15 shows the change in the current through the quartz crystal with different x-ray tube potential and bias voltage.

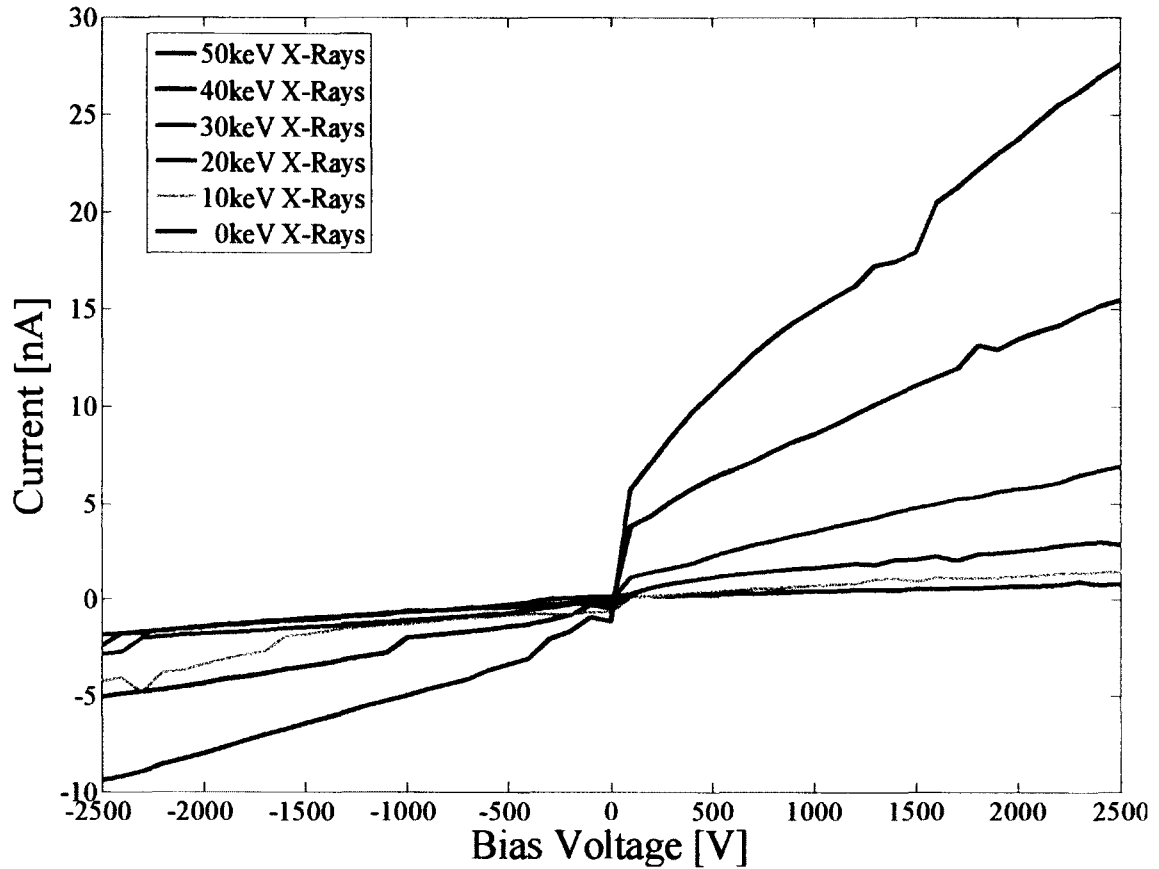


Figure 3.15. Voltage Versus Current For Quartz Crystals During Irradiation By X-Rays

The bias voltage was varied from -2500V to 2500V DC and the x-ray potential was varied from 10keV to 50keV. Figure 3.15 shows that the current through the quartz crystal varies with the bias voltage and the x-ray potential. There is a significant increase in the current through the quartz crystal as the bias voltage and the x-ray potential increases. The higher energy x-rays allow for more of the defect ions present in the quartz crystals to be released and they will eventually flow through the crystals due to the electric field being applied. For low energy x-rays the current through the crystal is not significant enough to produce any effect on the etch rate. However, with a bias voltage of 2500V and 50keV x-rays it was possible to push almost 30nA through the quartz

crystal. Figure 3.16 shows the current being induced through the quartz crystal at -5000V to 5000V at the 50keV x-ray potential.

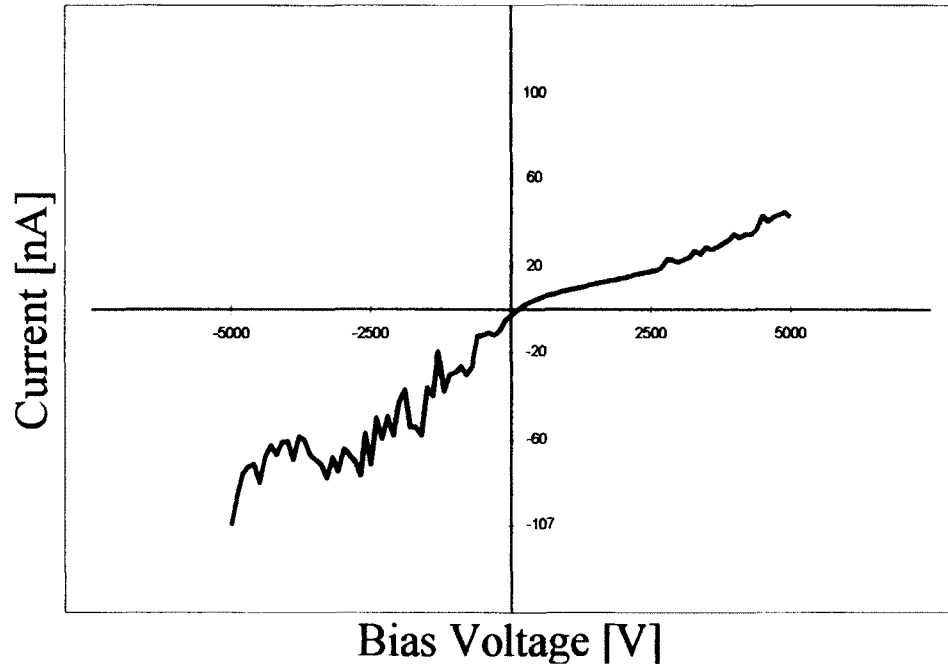


Figure 3.16. Current Induced Through Quartz 5kV to -5kV.

The maximum current measured at 5kV and 50keV x-ray potential produced a current of 45.6nA through the quartz crystal. And at the other end the bias voltage of -5kV with 50keV x-ray potential created a current of -107nA. There are three ways to increase the current through the quartz crystals further and are as follows: 1. Increase the DC bias voltage applied to the crystal, 2. Increase the energy of the x-rays that strike the quartz crystal, 3. Increase the radiation flux on the quartz crystal (done so by increasing the tube current). It would be possible to increase all three of these parameters. By increasing these parameters it could be possible to produce a higher amount of current

through the quartz crystals, which in turn could increase the etch rate of the quartz crystals. This will be looked at for future research by the author.

Now that it has been shown possible to pass significant current through the quartz crystals, it will be shown that the current will affect the etch rate of the quartz crystals. Figure 3.17 shows the resonant frequency of the two quartz crystal resonators while being etched for two hours. The data in Figure 3.17 was taken with the frequency data acquisition program built in Labview, which was discussed in Chapter 2 of this dissertation.

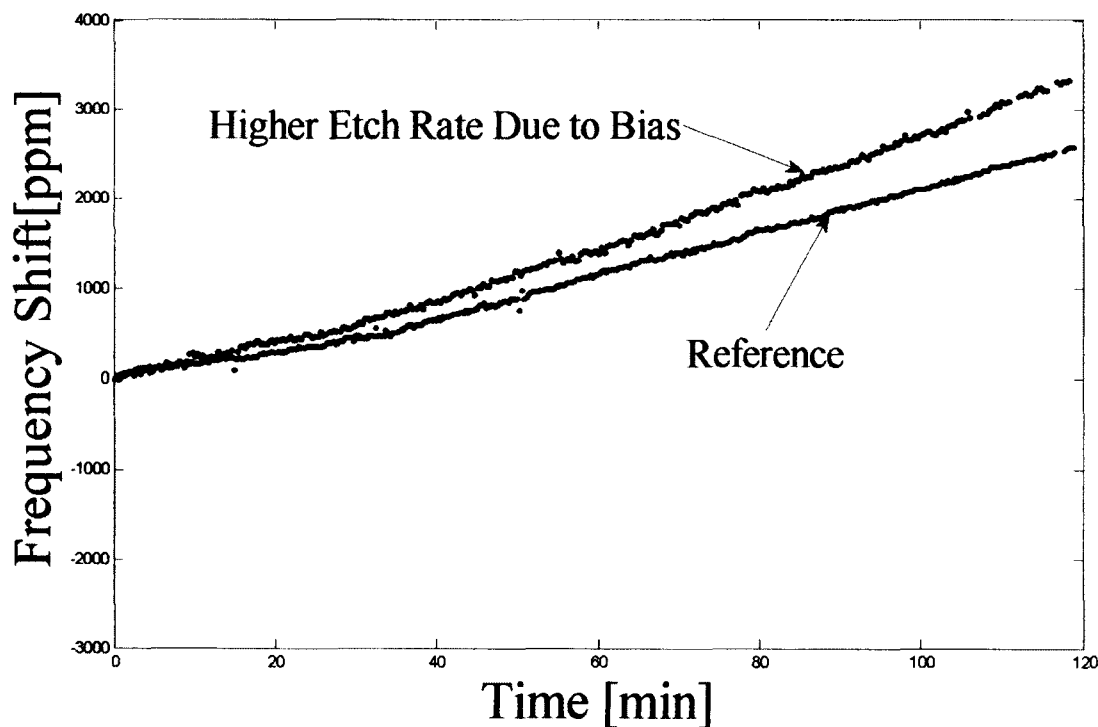


Figure 3.17 Frequency Measurement During Etching of Reference And Sample Irradiated By X-Rays

Both samples had their etchants heated to a temperature of 40°C. The reference crystal did not have bias voltage applied to it and no x-rays were irradiating the sample.

It is clear that the current going through the quartz crystal changes the etch rate. It is possible to increase the etch rate by 27% more than the reference (just 40°C and no x-ray or DC bias voltage). The etch rate (of the x-ray and bias sample) starts increasing higher after about 15 minutes during etching. It is the belief of this research that it takes a little time for the current to start affecting the etch rate through various tests showing this same phenomena. For Figure 3.17 the DC bias voltage applied with 50keV X-rays with a tube current of 2mA, which correlates to a flux of 4.5e19 photons/hr.

A surface profiler was used in order to verify the accuracy of the etch rate measurements taken by the frequency data acquisition program. Table 3.2 shows the etch rate measurements obtained by the frequency and surface profiler measurements.

Table 3.2 X-Ray Assisted Etching Results

| Measurement Type | Reference Etch Rate [nm/min] | X-Ray and Bias Voltage Etch Rate [nm/min] |
|---|------------------------------|---|
| Electrical Resonant Frequency Measurement | 11±1 | 14±1 |
| Profiler Measurement | 11±1 | 15±1 |

Table 3.2 shows that the electrical measurements and profiler measurements were accurate to within a standard deviation of 1 nm/min (60 nm/hr) for the etch rate.

To correlate the frequency change with the etch rate the following equation is used:

$$\frac{f_1}{f_2} = \frac{h_1}{h_2} \quad (3.12)$$

where f_1 is the initial resonant frequency before etching, f_2 is the final resonant frequency after etching, h_1 is the initial height (thickness) of the sample ($500\mu\text{m}$) and h_2 is the final height of the crystal after etching. For example with Equation 3.12, the 3000ppm frequency shift in Figure 3.15 corresponds to a 1770nm change in sample thickness. This 27% increase corresponds to an etch rate of 900 nm/hr. Usual wafer thickness variations are around 100 nm, so this increase in the etch rate is more than sufficient to compensate for the typical manufacturing variations encountered in quartz wafers. After verifying the increase in etch rate using the x-ray assisted electrochemical etching process, the next step of this research was to find out how long the process could last. Figure 3.18 shows the etching of the resonators at four hours.

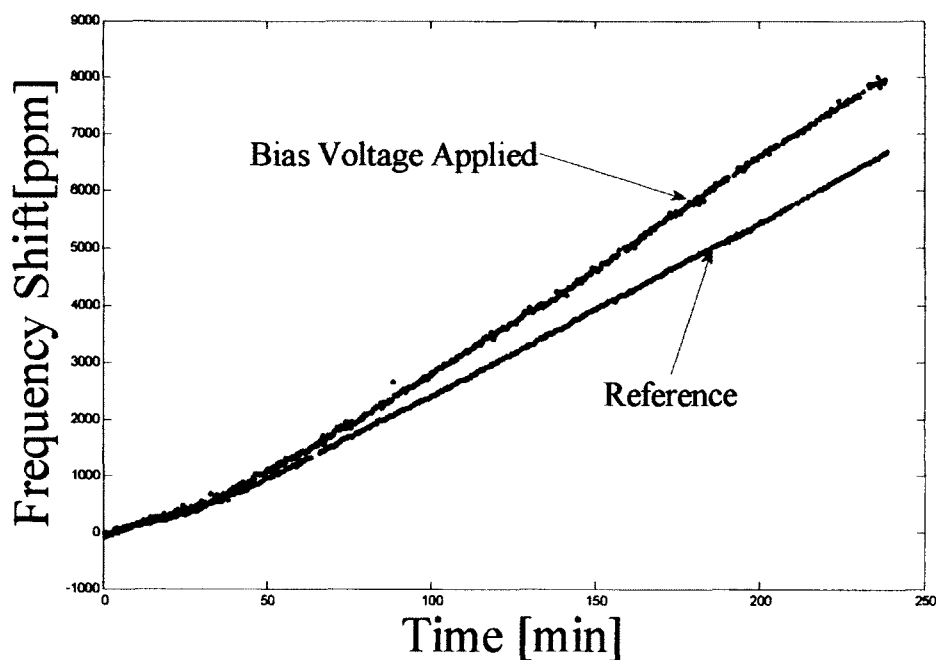


Figure 3.18 Four Hour Etch

The etch results in Figure 3.18 has the same conditions as data in Figure 3.17 except longer etch time. Figure 3.18 shows that the etch rate for the x-ray assisted electrochemical process continues to be above the reference. Also, this data shows that the x-ray assisted electrochemical process is not a transient effect and the etch remains stable. If the process was transient, it would not be useful for manufacturing quartz resonators. Since the effect is not transient in nature then it is possible to adjust the etch rate for long periods of etching.

The next aspect of this process was to investigate is the current profile created through the quartz crystal resonators. All current profiles produced through the experiments conducted for this dissertation's research can be divided into two sections. The first section is the surge section and the steady-state section. The current is initially high for about 30 minutes and then begins to decay to a relative steady-state value. The surge section typically lasts about 30 minutes for most of the experiments conducted and has a very unstable current flow. The steady-state section does not stay at a single current value but decays at a steady rate compared to the surge section of the current profile. Figure 3.19 shows the current that mainly occurs during a two hour experiment.

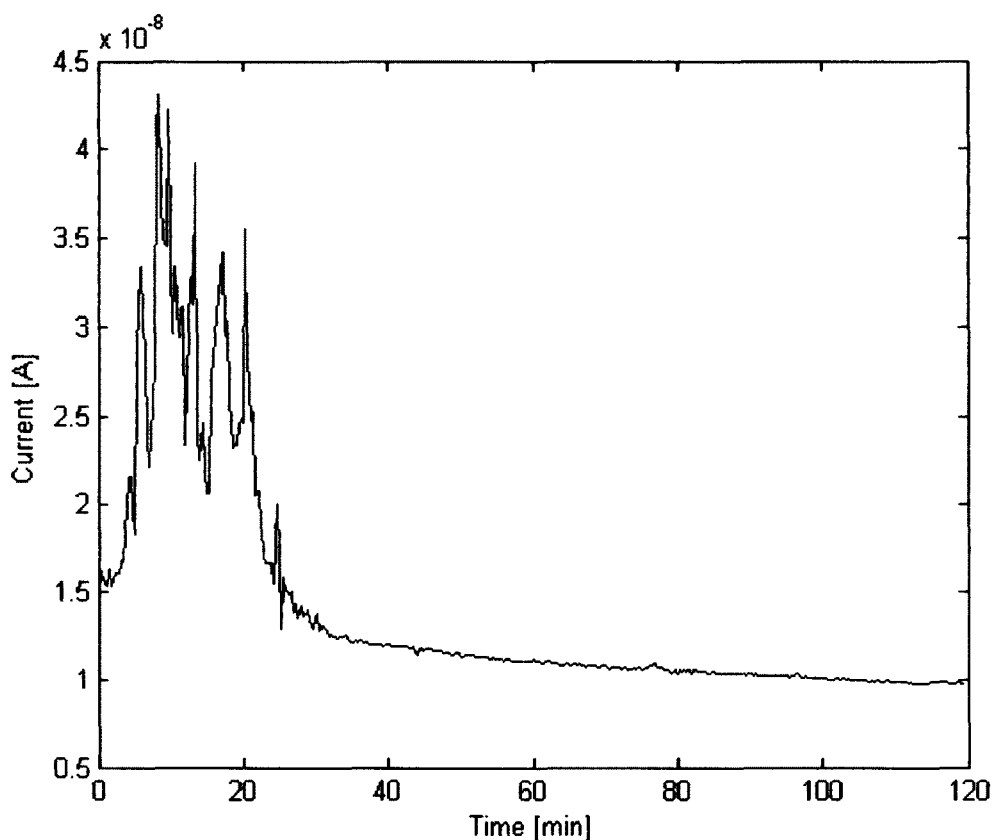


Figure 3.19 Radiation Induced Ionic Current

Figure 3.19 shows that after about 30 minutes the current decreases and enters into an exponential decay. For almost all of the experiments when the x-rays were applied with the DC bias voltage the current would start to have a steady decay around the 30 minute mark. This shows that the current induced in the quartz crystal is ionic in nature and that once the mobile ions within the quartz crystal is depleted, the current falls off and begins the exponential decay [41]. The etch rate does not change or fall off after the mobile ions start to become depleted but continues at the same rate [41]. This supports the fact that the bias voltage along with x-rays cause changes in the crystalline structure by removing the mobile ions. For Figure 3.19 the total charge transport in 30 minutes is approximately $6E-4 \text{ C/cm}^2$, which indicates that the initial ion density in the

quartz crystal was around $7E16/cm^3$ [41]. It is this researcher's belief that the depletion of the mobile ions inside quartz's crystalline structure causes unterminated bonds inside the crystal [41]. It is known that unterminated bonds will act as local initiation points for the dissolution of silicon dioxide during wet chemical etching [41]. Therefore one explanation for the increase in etch rate for the quartz crystals is due to the unterminated bonds that are produced from releasing the mobile ions [41].

Further explanation of the causes of the mobile ions will be further discussed. Through this experimental research into the x-ray assisted electrochemical process it was found that the current spikes in the initial surge current are more random in nature. The random surge current is due to the fact that not all quartz crystals are created equal. Each crystal will have a varying amount and type of mobile ions present in its crystalline structure. The current induced in quartz has long been studied in order to eliminate the mobile ions, which by doing so eliminates the quartz crystals sensitivity to ionized radiation. It is believed this random surge current is due to the multiple ion species moving through the thickness direction of the quartz crystals [39,97]. Previous researchers have concluded that the initial large current (surge current) is due to the alkali ions (present as defects) moving through the crystal [97]. The reason is the fact that alkali ions are the easiest bonds to break of the possible defects in the quartz crystals. The steady-state current is possibly due to hydrogen's OH- bond broken releasing the hydrogen ions [39, 94, 95]. Another likely mechanism for the steady-state current is from a single type of alkali ion species.

Table 3.1 shows the activation energies of the defects present versus atomic radii. For the alkali metal ions the activation energy increases as the size of the ion radius

increases. The most common impurity ions in quartz crystals are lithium and sodium and they have the lowest activation energy. The initial large surge current is most likely from lithium and sodium mobile ions. And if the steady-state decay current is from hydrogen, the strong bonding nature between hydrogen and oxygen atoms this explains why it remains hours longer after the surge current.

To sum up the extent of this section, it was shown that the etch rate is changed by depleting the mobile ions present in the quartz crystal. The depletion of the mobile ions creates unterminated bonds in quartz's crystalline structure. This increases the reaction rate of quartz and hydrofluoric acid causing the etch rate increase. Another important aspect to take away is the fact that the x-ray assisted electrochemical etching process is not transient in nature. This allows for it to actually be useful for the quartz crystal resonator industry as a new etching process.

3.8 Conclusion and Future Work

This chapter dealt with the x-ray assisted electrochemical etching of quartz crystal resonators in parallel to eliminate the need for individual frequency processing. It is possible to increase the etch rate of the quartz crystals by applying x-ray radiation in conjunction with bias voltage. The etch rate of the quartz crystals was increased by 27% over the reference. This electrochemical process gives another degree of freedom in the stagnate quartz industry in terms of improving upon the creation of quartz crystal filters and resonators.

Future work would involve increasing the x-ray tube potential, the tube current (increases the x-ray flux) and the bias voltage applied to the crystals during etching. The x-ray source can be varied in two ways. Increasing the x-ray potential higher than the

50keV that was used in this dissertation, which could allow more current to pass through the crystal and possibly increase the etch rate beyond 27%. Another factor that could possibly increase the current through quartz would be increasing the x-ray sources flux output. The final way for increasing the current through the quartz crystals is by applying a higher bias voltage. Protection circuits were created to limit the amount of voltage applied to the measurement instruments. Therefore the easiest way to increase the current through the quartz crystal resonators is either by increasing the x-ray potential or the x-ray flux.

Another objective for future work is to use this process for other insulating piezoelectric crystals such as the following: Langasite, Lithium Niobate, Lithium Tantalate, Lithium Tetraborate, and other piezoelectric (or insulating materials). All of these piezoelectric crystals are grown in a similar fashion as quartz, therefore, the same principles discussed in this dissertation can be used for processing them.

CHAPTER 4

LASER ASSISTED RAPID ETCHING

This chapter will show the ability to etch quartz crystal resonators with the combination of lasers and wet etching chemistry. It will be shown that by irradiating the quartz crystal with lasers the etch rate can be controlled through varying the laser's power density. Hot spots will develop at the areas being irradiated by the laser. These hot spots can create large temperature gradients allowing the etch rate to be increased safely beyond the current processing methods. Current processing methods require large amounts of HF acid to be bulk heated, with this method only the etchant in contact with crystal being irradiated will be heated. In order to measure the resonant frequency (which allows for measuring the thickness) of the crystals a metal thin film must be deposited on the front-side of the crystal. The metal thin film will also be used as an absorber allowing for the etch rate to be increased. Figure 4.1 shows a conceptual drawing of the laser assisted wet etching of the quartz crystals.

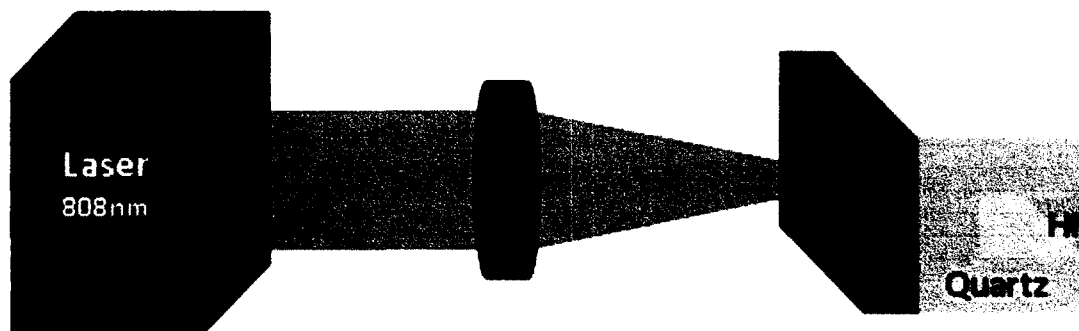


Figure 4.1 Laser Assisted Wet Etching of Quartz with Cr Thin Film

From Figure 4.1 it can be seen that at the laser's focal point the etch rate of the quartz crystal will be hotter than the surrounding areas. The area around the focal point of the laser will still etch; however, this is much slower than the area where the laser is being focused. Figure 4.2 shows a sample that was etched with a laser power density of 4 W/mm^2 .

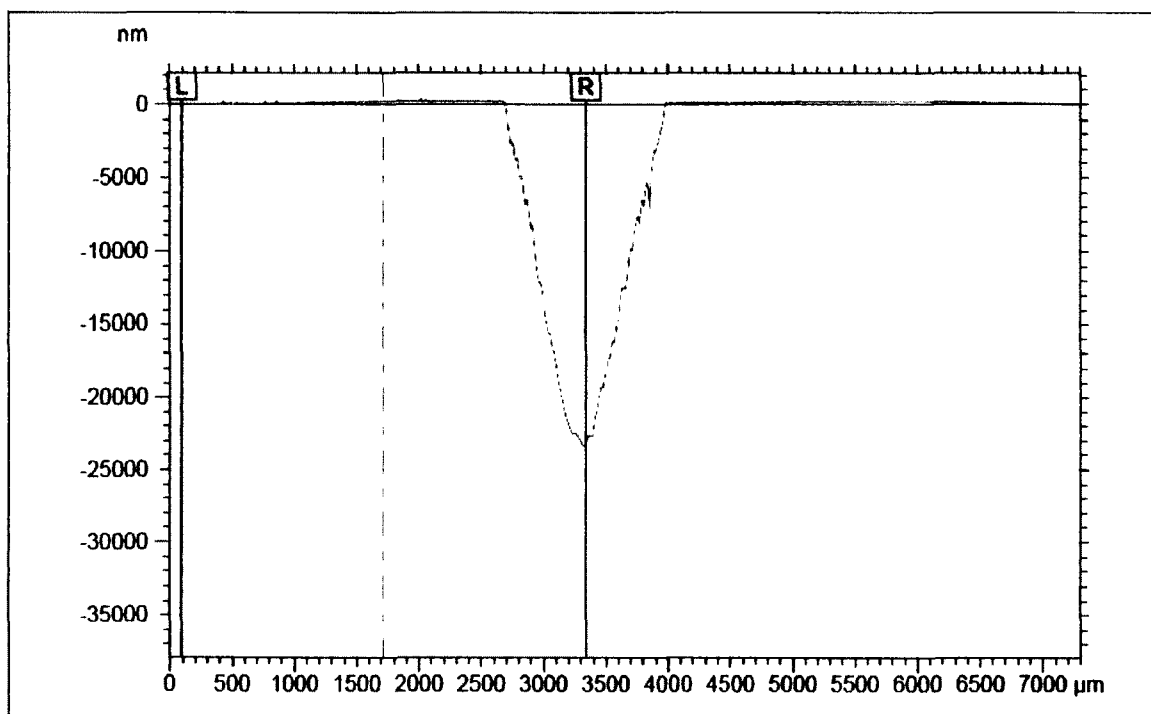


Figure 4.2 Etch Profile of Laser Assisted Wet Etching of Quartz.

The whole area shown was in contact with the wet etchant; however, the only portion of the crystal etched was the area being irradiated by the laser beam. The etch profile is Gaussian in nature due to the shape of the laser beam, however, this shape can be varied which will be discussed later in this chapter.

4.1 Literature Review for Laser Etching of Quartz

Laser assisted etching of quartz has been done by various research groups [98-102]. The works by previous researchers use lasers with large power densities to etch quartz and glass, all of these processes will melt the quartz crystals [98-102]. These processing methods are known as laser ablation. Another type of laser assisted etching of quartz does not ablate the crystals, it creates amorphous areas in the crystalline structure then they are dipped in a HF solution [102]. This laser process will not be discussed further due to the fact that it is a multistep processing method and it damages the crystal [102].

The first type of optical etching of quartz to be discussed involves using only a laser during fabrication and no wet etchants. This process is strictly laser ablation. Laser ablation requires laser that pulse small amounts of energy (mJ). These pulses occur typically at a rate between nanoseconds to femtoseconds. By hitting materials with very high rate of pulses even small amounts of energy can ablate the material. The pulsed laser beams with nanosecond and femtoseconds pulse widths will excite electrons. These electrons excited by photons are called free electrons. The freed electrons will go and interact with other electrons creating avalanche ionization. At a certain point during the avalanche ionization a plasma plume is created. This is the effect that creates laser ablation without using chemicals. It was found that a laser at a wavelength of 790nm and

with pulse lengths from 100 to 200 femtoseconds (fs), can produce microchannels that are ablated in the quartz crystals [99]. There is no chemical etchant being used in this process. They could reach an etched depth of 500 μm in about one minute in a vacuum environment and in atmosphere they reached 500 μm in about two and half minutes [99]. This process can etch quartz crystals rapidly, however, the ablation of the quartz crystals damages it as a material that could be used for resonators. For quartz crystal resonators any damage to the surface will cause the quality factor to decrease dramatically and with no piezoelectricity there is no resonator. It has been found that damage and the roughness of the quartz sample for a resonator will decrease its quality factor [87]. Another damage factor is the fact that laser ablation causes the quartz crystal to become amorphous. Amorphous silicon dioxide does not have piezoelectric properties and is useless for resonators applications. The goal of this dissertation is to create quartz crystals that have their piezoelectric properties intact after processing.

The final process to discuss is one of the most commonly used laser assisted etching of quartz and it is called Laser Induced Backside Wet Etching (LIBWE) [98]. It combines optical and chemical processes to etch materials [98]. A 248nm laser is used in the experiments, and the laser is attenuated by a dielectric mirror positioned at the laser output [98]. The etchant used on the backside of the quartz crystal is acetone with pyrene [98]. The laser passes through a mask, and then it is focused through a lens at the etchant, which then heats up and etches the shape of the mask on the backside of the quartz crystal plate [98]. Figure 4.3 shows the LIBWE optical chemical etching setup [98].

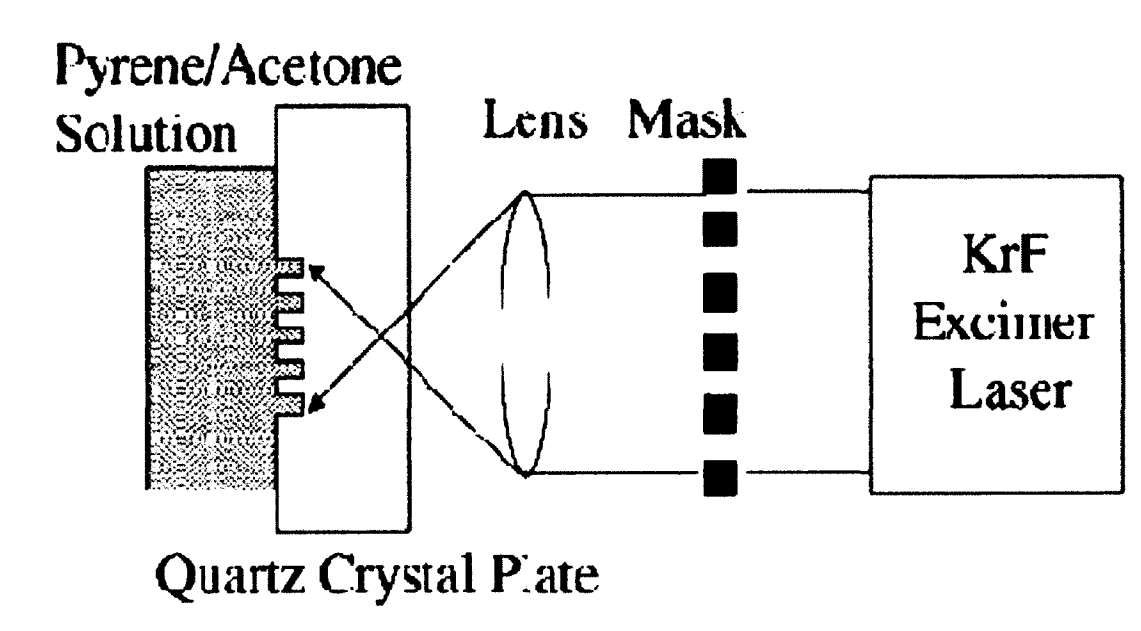


Figure 4.3 LIBWE(Laser Ablation) Etching Setup [98]

The etch rate for this system setup is about 25nm/pulse and with a repetition rate of 2Hz it is possible to have an etch rate of 3 μ m/minute [98]. What happens in this process is very simple; the etchant that is used will absorb most of the UV light from the laser. The etchant absorbs the laser energy and then this will increase the temperature and the pressure of the etchant, which in turn etches the quartz [101]. The previous uses of this setup are in fabricating optical lenses out of quartz samples [101]. The temperatures created in this process exceed that of the melting point of quartz which is 1670°C. Therefore like the previously discussed laser ablation setup this process cannot be used for creating quartz crystal resonators. The LIBWE technology created by Wang *et al.* is ideal for etching through quartz crystals, however it cannot be used to create piezoelectric devices out of quartz crystals (due to damage created by the laser ablation process). The system created during this dissertation's research is a one step process of etching the quartz crystals and measuring the resonant frequency, thus eliminating the

need for final frequency trimming. Also, with the laser assisted etching setup it is possible to create various etch patterns in the quartz crystals without damaging its' piezoelectric properties.

4.2 Laser Etching Setup for Creating BAW QCRs

This section of the chapter will discuss the equipment used in the creating the laser assisted wet etching experiments. The laser assisted wet etching setup created for this dissertation is a simple one step process. The laser assisted wet etching process consists of an 808nm laser, a Fresnel lens, and a network analyzer. Figure 4.4 shows the experimental etching setup for the laser assisted wet etching process. Also, Figure 4.4 shows that this process is very simple and much cheaper than plasma etching systems. The most expensive piece of equipment is the network analyzer. The laser being used is an off the shelf 808nm laser under \$3000. Using the switching unit discussed about in Chapter 2 it is possible to measure multiple resonators, thereby needing only one network analyzer keeping the costs of the overall system down.

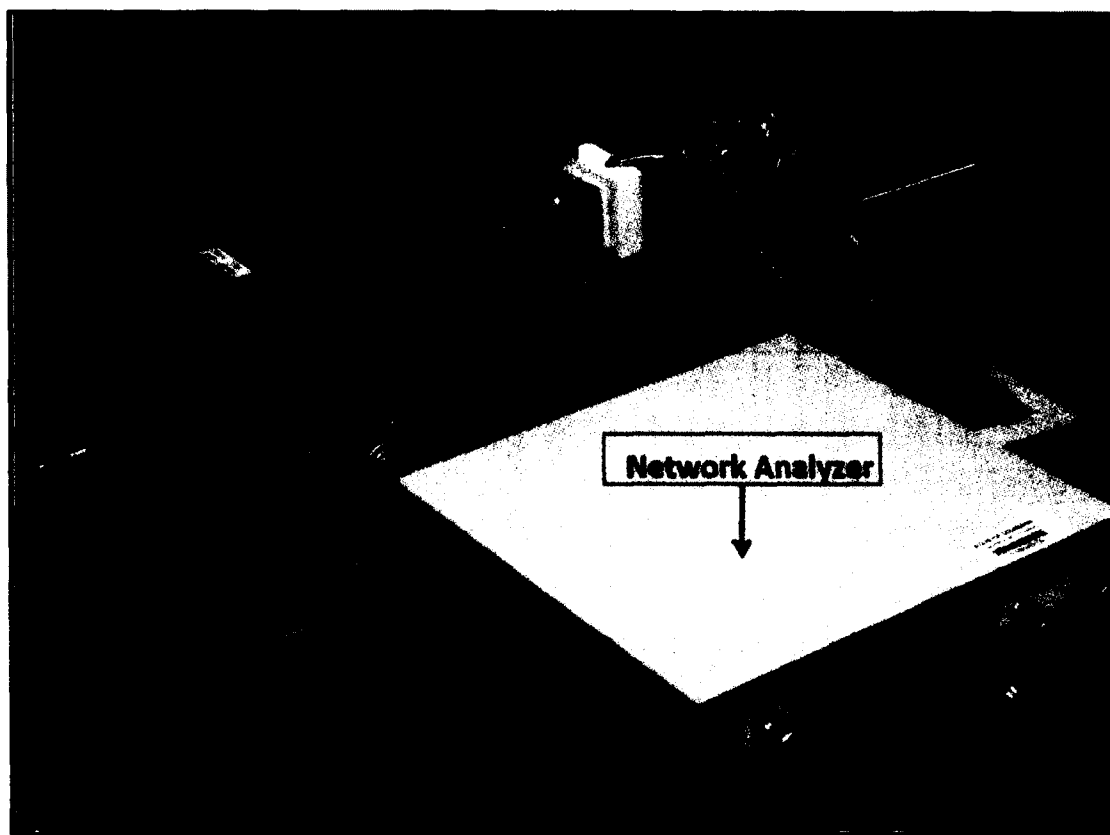


Figure 4.4 Laser Assisted Etching Setup with Fresnel Lens

An 808nm continuous wave 5W laser from OEM Laser Systems was used for the majority of the experiments in this dissertation. The laser in this setup is focused by a Fresnel lens. This allows for the laser to selectively heat specified areas of the quartz crystal. The network analyzer allows for the monitoring of the thickness of the quartz resonators by measuring their resonant frequency. The quartz crystal holder is made out of PTFE due to its chemical resistance to HF acid, its ability to be used over a large temperature span, and the low optical absorption coefficient for the wavelengths of light used in this dissertation. The setup in Figure 4.4 will create a Gaussian etch profile. By adding an optical diffuser it is possible to create a Top-Hat etch profile similar to a wet etch anisotropic etch pattern.

The laser used in this test setup is a continuous wave semiconductor diode laser.

Table 4.1 shows the parameters for the 808nm OEM laser diode system.

Table 4.1 [103] 808nm Laser Properties

| Laser Specifications | |
|--|-------------------------------------|
| Wavelength | 808+/-3nm |
| Laser Type | Diode |
| Output Power | 5 |
| Transverse Mode | Near TE ₀₀ , Square Beam |
| Operating Mode | CW |
| Power Stability[RMS over 4 hours] | <5% |
| Warm-Up Time[minutes] | <5 |
| M ² Factor | <20 |
| Beam Divergence[mrad, full-angle] | <3.0 |
| Beam Diameter[mm, at aperture] | ~5x8 |
| Beam Height[mm, from base plate] | 29 |
| Pointing Stability[mrad,after warm-up] | <0.05 |
| Polarization Ratio | >50:1 |

This laser was selected in order to test a wide range of power densities and their effect on the etch rate of quartz crystals. Figure 2.9 showed the etching setup for two IIIb 635nm lasers etching two different resonators on the same quartz die. Figure 2.9 shows the ability to etch multiple resonators on the same die with cheap off the shelf lasers. Variability of this laser assisted wet etching process allows for the ability to bring this to

a commercial setting. It requires little effort to configure this setup for controlling multiple resonator's etch rate at the wafer level. Details of the principles of operation for a laser will be discussed in the next section.

4.3 Laser Principles of Operation

Basic principles of laser operation will be discussed in order to give the reader a general idea of how semiconductor laser diodes perform. There are various types of lasers that have been created over the years such as: Gas (Helium-Neon), Chemical (Hydrogen Fluoride), Dye, Metal-Vapor (Helium-Cadmium), and Solid State (Nd:YAG). Solid State lasers will only be discussed, since this is the only type of laser used in this dissertation. This chapter will cover work using semiconductor lasers, such as laser diodes and diode pumped solid state (DPSS) lasers. However, Appendix A will feature results using LED's as the heating source for wet etching quartz crystals.

Lasers also can be classified as either continuous wave or pulsed. This dissertation will deal with only continuous wave semiconductor laser diodes. The literature review in Section 4.1 covered etching processes assisted by lasers that used pulsed operations. Pulse laser systems are designed to irradiate samples with laser fluences at ns, ps, and fs intervals. Also discussed in Section 4.1, was that pulsed laser systems ablate the crystal, which can either damage the surface (lowering the Q factor) or eliminate the crystals ability to be used as a resonator (destroying the piezoelectric properties). Continuous wave lasers allow for lower amounts of energy to irradiate the sample's surface. The power densities used for this dissertation work are less than 10^3 W/cm², whereas the pulsed laser etching processes use power densities in the range from 10^8 to 10^{14} W/cm². The small power densities used in this dissertation do no damage to

the quartz crystals crystalline structure or its piezoelectric properties. The next topic will cover the basic physics of semiconductor lasers.

4.3.1 Laser Pumping

Radiative recombination of electrons and holes can occur in two ways in semiconductors, either through electrical pumping or optical pumping. Pumping is the process in which photons are created in order to start up the reaction needed to produce a laser. Laser diodes use electrical pumping and diode pumped solid state lasers (DPSSL) use a laser diode as the pumping mechanism.

Electrical pumping requires a p-n junction semiconductor to inject photons created through recombination into the optical resonator cavity. Once photons are present inside the optical resonator cavity they are amplified up until a certain point and then are emitted as electromagnetic radiation. Electrical pumping takes place when the p-n junction is forward biased. The forward bias will create an excess of electrons and holes at the junction (active area) of the semiconductor. The recombination process will create population inversion (excess of electrons in conduction band), which will allow for the production of photons to be injected in the optical resonator.

Optical pumping uses the laser diode (or a flash tube) to create population inversion. The laser diode passes through the gain medium crystal. After passing through the gain medium the laser diodes' wavelength will be converted. A 808 nm laser diode will pass through a Nd:Glass crystal, which will convert the 808 nm wavelength to 1.06 μm . The transitions that can produce photons will be discussed briefly in the next section.

4.3.2 Transitions

There are three types of optical transitions that can take place inside a semiconductor laser and they are as follows: absorption, spontaneous emission, and stimulated emission. The first transition possible is absorption, when a photon strikes the semiconductor material, the material will absorb the energy and if the energy is greater than the band gap an electron will move from a lower state to a higher energy state.

The second transition is spontaneous emission, which takes place when an electron from the higher energy level spontaneously moves to a lower energy state and produces a photon. The phase and polarization of spontaneous emitted photons are random and the direction that the photons will be emitted is unknown. Light emitting diodes (LEDs) use spontaneous emission as the main source to create photons.

The third transition is stimulated emission, when a photon hits a material causing an electron to move to a lower energy state emitting another photon. Therefore, two photons leave the system after stimulated emission. Unlike spontaneous emission, photons created by stimulated emission will have the same frequency, phase, polarization and photon emission direction. Stimulated emission is the principle that must take place in order to produce a laser beam. The stimulated emission takes place in an optical resonator to build up the laser's energy until enough energy is created it can leave the optical resonator.

4.3.3 Polarization Ratio

Every laser system that is used will have some spontaneously emitted photons. Spontaneous emitted photons will produce noise in the laser system; therefore it is

important to characterize it for each laser system [104]. As shown in Table 4.1 the OEM laser used in this dissertation has a polarization ratio of 50:1. This means that for every fifty stimulated emitted photons, one of the photons will be produced by spontaneous emission. The top of the line laser systems typically have a polarization ratio of only 100:1. The next section will discuss the M^2 factor of a laser beam.

4.3.4 M^2 Factor

The M^2 factor determines the quality of the beam in relation to it having a pure Gaussian profile. When the M^2 factor is equal to a value of one the laser profile is a perfect Gaussian. Therefore the M^2 measures how much the laser beam profile deviates from the Gaussian profile. The M^2 factor is calculated using the following equation:

$$M^2 = \frac{1}{\theta} \left(\frac{\lambda}{\pi * w_0} \right) \quad (4.1)$$

where θ represents the half-angle beam divergence of the laser (the beam divergence is how fast the laser will expand with distance from its waist), w_0 is the waist of the beam meaning it is the point at which the beam will have the smallest diameter [105].

4.4 Optical Elements

Various types of optical elements are used in this etching system. Three different types of lenses were used to vary the size of the beam diameter for the NIR laser. The three types of lenses used are the plano-convex, biconvex, and the Fresnel lens. A quick review of the basic principles of lenses covering focal length and its effect on the spot size of the beam will be discussed. The final topic of this section involves beam shaping.

4.4.1 Optical Lenses

The principles of optical lenses used in this work will be discussed briefly in this section.

The first thing to look at for optical lenses is the focal length of the lens. There are a few ways to calculate the focal length of a given lens. The focal length can be found using the following relation:

$$\frac{1}{f} = \frac{1}{o} + \frac{1}{i} \quad (4.2)$$

where the focal length is represented by f , the object distance from the lens is designated by o , and i represents the distance of the image created through the lens. The other focal length equation to be discussed is the well known Lens-Maker's equation:

$$\frac{1}{f} = \left(\frac{n_1}{n_0} - 1 \right) \left(\frac{1}{R_1} - \frac{1}{R_2} \right) \quad (4.3)$$

where n_1 and n_0 are the index of refraction of the lens material and the medium around the lens respectively. The R_1 and R_2 are the radius of curvature of the front and back side of the lens. These values determine the actual shape of the lens, for example whether the lens is concave or convex. Another important aspect to calculate for a lens is the spot size of the laser beam in order to get the highest possible power density. The beam waist of a Gaussian beam can be found by the following equation:

$$w(z) = w_o \left[1 + \left(\frac{\lambda z}{\pi w_o^2} \right)^2 \right]^{1/2} \quad (4.4)$$

where w_o represents the area of the beam when it has an intensity of $1/e^2$, λ is the wavelength of the beam, z represents the distance of the laser beam [105]. Equation 4.4

shows how to calculate the beam waist of the Gaussian beam at any given distance from the source.

Finding the smallest spot size that can be created for a given laser beam is of utmost concern of this research. The way to calculate the smallest possible spot size of the laser beam after focusing while taking into account for diffraction:

$$\text{Spot Size} = \frac{4 * \lambda * M^2}{\pi * D} \quad (4.5)$$

where λ is wavelength of the laser, M^2 is a factor that shows how close the laser beam output shape is to a perfect Gaussian profile, D is the diameter of the laser beam before it reaches the lens. The focal length of the Fresnel lens used in this research is 12.7cm. The smallest spot size that would theoretically be possible if the laser had a perfect TE00 profile and not diffraction limited, would be 14.48 μ m. However, it is difficult to get a spot size in the 14.48 μ m without a beam profiler to measure the spot size. For this research the smallest spot size used was 0.5mm. It is possible to obtain a smaller spot size, and this would allow for small size etching profiles and lower overall laser power.

Since the laser profile was TE00 and we are focusing it with a Fresnel lens, it will have a Gaussian pattern. The intensity of a Gaussian Laser beam at a specific distance is found by the following expression:

$$I(r, z) = I_0(z)e^{-2r^2/w(z)^2} \quad (4.6)$$

where I_0 is the maximum power of the laser beam, r is the radius of the beam [105]. Figure 4.5 shows the Gaussian profile when the laser is focused down to have a max power density of 12.7 W/mm².

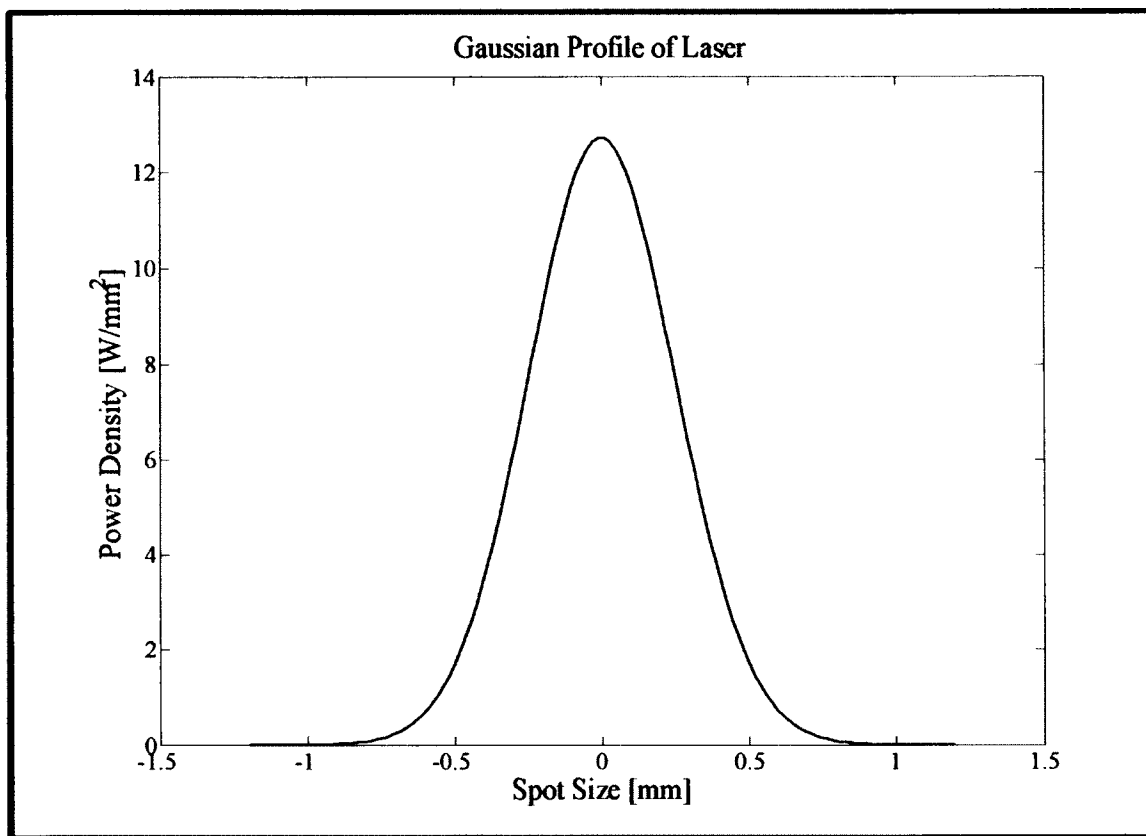


Figure 4.5 Gaussian Profile with a Maximum Power Density of 12.5 W/mm².

There are only two ways to vary the spot size of a laser, since the wavelength and the M^2 factor are determined during manufacturing. The two ways to vary the spot size of the laser is to vary the laser beam before it enters the lens or to vary the lens distance from the sample. In order to increase the laser beams diameter before it enters the lens requires other optics and therefore the faster way to change the spot size is to vary the lens distance from the sample. The next section will discuss varying the shape of the laser beam from a Gaussian distribution to a Top-Hat distribution.

4.4.2 Optical Diffuser

The beam profile can be adjusted by varying the type of optical element in front of the laser. To change the beam profile from Gaussian to Top-Hat distribution an engineered diffuser created by RCP Photonics was used [106]. Figure 4.6 shows the laser beam profile with a Top-Hat distribution created using the engineered diffuser and focused with the Fresnel lens.

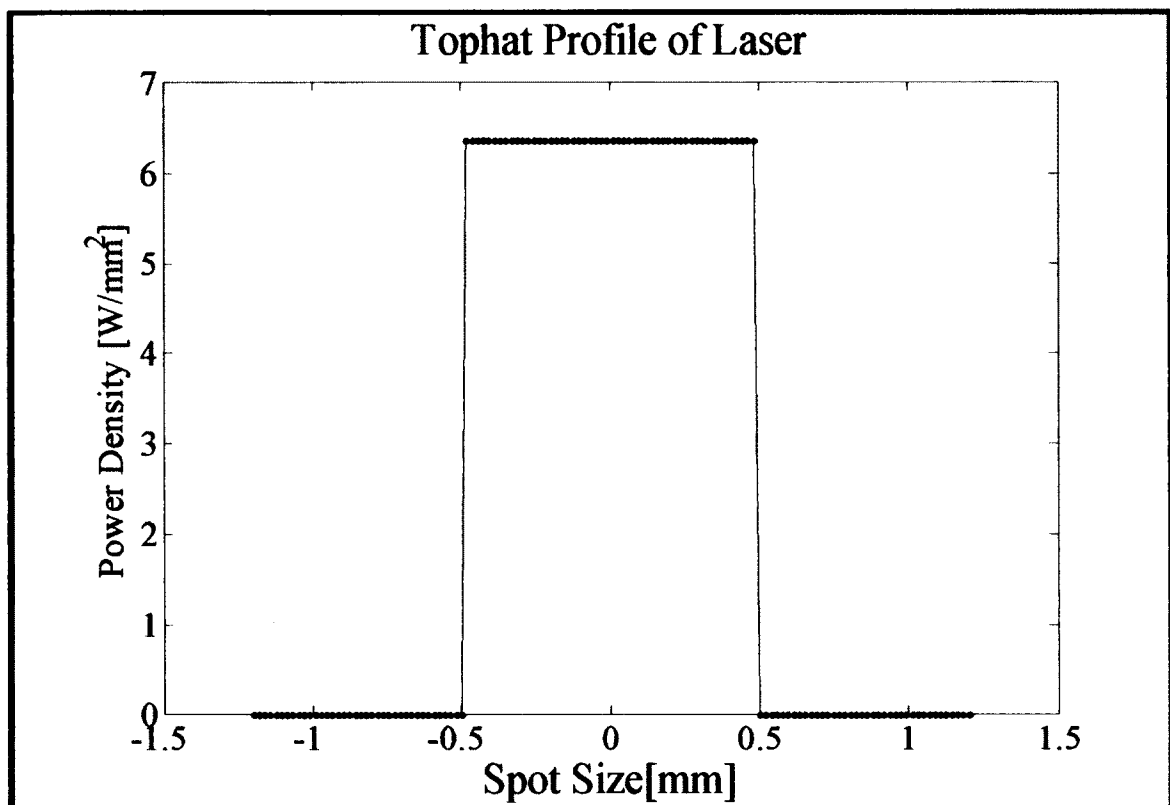


Figure 4.6 Top-Hat Profile with Maximum Power Density of 6.5 W/mm².

The Top-Hat profile has the same power and spot size of the Gaussian Profile in Figure 4.5. The Top-Hat profile will have a power density that is roughly half of the power density of a Gaussian profile. The Top-Hat beam profile will create etching

profiles with steep sidewalls. This profile will be the most useful for creating a quartz crystal resonator, since it will make it easier to have efficient energy trapping. The energy trapping is important in order to maintain a high quality factor. Figure 4.7 shows the schematic for creating shapes for a Top-Hat profile using the engineered diffuser from RCP Photonics tutorial [106].

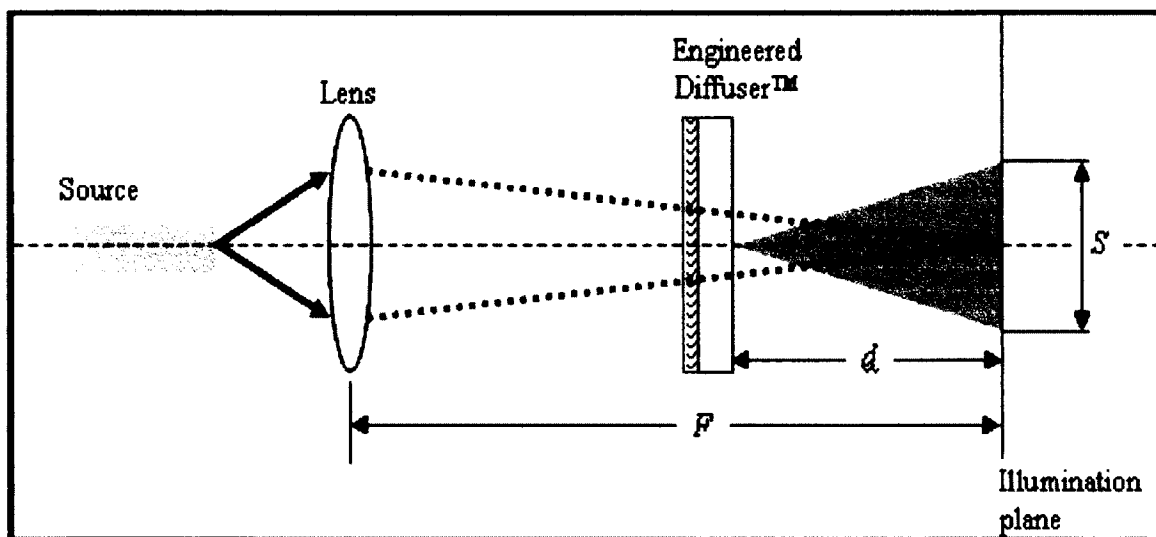


Figure 4.7 Schematic for Creating Top-Hat Beam Profile [106].

The size of the beam through the engineered diffuser can be calculated using the following equation:

$$\text{Illumination Size (S)} = d \times \tan \theta \quad (4.7)$$

where d is the distance from the diffuser to the sample, θ is the angle that is specified by engineered diffuser [106]. The next section of this chapter will discuss the actual mechanisms involved with the wet etching assisted by the 808nm laser.

4.5 Etching Mechanism

This section of the dissertation will go into more detail in explaining the etching mechanisms that take place in the laser assisted process. The laser assisted process involves one etch step due to the measurement system used in combination. The mechanism for increasing the etch rate of the quartz crystals is the absorption of laser radiation. The quartz crystal and the HF etchant will absorb laser radiation. However, the percentage of absorption is quite small, experimentally it was found that the quartz samples used absorbed five percent laser radiation. The laser absorption of HF acid was measured to be four percent. In order to measure the resonant frequency of the quartz crystal during etching, a metal thin film is deposited on the front side of the crystal. This metal thin film also acts as an additional absorption layer. The absorption of the metal thin films used in this research is 6X larger than quartz and the HF etchant. Figure 4.8 shows the etching mechanism of the LASER ASSISTED process.

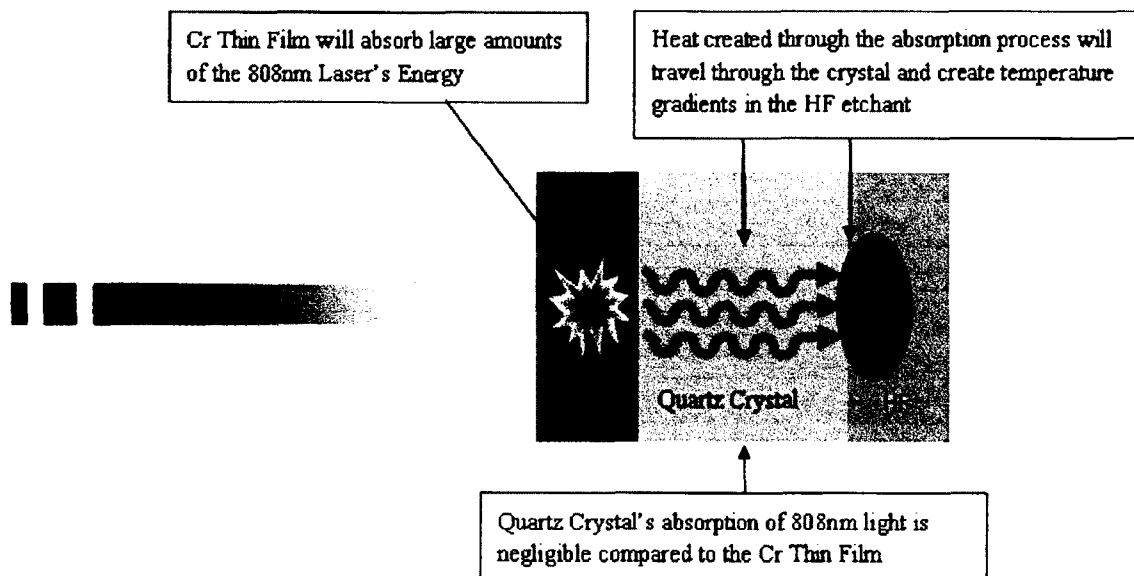


Figure 4.8 Etch Mechanism of the Laser assisted Process.

The metal thin film deposited on the front side of the quartz crystal absorbs a large percentage of the 808nm laser radiation. The heat that is produced by this initial absorption process will flow through the quartz crystal to the HF etchant located on the backside of the crystal. The most important aspect of the LASER ASSISTED process is the metal thin film absorbing the majority of the laser's radiation. Therefore it is very important to select the right metal thin film to be deposited on the quartz crystal.

4.5.1 Metal Thin Film Selection

Research was done on finding which metal thin film had the highest absorption coefficient for 808nm. Figure 4.9 is the percent absorbed of various metals with varying thickness layers at the 808nm wavelength [107].

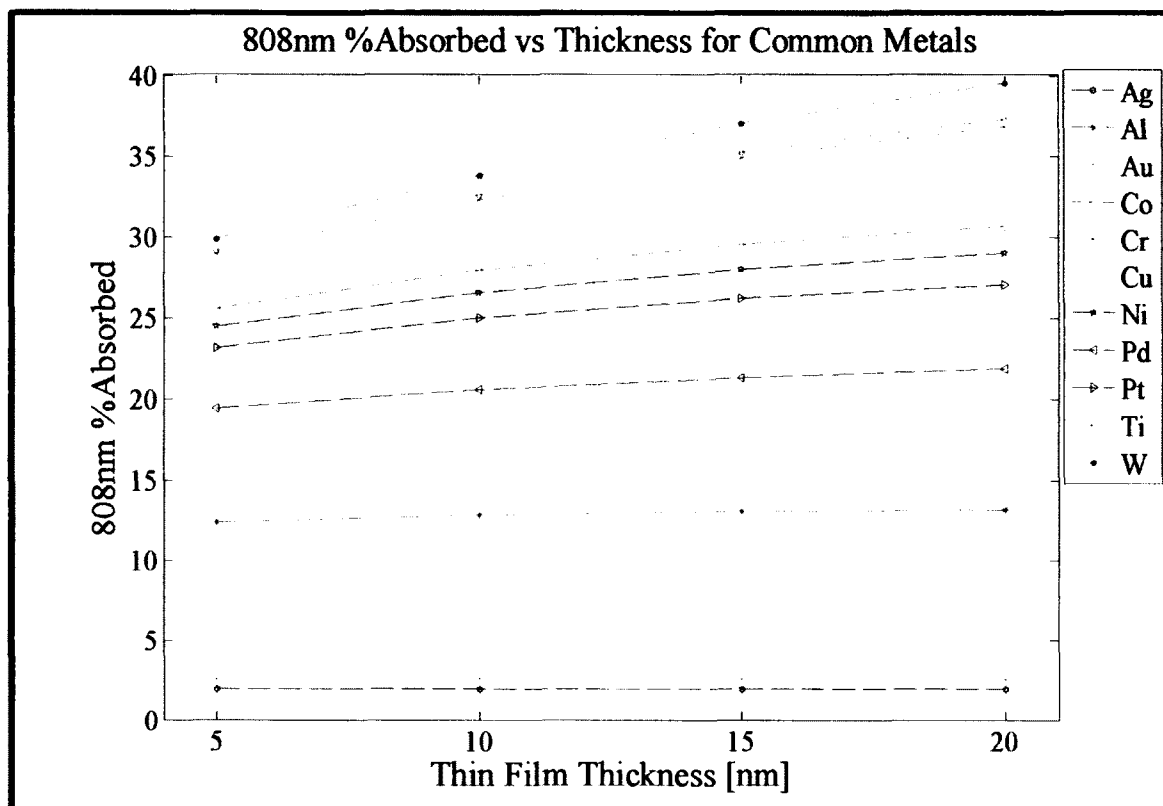


Figure 4.9 Amount of 808nm Laser Radiation Absorbed By Common Metals.

The data from Figure 4.9 comes from the online database site refractiveindex.info [107]. This database is collected from various journal papers and other references [107]. From Figure 4.9 it can be seen that the best metals to use as thin film absorption layers for the 808nm wavelength are Chromium (Cr), Titanium (Ti), and Tungsten (W). Even though Cr and Ti thin films are not the best absorbing metal thin films at 808nm wavelength, they have the ability to adhere to quartz crystals without an adhesion layer. Chromium and Titanium thin films of around ~5nm are used as adhesion layers for other metals used as electrodes on quartz crystals. Tungsten has a higher absorption percentage, but does not adhere well to the quartz crystals. Chromium thin films were chosen due to the fact it is the most common adhesion layer for quartz resonators.

Figure 4.9 is the absorption percentage of radiation at the 808nm wavelength. However, the data in Figure 4.9 is based on optical properties of bulk Chromium. Therefore the absorption coefficient was measured for various Chromium thin film thicknesses on a quartz substrate, these results are shown in Table 4.2

Table 4.2 Absorption of Materials

| Material | Absorption Coefficient [1/cm] for 808nm Radiation |
|----------------------|---|
| Quartz (500µm) | 0.35 |
| Quartz w/ 5nm of Cr | 16.76 |
| Quartz w/ 10nm of Cr | 18.62 |
| Quartz w/ 15nm of Cr | 23.94 |
| Quartz w/ 20nm of Cr | 26.10 |

The data obtained in Table 4.2 was found by calculating the reflectance of Chromium thin films with the following equation:

$$R = \frac{(n - 1)^2}{(n + 1)^2} \quad (4.8)$$

where n is the index of refraction for chromium, which is 3.17386 for a wavelength of 808nm. The reflectance was calculated to be 0.2712 for Chromium. The absorption coefficient then can be calculated by the following equation:

$$I_t = I_o(1 - R)^2 e^{-\alpha x} \quad (4.9)$$

where R is the reflectance calculated using Equation 4.8, x is the thickness of the sample, α is the absorption coefficient (1/cm). Both I_o and I_t were measured, I_o is the initial power of the laser before entering the sample and I_t is the power of the laser after passing

through the sample. Equation 4.8 can be rearranged in order to easily calculate the absorption coefficient, shown in the following equation:

$$\alpha = -\frac{1}{x} \ln\left(\frac{T}{(1-R)^2}\right) \quad (4.10)$$

where T is the transmittance which can be expressed as:

$$T = \frac{I_t}{I_o} \quad (4.11)$$

where I_t is the beams transmitted intensity and I_o is the beams initial intensity.

Experiments were conducted in order to verify that the etch rate of the quartz crystals could be varied by increasing the Chromium thin films thickness. This would allow another degree of freedom in varying the etch rate of quartz crystal resonators. Table 4.1 results show an increase in the absorption percentage of 808nm laser radiation for Cr thin films as the film thickness is increased. Figure 4.10 shows the etch rate for different thicknesses of Cr thin film and the quartz crystal without any thin film.

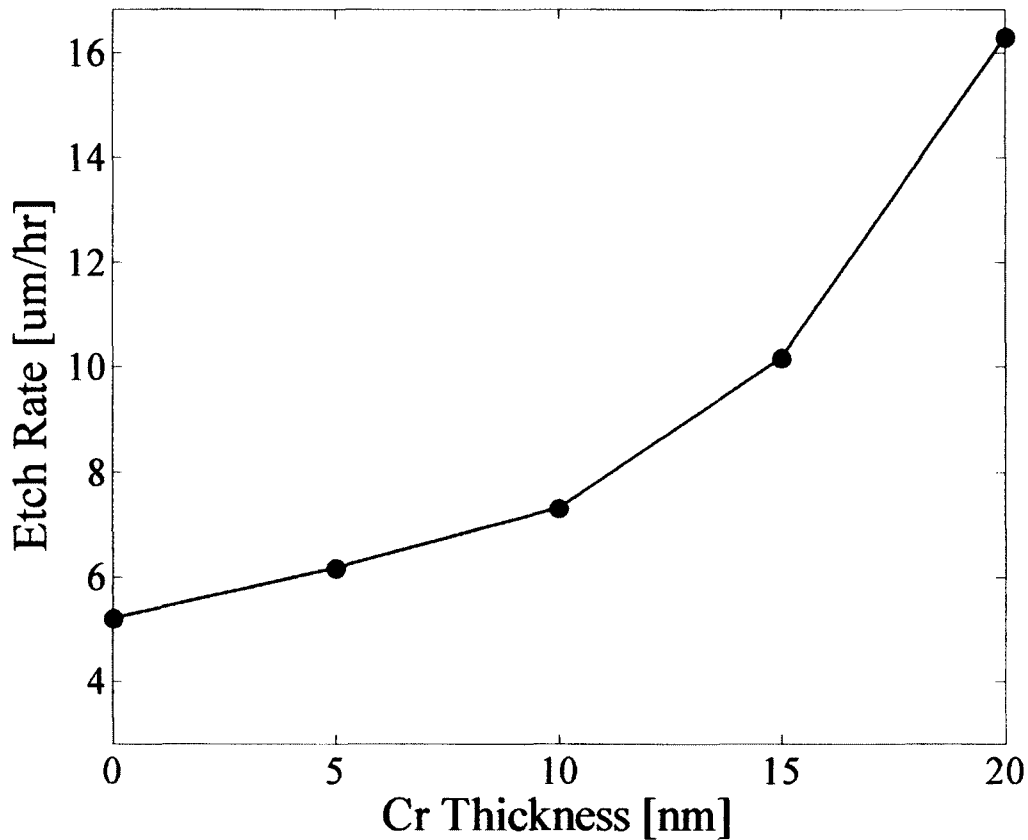


Figure 4.10 Etch Rate Vs Thickness of Cr Thin Film.

Figure 4.10 shows that the etch rate of the quartz crystals can be varied by increasing or decreasing the Chromium thin film thickness. Thereby allowing the etch rate of the quartz crystals to be increased by increasing the Chromium thin film thickness. The experiment conducted used a laser power of 1.5W with the laser beam focused with a 2mm spot size. The power densities used in these experiments are not high enough to etch the quartz crystals without a wet etchant.

Figure 4.10 shows that in fact the Chromium thin film is absorbing the laser radiation. If the quartz crystal, Chromium thin film and etchant did not absorb the laser radiation no etching would take place. The quartz/thin film interface absorbs the laser radiation creating a temperature gradient, which in turn heats the etchant that causes the

etch rate to increase. When the Cr thin film thickness increases the etch rate of the quartz will increase due to the Cr thin film absorbing more energy and heating the etchant to a higher temperature. This higher temperature increases the etch rate of the quartz crystal. With the thin film it is possible to etch the quartz crystals with the laser and etchant in a one step process.

4.6 Modeling of Laser Assisted Process

This section will cover modeling the Laser Assisted process in order to verify that the etch mechanism of laser absorption is the key component of the Laser assisted process. The quartz crystals were modeled in Comsol Multiphysics through the Louisiana Tech University license in Nethken Hall Room 209. The quartz crystal along with the Chromium thin films will be modeled using finite element analysis. The finite element modeling is to be used to model the laser interacting with the quartz crystal with chromium thin film while in contact with the etchant. To simulate the temperature gradients the laser causes and how it thermally conducts throughout the sample. During the experimental research it has been observed that if the laser is focused down to a spot size of 0.5mm, the surrounding area (area not being irradiated) has a much lower etch rate. For example a sample etched at 3W focused down to a spot size of 0.5mm, the etch rate of the irradiated area was around 25 μ m/hr, whereas the surrounding part of the sample still in contact with the etchant but not the laser radiation the etch rate was less than 1 μ m/hr. Therefore, the simulation will be able to show the temperature gradients created during the laser assisted wet etching of the quartz crystals.

4.6.1 Laser Heating Modeling Theory

This section will detail out the overall theory of laser assisted wet etching of quartz crystals. The first part of this section will cover the Drude-Lorentz model for dielectrics and metals. With the final part of this section will discuss Fourier's law of heat conduction in one dimension.

This model explains how dielectrics and metals interact with electromagnetic radiation. As discussed in Chapter 3, quartz crystals have a band gap of 9eV, which corresponds to a wavelength of 137 nm. Therefore the 808nm radiation will not excite electrons in the valence band enough to move across to the conduction band. However, the impurities that are present allowing for current to move through the quartz crystal during etching with irradiated with x-rays can also be used for etching the crystal with 808nm radiation. For instance Aluminum and Lithium both impurities present in quartz have absorption coefficients at 808nm higher than Chromium. Therefore, it is reasonable to believe that these impurities influence the etch rate when irradiated with the 808nm radiation.

The interaction between the Chromium thin film and 808nm radiation can be explained by the Drude-Lorentz model. By taking the inverse of the absorption coefficient will yield the penetration depth (δ). For bulk chromium, the penetration depth of 808nm laser radiation is 18.6 nm. For metals when deal with optical radiation, the main mechanism for optical absorption is due to the free electrons present [108]. These free electrons can become energized by EM radiation, this allows for the electrons to collide with phonons in the lattice of the metal structure [108]. These collisions allow for

the heating up of the metal. Another important parameter for metals when dealing with optical absorption is the plasma frequency, represented by the following equation:

$$\omega_p = \sqrt{N_e e^2 / m_e \epsilon_0} \quad (4.12)$$

The electron density is represented by N_e , e is the electric charge, m_e is the mass of the electron, and ϵ_0 is the permittivity of free space [108]. Any optical frequency below the plasma frequency will either be reflected or absorbed [108]. Any optical frequency above the plasma frequency will be transmitted through the metal [108]. For this dissertation, the optical frequency of the EM radiation is below the plasma frequency of chromium. However, some of the 808nm radiation will be transmitted through the chromium thin film due to the thickness of the film being smaller than the optical penetration depth.

This final section will discuss the basic theory of thermal conduction in one dimensional geometries. Thermal conduction, which is also known as Fourier's law can be expressed in one dimension as:

$$q = -kA \frac{dT}{dx} \quad (4.13)$$

where k is the thermal conductivity of the material, A is the cross-section area of the material, dT/dx represents the temperature gradient created. Another important parameter of heat transfer is the flow rate of heat, which can be expressed as follows:

$$\frac{dQ}{dt} = -kA \frac{dT}{dx} \quad (4.14)$$

where dx is the distance the heat flows, and dT is the temperature change between those two points for the amount of heat flowing through the material in a given time dQ/dt . For quartz its thermal properties are not isotropic, therefore it is of importance to look at heat transfer in more than one dimension.

4.6.2 Comsol Simulation Setup

This section will go through the various steps to setup the finite element method (FEM) simulation. The sections that will be covered on the FEM modeling of the laser assisted process are as follows: Laser Profiles, Mesh Refinement, and Heat Transfer Module. The heat transfer module will cover the thin film and quartz crystal interface; also it will cover the convective cooling that takes place in the laboratory vent hood and HF etchant in contact with the crystal.

This section will discuss briefly the equations used to model the Gaussian and Top-Hat profiles of the laser during the etching process. The Gaussian laser profile is a simple 2D Gaussian distribution on a xy-plane [109]. The following equation shows the Gaussian profile of the continuous wave laser:

$$Q(x, y, z) = Q_0(1 - R_c) \frac{A_c}{\pi\sigma_x\sigma_y} e^{-\left[\left(\frac{(x-x_0)^2}{2\sigma_x^2} + \frac{(y-y_0)^2}{2\sigma_y^2}\right)\right]} e^{-A_c z} \quad (4.15)$$

where Q_0 is the input power of the laser, R_c is the reflection coefficient, A_c is the absorption coefficient of the material, the x and y components are for the 2D Gaussian distribution [109]. Figure 4.11 shows the Gaussian distribution of the laser applied during modeling.

Gaussian Distribution

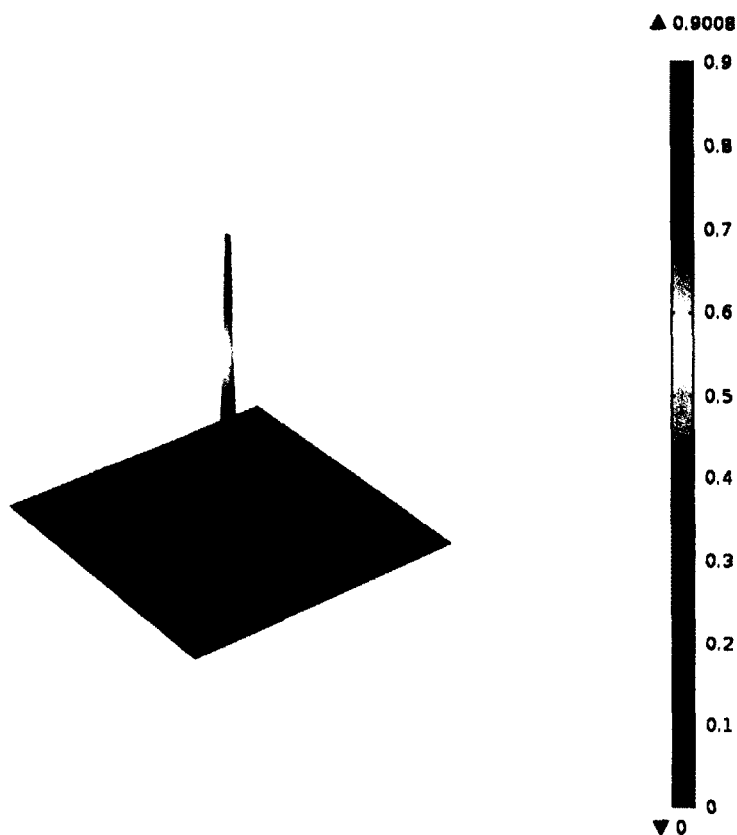


Figure 4.11 Gaussian Profile of Laser Modeled In Consol.

The next distribution to look at is the Top-Hat profile; this is created with the super-Gaussian equation. The super-Gaussian equation used was the following:

$$Q(x, y, z) = Q_0(1 - R_c) \frac{A_c}{\pi\sigma_x\sigma_y} e^{-\left[\left(\frac{(x-x_0)^2}{2\sigma_x^2} + \frac{(y-y_0)^2}{2\sigma_y^2}\right)^n\right]} e^{-A_c z} \quad (4.16)$$

where n is the variable controlling the Gaussian distribution [110]. As n is increased the Gaussian distribution flattens out creating a Top-Hat profile. The Top-Hat profile used during the modeling is shown in Figure 4.12.

Top-Hat Distribution

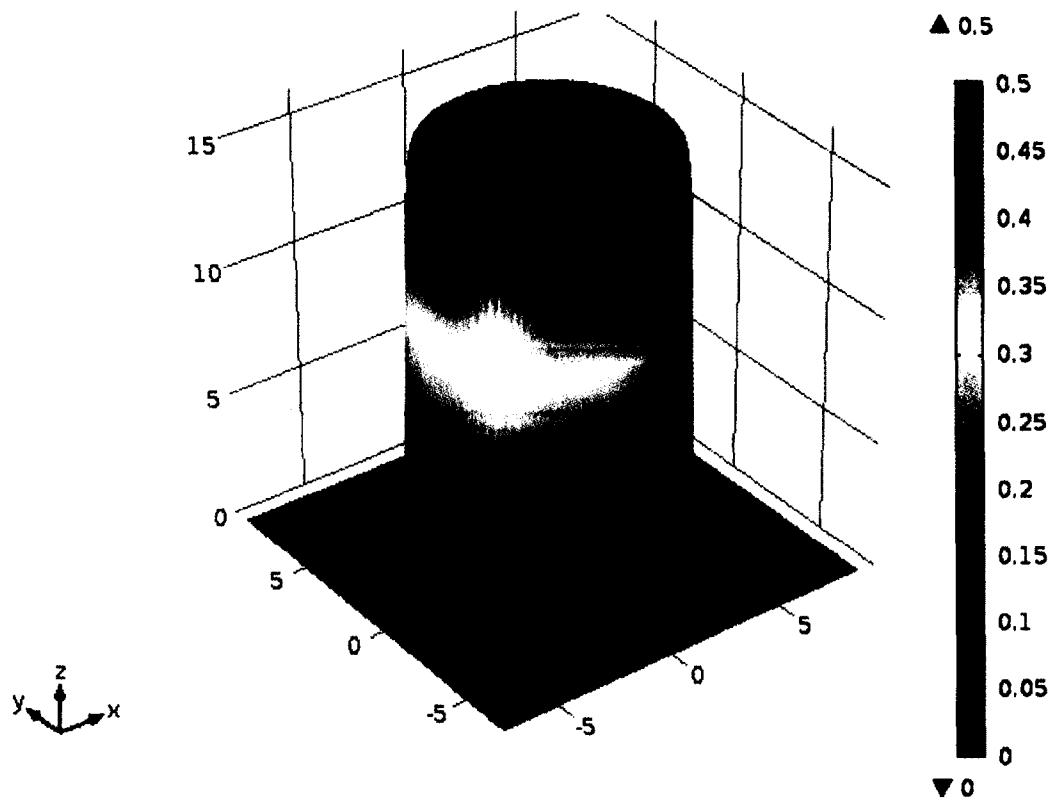


Figure 4.12 Top-Hat Profile of Laser Created Diffuser Optics Modeled in Comsol.

The model using the equations in finite element software follows what was seen in experimental results, where the TopHat profile has an intensity roughly half of the Gaussian profile.

The most important aspect to modeling in a finite element program is the meshing. The finer the mesh, the final results will be more accurate and detailed. The problem with a fine mesh is the longer computational times required. The finite element mesh that was created allows for the most accurate data and fastest possible computation times. The type of element used during all of the simulations was the triangle, due to the fact that the irradiated area is a circle. The triangle element shape allows for solutions to

converge due to the geometry used for the laser is circular. Figure 4.13 shows the mesh that was used for most of the modeling.

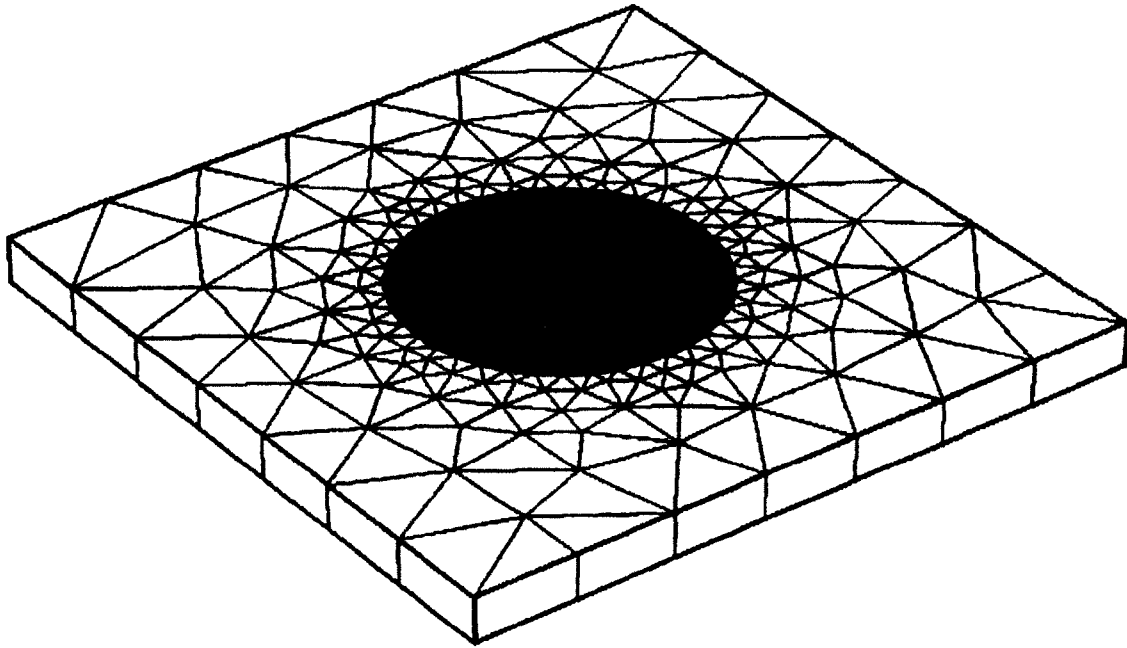


Figure 4.13 FEM Mesh of Quartz Crystal

The next aspect of this section will discuss the different variables that can be adjusted in the heat transfer module in Comsol. Heat transfer can be broken down into conduction, convection and radiation. For this work all three of these areas are of importance. Conduction comes into play from the heat being produced through radiation in the Chromium thin film flowing through the quartz crystal into the etchant on the backside. Convection is produced by the etchant in contact with the backside of the crystal and by the hood that the etchant holder is placed. The etchant holder is in the hood for safety concerns due to the hazardous nature of heating hydrofluoric acid. Radiation is from the chromium thin film and the quartz crystal absorbing the photons emitted from the laser. Heat transfer equations in fluids and solids will be discussed.

The first heat transfer equation to be discussed is the heat transferred in fluids. For a 3D model the heat equation for fluids is as follows:

$$\rho C_p \frac{\partial T}{\partial t} + \rho C_p \mathbf{u} \cdot \nabla T = \nabla \cdot (k \nabla T) + Q \quad (4.17)$$

The important terms in Equation 4.16, are as follows: ρ is the density (kg/m^3), C_p is the heat capacity of the fluid at a specific pressure, k is the thermal conductivity of the fluid, \mathbf{u} is the velocity field of the fluid, and Q is the heat source in the system [111]. The next important equation used for modeling is the heat equation for solids. The 3D model of the heat equation for solids is the following:

$$\rho C_p \frac{\partial T}{\partial t} - \nabla \cdot (k \nabla T) = Q \quad (4.18)$$

The main difference between the heat equation for fluids and solids is the velocity field [111]. For both equations the steady state solution eliminates the first term. The steady state solution for solids follows:

$$\nabla \cdot (k \nabla T) = Q \quad (4.19)$$

The reason for the first term to eliminate is the fact that the temperature is at steady-state, therefore it is not changing and the derivative term goes to zero [111]. For this dissertation work we will look at the transient stages of heat transfer as well as the steady-state, therefore both set of equations are of importance.

The next set of equations to discuss involve convective cooling. Convective cooling takes place by having the etchant in contact with the backside of the quartz crystal and by the air movement in the hood. As stated previously the etchant holder was placed in the chemical hood for protection from HF acid vapors. The main equation used in COMSOL for convective cooling is the following:

$$-\mathbf{n} \cdot (-k\nabla T) = h(T_{inf} - T) \quad (4.20)$$

where T_{inf} is the temperature of the fluid away from the boundary and \mathbf{n} is the normal vector of the boundary [111]. Comsol allows for the ability to model various convective cooling parameters. There are four methods for modeling convective cooling and are as follows: External Natural, External Forced, Internal Natural, and Internal Forced. The internal natural convective cooling was chosen for both the etchant in contact and the air flow from the chemical hood. Why was natural convection selected? Forced convection is used when a mechanical or some external force such as a fan creates the flow in the substance [111]. Natural convection is used when the convection is created by a variation in temperature and the expansion that occurs in the liquid. The heat transfer coefficient h , for the internal natural convective cooling in a narrow chimney (circular tube) is represented by the following equation:

$$h = \frac{k}{H} \frac{1}{128} Ra_D \quad (4.21)$$

where Ra is Rayleigh's Number, D is the tube diameter, H is the height of the tube, k is the thermal conductivity of the fluid. Rayleigh's number for the convective cooling geometry for a cylinder can be expressed as follows:

$$Ra_D = \frac{g |(\partial\rho/\partial T)|_p |\rho C_p| T - T_{ext} |D^3}{k\mu} > 10^9 \quad (4.22)$$

where g is the acceleration of gravity (9.81m/s^2), ρ is the density of the fluid, C_p is the heat capacity of the fluid, μ is the dynamic viscosity [111].

The chromium thin films were modeled using the highly conductive layer present in Comsol. It was used due to the difficulty of modeling macro-size elements combined with nanometer thin films. Meshing problems occur when the mesh elements from the quartz crystal and the chromium thin film are combined due to converging problems

when the highly conductive layer option is not used. The converging issues make it impossible to accurately mesh the combination of the two structures that have large aspect ratios. Therefore another solution was sought after and found by using the highly conductive layer option in Comsol. There are two requirements in order to use the highly conductive layer option. The first requirement is that the material being modeled (as a highly thermal conductive layer) is considered a thin film in respect to the substrate layer [111]. The quartz crystals used in this work were 500 μm thick and the thickness of the chromium thin films ranged from 5 to 20 nanometers. The quartz crystal is orders of magnitude larger than the chromium thin film therefore it meets the first requirement. The second requirement is that the material must be a better thermal conductor compared to the substrate material [111]. Chromium has a thermal conductivity of at least 5X larger than quartz. The thermal conductivity of chromium is 93.9 W/(m·K) and quartz largest thermal conductivity (quartz is anisotropic) is 12.1 W/(m·K). Therefore this model meets both of the requirements needed to use the highly conductive layer option. The following equation is the heat transfer equation used for highly conductive layers [111]:

$$d_s \rho_s C_s \frac{\partial T}{\partial t} + \nabla_t \cdot (-d_s k_s \nabla_t T) = q_{\partial\Omega} - q_{\Omega} + d_s Q_s = -q_s. \quad (4.23)$$

The variables in the first term in the equation are as follows: d_s is the thickness of the conducting layer (m), ρ_s is the density of the conducting layer (kg/m^3), and C_s is the heat capacity of the conducting layer ($\text{J}/\text{kg}\cdot\text{K}$) [111]. The second term of the equation variables are the following: The boundary condition for the general heat flux equation is the following: where ∇_t represents the del operator that will be projected on the plane of the conductive layer, and k_s is the thermal conductivity of the conductive layer [111].

The rest of the variables of the equation are as follows: $q_{\partial\Omega}$ is the heat flux of the area around the conductive layer, q_{Ω} is the heat flux from the conductive into the domain, q_S is the net outward heat flux dissipated through the conductive layer, and the final variable Q_S is the internal heat sources placed on the conductive layer [111].

The final part of this section will compare the experimental and modeled results obtained for the etch rate versus the chromium thin film thickness. Previously shown in Figure 4.10 shows the experimental etch rate of the quartz crystals with varying layers of chromium thickness. Modeling in Comsol was conducted in order to prove the hypothesis that the quartz crystal and chromium thin film absorbed the laser's energy to increase the etch rate of quartz. The parameters discussed in the previous sections were used to simulate the etching experiment. Not all models are exact or represent all variables that could be present in an experiment. The goal is to use the variables that are known during the experiment and implement them into the model. The results obtained are shown in Figure 4.14 compared with the experimental results.

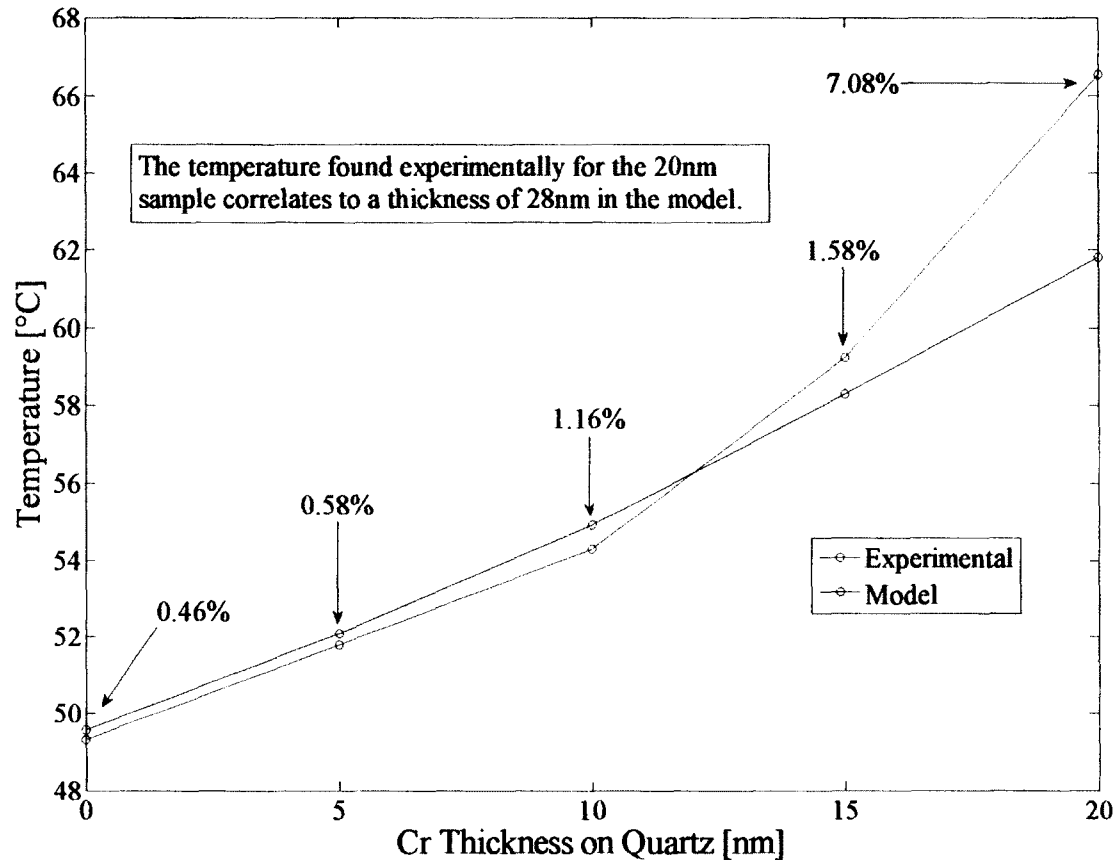


Figure 4.14 Experimental Results versus Model Created in Comsol Multiphysics™

The etch rates have been changed to the etchant temperatures obtained by the Arrhenius equation. The modeling results do not completely match up with the experimental results. The modeling results for 5nm and 10nm are less than one percent different from the experimental results (temperature difference less than 0.5°C). The difference occurs with the 15nm and 20nm thin films. By varying the model thickness it was found that the temperatures line up with chromium thicknesses of 18 and 28nm.

Attempts were made to measure the thickness of the chromium thin films. The thickness measurement previously reported was taken from the deposition monitor on the e-beam deposition system. A Filmetrics F10-RT model, which can measure the thickness of a thin film, has a thickness measurement range of 15nm to 70μm and has a thickness

accuracy of 2nm (thickness accuracy is based on material properties) [112]]. This instrument can be used for the 15nm and 20nm chromium thin films, however, it is not possible to get an accurate reading on the 5nm and 10nm samples. The F10-RT uses spectral reflectance/transmittance to measure the thickness of thin films [112]. A white light source with wavelengths ranging from 380 to 1050nm is shine at an angle of incidence of zero (perpendicular to the sample). The instrument then measures the reflectance and transmittance over the entire spectra of light irradiating the sample. Measuring the thickness using spectral reflectance/transmittance is based on the following equation:

$$2d * \sqrt{n^2 - \sin^2 \theta} = i * \lambda \quad (4.24)$$

where d is the thickness of the sample, n is the index of refraction, θ is the angle of incidence, i is the number of fringes in wavelength range measured, and λ is the wavelengths used for the calculation [112]. For the Filmetrics F10-RT, the angle of incidence is zero therefore the equation can be reduced to the following:

$$2dn = i\lambda \quad (4.25)$$

the expression has been simplified, however, for complex structures it might be nessercery to used elliposmetry to find thickness of the thin film [112]. Table 4.3 shows the data taken for the 5nm, 10nm, 15nm, 20nm samples.

Table 4.3 Film Thickness Measurements

| Thickness Taken From E-Beam[nm] | Measured Transmission [%] | Measured Thickness [nm] | Goodness of Fit |
|---------------------------------|---------------------------|-------------------------|-----------------|
| 5 | 21.881 | 17.08 +/- 9.55 | 0.9640 |
| 10 | 20.574 | 23.95 +/- 9.88 | 0.9799 |
| 15 | 14.402 | 22.42 +/- 6.16 | 0.9699 |
| 20 | 13.903 | 17.88 +/- 9.78 | 0.9723 |
| 20 | 13.619 | 24.31 +/- 9.89 | 0.9806 |

The thicknesses shown in the first column are taken from the deposition monitor on the e-beam system. The measured transmission shows good agreement that as the sample thickness increases the amount of light transmitted through the sample decreases. The measured thickness is found through the F10-RT software, which uses Equation 4.23 to calculate the thickness of the thin film, and this is rated by the goodness of fit. The goodness of fit shows that the data measured has some of the highest accuracy possible. This shows that the data taken is as good as the instrument can produce. Table 4.3 shows that the 5 and 10 nanometer samples have the most light transmitted through them, however, the F10-RT system can only accurately measure down to a 15nm thin film thickness. The measured thickness cannot be verified for the 5 and 10 nm thick samples. For the 5 and 10 nm thick samples, the experimental data was less than 1% difference from the model created in COMSOL. The variation of the measured thickness using the F10-RT system is the non-uniformity of the sample. This non-uniformity could be roughness or any variation in the thickness of the thin film [112]. The model created in COMSOL predicts that the actual chromium thin film thickness for the 15nm and 20nm samples should be 18 and 28nm. Table 4.3 shows that the measured thickness from the F10-RT system falls within the 18 and 28nm thickness for the 15 and 20nm samples.

The deposition or measurement of thin films with nanometer thicknesses can be skewed by a number of variations. One possible explanation in the difference in the thicknesses of the metal thin films can be explained by the equipment used to deposit the chromium films onto quartz. The chromium thin films were deposited onto the crystals by a CH industries E-beam system. The e-beam system has a slow deposition rate initially, and the rate increases with time as the material being deposited heats up. Also,

when the correct amount of material is deposited on the substrate, a mechanical shutter closes in order to stop the deposition. The lower film thicknesses are most likely more accurate due to the slower deposition rate. The thicker the metal thin film being deposited the less accurate the thin film thickness, due to a higher deposition rate and the mechanical shutter taking seconds to close completely. Another possible reason for the discrepancy is the model itself. Various changes could be made in the future of the model to give an even more detail of the laser etching system. The next section will show the results obtained by the laser etching system.

4.7 Etch Results and Discussions

This section will cover the results obtained by etching quartz crystals with an 808nm laser while the samples are in contact with hydrofluoric acid. The goal of this section is to show the possibilities of using a laser in conjunction with wet etching. The experiments conducted in this section did not use the PID control system detailed in Chapter 2. The reason for not including the PID control system is to allow for the determination of the maximum potential of increasing the etch rate of the quartz crystals using a high power laser. However, the high power laser or even multiple high power lasers can be incorporated into the PID control system shown in Chapter 2.

4.7.1 Etching with Gaussian LASER Profile

The first results to be discussed involve creating a Gaussian beam profile using a Fresnel lens. Gaussian beams as discussed previously produce a very high power density, which allows for an increase in the etch rate of the crystals without heating the

entire solution. Figure 4.15 shows the results obtain by varying the power density of a Gaussian beam and its effect on the etch rate of quartz while being wet etched.

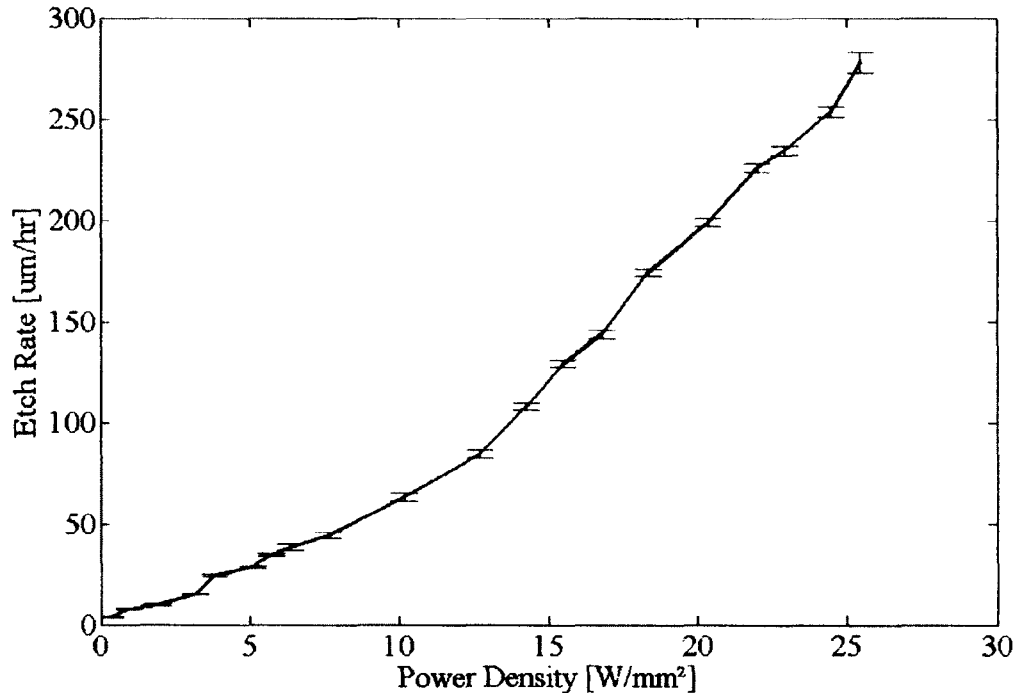


Figure 4.15 Etch Rate Data From Gaussian LASER Profile

The results from the Gaussian beam profile etching shows that with a 5nm sample it is possible to increase the etch rate of quartz crystals to 278 $\mu\text{m/hr}$. The etch rate might seem high for quartz processing, however, Vallin *et al* proved that at 130°C the etch rate was 324 $\mu\text{m/hr}$ with a variation [27]. Also, with our process by varying the power density from 0.3 W/mm^2 to 25 W/mm^2 allows for a variation of the etch rate from 3.8 $\mu\text{m/hr}$ to 278 $\mu\text{m/hr}$. However, it is possible to have a slower etch rate by cutting the laser's power and allowing the sample to be etched at room temperature. The standard deviation at 278 $\mu\text{m/hr}$ was found to be $\pm 5.256 \mu\text{m/hr}$ and the uncertainty (relative standard deviation) was found to be 1.89%. The lower the percentage indicates a lower

variability in the data. This proves that the process is repeatable even at the higher end of the power densities used in this research. Vallin *et al* using the standard chemical wet etching with a bulk solution of saturated ammonium bifluoride heated the traditional way they had an etch rate variation of 30.06 $\mu\text{m/hr}$ [27]. The PID controller was not used in these experiments in order to obtain the fastest etch rate possible. Therefore just using a stable laser as the heating source and no control system allows for less variability than heating a bulk solution on a hot plate. Using the PID controller two different resonators can be brought within 30ppm, which translates to a variation of 0.014 μm (14nm).

The statistical analysis of the experiments were conducted to understand the repeatability of each experiment. This is useful just from a research perspective but also it is even more important on the industrial level. The standard deviation was incorporated to quantify how much variation was present between experiments while keeping the same number of variables. The uncertainty is the relative standard deviation, which is the mean divided by the standard deviation and is expressed in a percentage. The uncertainty is an expression for displaying the precision and the reliability of an experiment. Therefore taking our example of standard deviation of 5.256 $\mu\text{m/hr}$, we have an uncertainty of 1.89%. Now comparing our processing to Vallin *et al*, which used wet etching only, and they had an uncertainty ranging from 11.25% to 16%. Therefore for these experiments the variability is quite low, however in order to be able to process the quartz crystals on an industrial scale it requires better control. This is done by allowing the etching system to control the heating mechanism through the PID controller to vary the voltage input to the laser. As discussed in Chapter 2 the system measures the

frequency and decides whether to decrease or increase the power of the laser based on the difference between frequencies.

The statistical analysis shows that there are some variations in each experiment. The possible variables that contributed to each experiment having some variation will now be discussed. One mechanism discussed previously that could explain some of the variations in etch rate is due to the chromium thin films thickness. Another variation of the etching setup is the power stability of the laser system used. Table 4.4 shows data taken using Coherent LabMax-TO power meter.

Table 4.4 Laser Standard Deviation Measurements

| LASER Power Stability | |
|-----------------------|--------------------|
| Power | Standard Deviation |
| 1W | $\pm 2.3\text{mW}$ |
| 2W | $\pm 3.6\text{mW}$ |
| 3W | $\pm 4.1\text{mW}$ |
| 4W | $\pm 5.5\text{mW}$ |
| 5W | $\pm 6.2\text{mW}$ |

The Coherent LabMax-TO power meter takes measurements for 20 seconds. The variations in power are quite small, but equating this to power density the 6.2 mW would

be for the maximum etch rate around 31 mW/mm^2 or 3.1 W/cm^2 . The second variation comes from placing the etching system inside of a fume hood. This was done due to the health hazards produced from hydrofluoric acid. As can be seen from the Figure 4.15, as the etch rate increases the standard deviation becomes larger. This makes sense since the faster the etch rate, the more variations that would occur in the cooling down cycle. A quick study was conducted to test the cooling and heating rates in various situations, this data is presented in Table 4.5.

Table 4.5 Heating and Cooling Measurements

| Testing of Heating and Cooling Rates In and Out of Chemical Hood | | |
|--|-----------------------------------|-------------------------------|
| Quartz Only | Outside Chemical Hood [°C/min] | Inside Chemical Hood [°C/min] |
| Heat Rate | 0.55 | 0.45 |
| Cool Rate | 0.55 | 0.45 |
| Holder and Quartz | | |
| Heat Rate | 1.67 | 1.75 |
| Cool Rate | 1.67 | 1.75 |

As can be seen from Table 4.5, the chemical hood has a profound effect on the cooling and heating rates. To sum up this section, there are a couple of mechanisms that can cause the variation reported. The variation between quartz crystals is at its apex,

because a small amount of impurities will typically always be present. The variation of the thin film thickness is difficult to control to an even better accuracy.

The etch profiles created with the Gaussian shaped laser beam will be shown and discussed. Figure 4.16 shows an image of a profile that was obtained using a KLA Tencor Alpha-Step 500 Surface Profiler after the quartz crystal was etched.

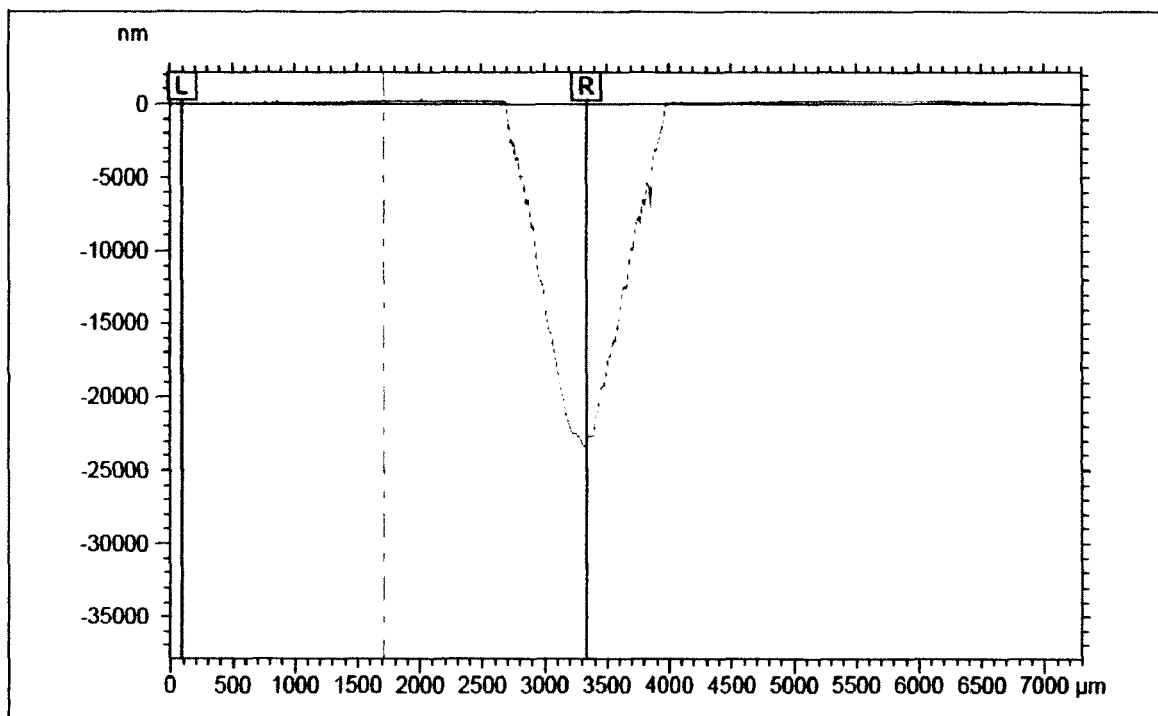


Figure 4.16 Gaussian Etch Profile with Power Density of 4 W/mm^2

The quartz sample shown in Figure 4.16 was wet etched while being irradiated with the 808nm laser. It shows the selectiveness of this etching system, the entire profile shown was in contact with the wet etchant. However, as clearly shown the only part that was etched was the area being irradiated with the 808nm laser. This data shows that the laser is selectively heating specific areas of the crystal. Figure 4.17 shows the etch

profile using a Gaussian beam that was taken using a Hitachi S-4800 Field-Emission Scanning Electron Microscope (SEM).

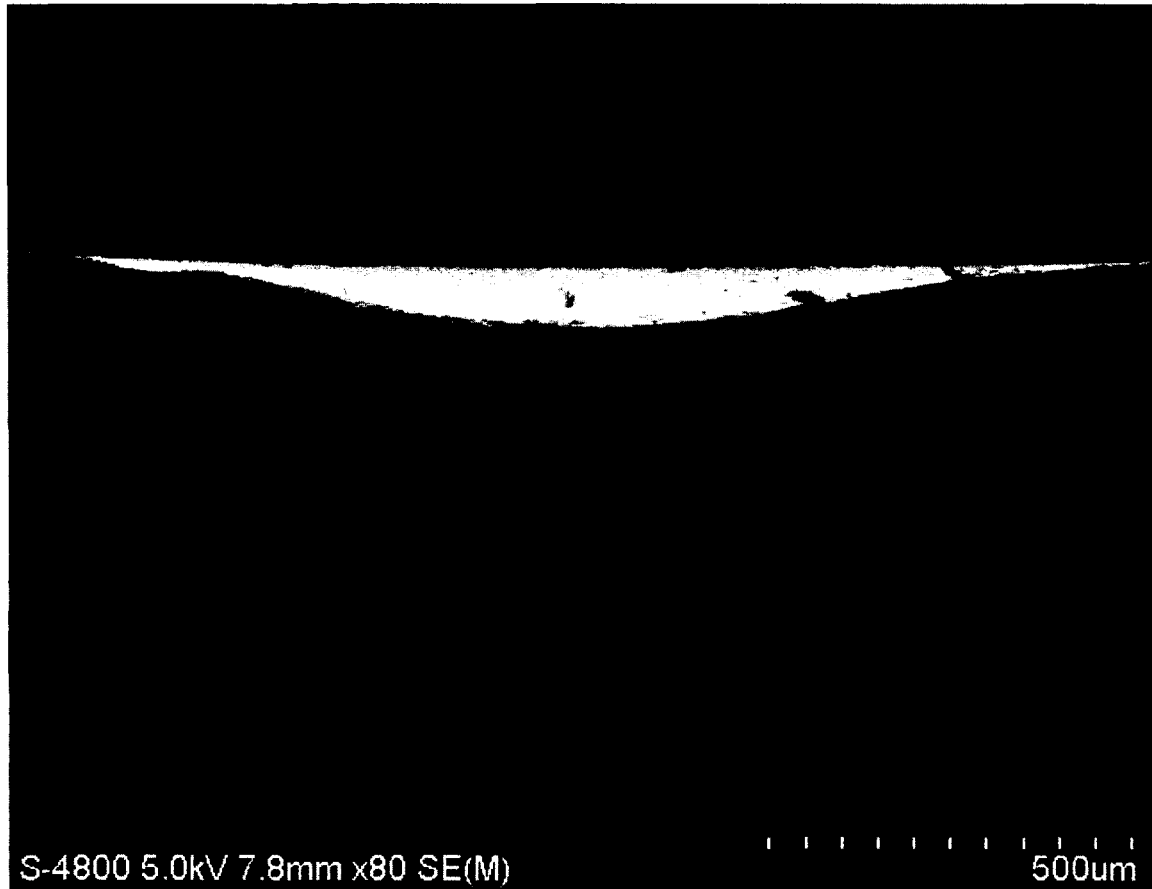


Figure 4.17 SEM Image of Quartz Sample Etched with Gaussian Beam.

The previous results were with a Gaussian beam; however, it is also practical to etch the quartz crystals to have shapes besides the Gaussian profile. In order to create a functional quartz crystal resonator, the laser beam was varied using a diffuser in order to create a Top-Hat profile.

4.7.2 Etching with Top-Hat LASER Profile

The Top-Hat profile was created as discussed in Section 4.4.2 of this dissertation. The Top-Hat profile allows for etching planar profiles. The power density of a Top-Hat is roughly half of a Gaussian profile compared at the same laser power. Therefore for the Top-Hat profile to get decent etch rates compared to the Gaussian profile, a thicker Chromium thin film was deposited on the crystal. Figure 4.18 shows the first results on using a Top-Hat profile irradiating a quartz crystal with a Cr thin film thickness of 15nm.

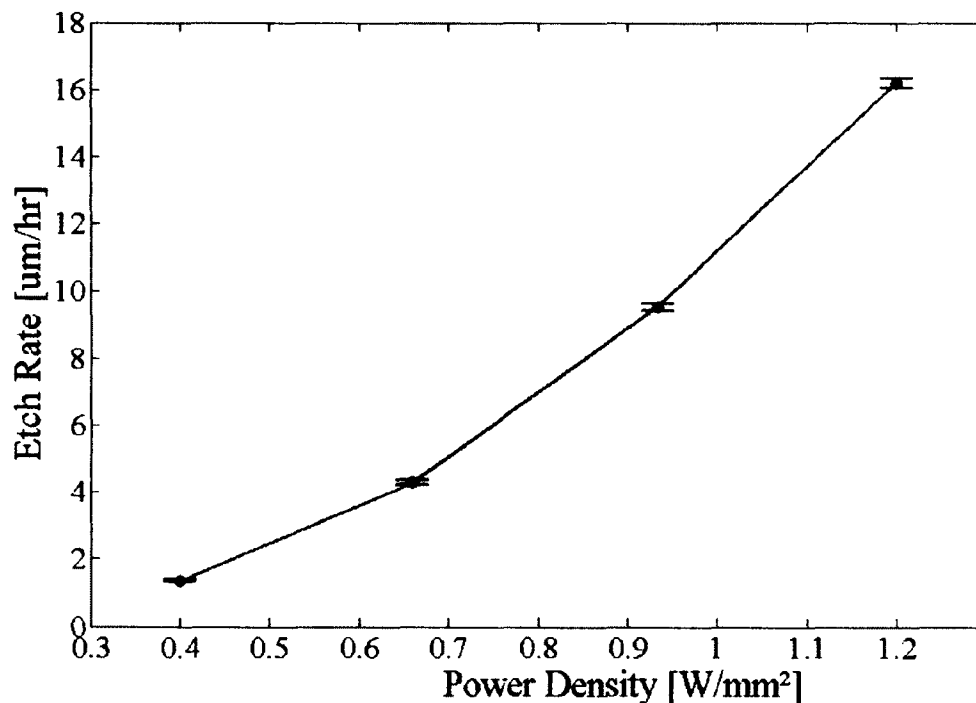


Figure 4.18. Top-Hat Profile, Cr Thickness of 15nm.

Figure 4.18 shows a nice steady increase in the etch rate versus the power density when using the optical diffuser. Also, shown in Figure 4.18 is the error bars, they are extremely small which occurs as the etch rate is slower. Compared to the Gaussian laser

profile is slow and requires a thicker absorber. The benefit of the Top-Hat is the nice profile it produces allowing for a better pattern to create a quartz crystal resonator. The Top-Hat profile can be used to create the commercial resonators, which are called inverted mesa structured crystal resonator. The next experiment was to see what effect an increase in the absorbing material thickness would have on the etch rate. The next set of experiments involved using a Cr thin film thickness of 20nm. Figure 4.17 shows the results of the 20nm Cr thin film thickness using a Top-Hat etch profile.

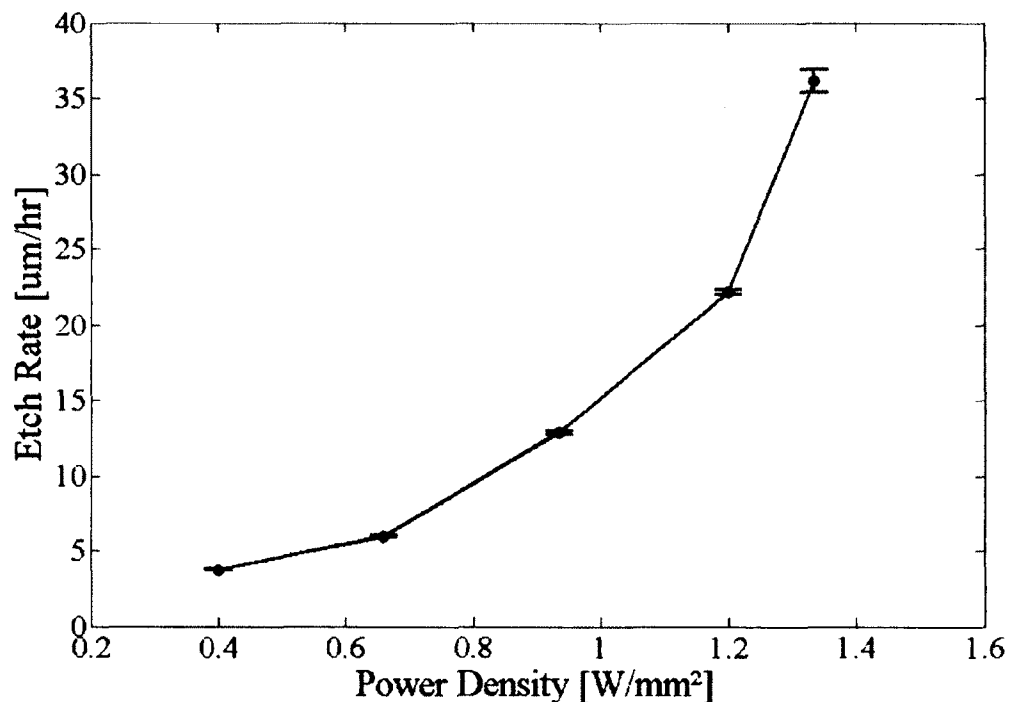


Figure 4.19. Top-Hat Profile with Cr Thin Film Thickness of 20nm

Figure 4.19 shows that an increase of the Cr thin film thickness increases the etch rate. The maximum etch rate was around 35 $\mu\text{m/hr}$, with an absorption layer of 20nm. The Top-Hat profile is ideal for producing resonators, therefore to increase the etch rate

various mechanisms can be changed. First the thickness of the Cr thin film can be deposited on the crystal. The thicker the Cr thin film, the higher the chance of the laser photons being reflected back. Another way to increase the etch rate could be from changing the metal thin film material. For instance tungsten has a higher absorption of 808nm laser radiation, therefore it could be deposited at 20nm. This would theoretically increase the etch rate without further increasing the thin film thickness. Another mechanism would be to change the laser wavelength from 808nm to 1064nm or even a laser with an ultraviolet wavelength. This change would also require an investigation into the absorbing material for the new laser wavelength. Then the final mechanism to change in this etch system is the power density of the Top-Hat profile. The optical diffuser equation shows that the closer the diffuser is to the sample being etched will increase its power density. Therefore the entire system can be redesigned to The next figures shown in this dissertation are SEM images of etch profiles created using the Top-Hat laser profile. Figure 4.20 is a SEM image of an etch profile using the Top-Hat profile.

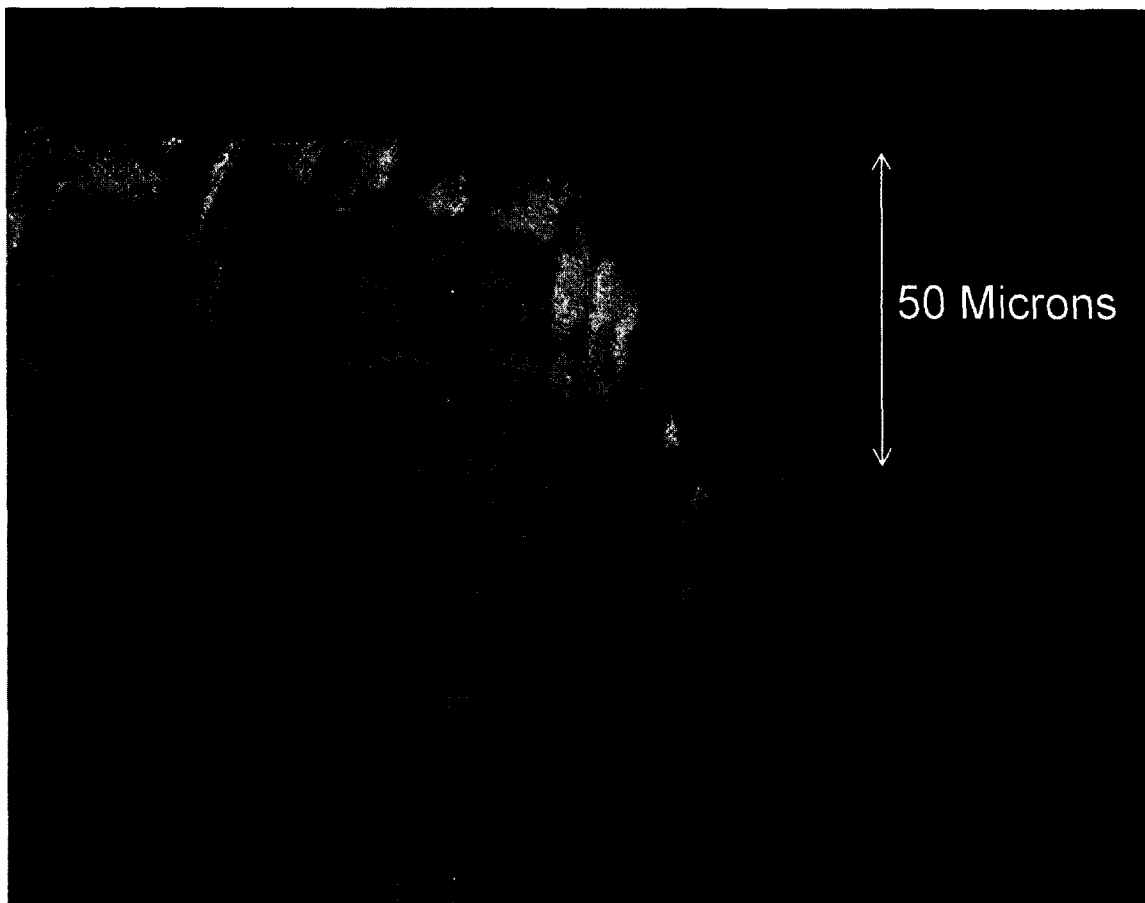


Figure 4.20 Side Image of Top-Hat Etch Profile

Figure 4.20 shows an SEM image with an etch depth of 50 μm . As can be seen from this image is the sidewalls created from Top-Hat profile. The next step was to image a quartz crystal that had been etched with the Top-Hat laser profile with an etch depth larger than 50 μm . Figure 4.21 shows an SEM image of a sample that has an etch depth larger than 100 μm .

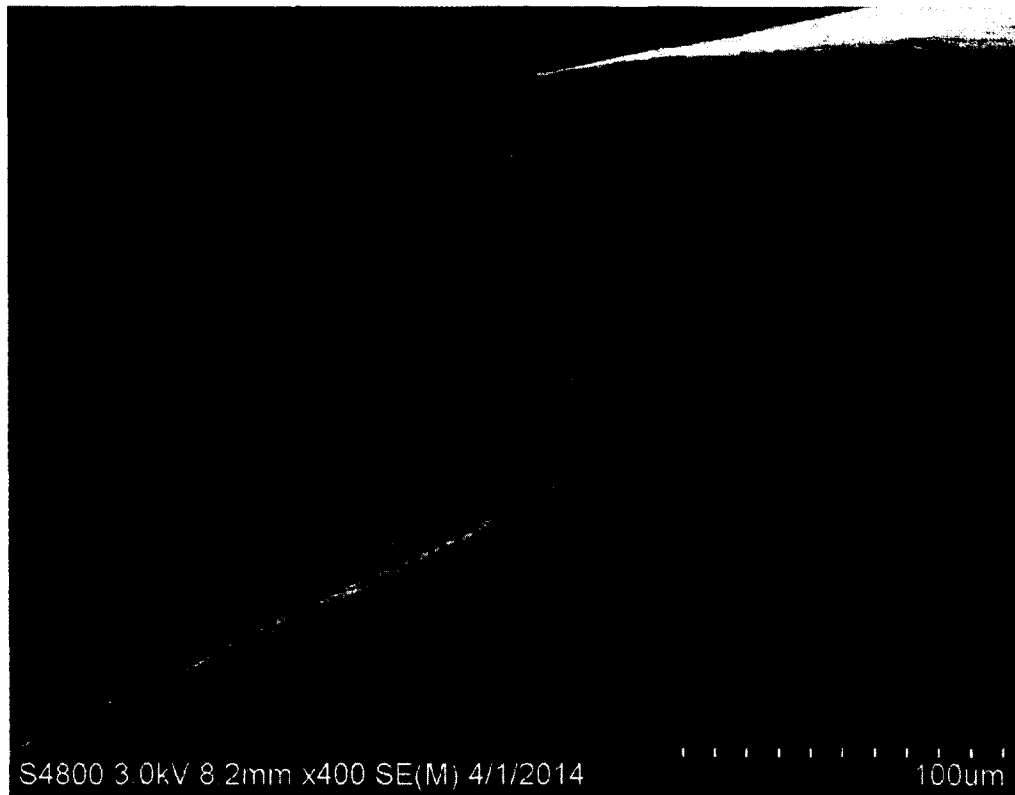


Figure 4.21 SEM Image of Top-Hat Profile with Etch Depth Larger than 100 μm

As can be seen from Figure 4.21 shows a sidewall etched with the Top-Hat beam profile with an etch depth greater than 100 μm . The etch setup is as follows: the quartz sample is in contact with an o-ring limiting where the hydrofluoric acid etchant, then the laser heats up the material thereby heating the etchant. The o-ring is circular giving the circular etch profile appearance. Figure 4.22 shows another SEM image using the Top-Hat laser profile from a more side view with a larger etch depth than Figure 4.20.

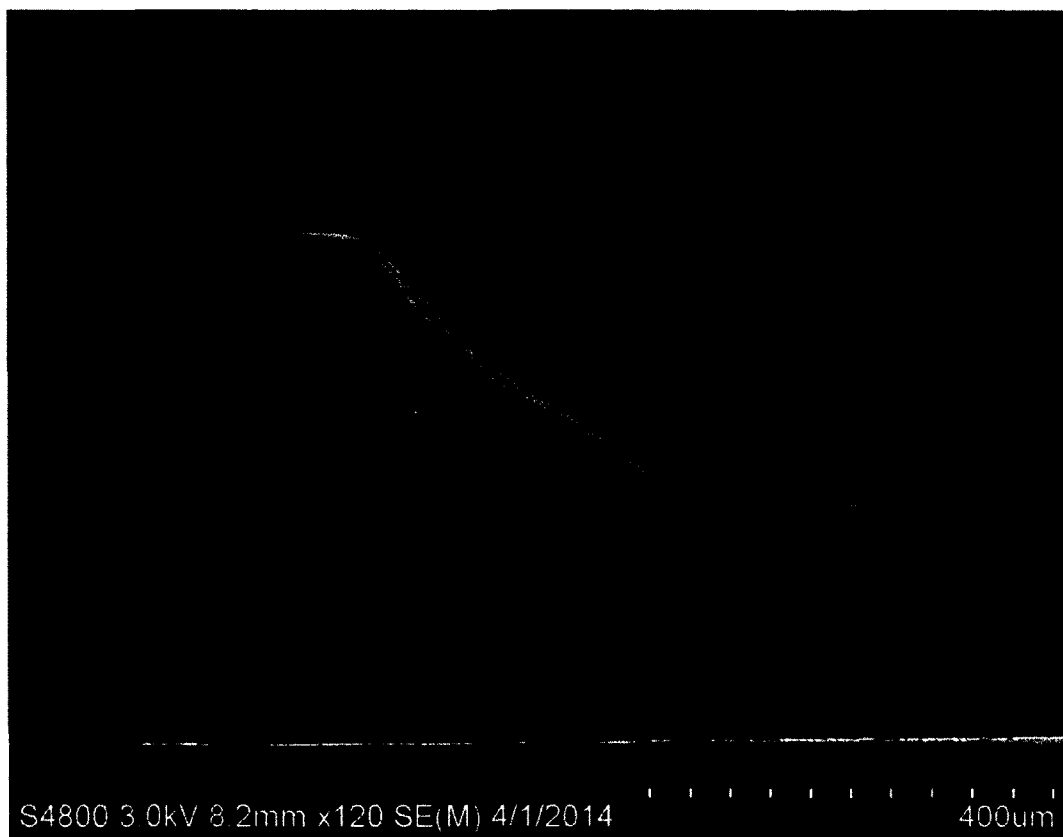


Figure 4.22 SEM Image of Top-Hat Profile Side View

Figure 4.22 shows an SEM image of the side view of a sample etched with the Top-Hat laser beam profile. The next two figures to be shown are presented to show the sidewalls that can be produced from the Top-Hat profile. Figure 4.23 is the SEM showing the back of the sample sidewalls.



Figure 4.23 SEM of Sidewalls

This image allows for showing the steepness of the sidewalls being created by the laser etching system. The etch depth of this sample is a little greater than 200 μm . These steep sidewalls with a flat middle portion (called vibration area) allow for the creation of a quartz crystal resonator.

4.8 Conclusion and Discussions

This chapter focused on the rapid etching of quartz crystals using a laser. Etch profiles of Gaussian and Top-Hat were created with the laser and optical elements. It is possible to increase the etch rate of the quartz crystals by using a laser in conjunction with an absorbing material on the quartz crystal. The etch rate of the quartz crystals can

be varied from $3.8 \mu\text{m/hr}$ to $278 \mu\text{m/hr}$. The etch rate can be lowered by decreasing the power density further or by allowing the material to be etched at room temperature. By combining the results from this chapter using the higher power densities along with the PID controller from Chapter 2 it is possible to etch multiple resonators on the wafer scale. By combining this into one laser system it will be possible to create resonators using the Top-Hat profile and getting them all within $\pm 30\text{ppm}$ of each other. The wafer level laser etching system with multiple lasers is shown in Figure 4.24.

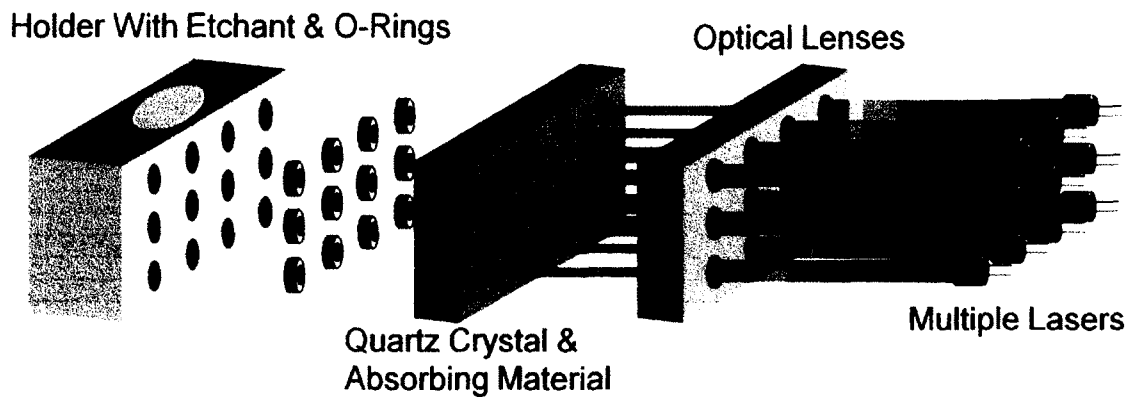


Figure 4.24 Wafer Level Laser Etching System.

Figure 4.24 shows one conceptual idea for implementing the wafer level laser etching system. This system can be used for piezoelectric materials when used with the PID control measurement system. Any insulating material can be etched this way with the absorbing material. Through this chapter I have shown that it is possible to vary the etch rate of quartz crystal using only an off-the-shelf laser.

APPENDIX A
CREATION OF QUARTZ CRYSTAL RESONATOR

This chapter will discuss the application of quartz using the technologies presented in this dissertation. Quartz crystal resonators that were created with our quartz technologies will be presented in this chapter.

A.1. Types of Devices Possible with Quartz Crystals

The various devices that are possible to create with quartz crystals will be discussed briefly. The main applications of piezoelectric materials are the following: Filters, Gyroscope, and Resonators. Quartz crystals can be used as electronic filters, however, due to its low piezoelectric coupling factor they are not the best choice. The next type of device created with quartz is the gyroscope. With increase interest in the consumer market for motion capture gaming, gyroscopes must be decreased in size. Smart phones are implementing MEMS-gyroscopes stabilizing the camera to get quality pictures, and also allowing the screen to change orientation as the smart phone is rotated. Therefore MEMS-gyroscopes are one of the top selling MEMS devices at the moment. Quartz crystals were the first MEMS-like gyroscope devices on the market, in the way of tuning forks. Epson Toyocom was one of the first to commercialize quartz crystal gyroscopes. According to Epson Toyocom their quartz crystal gyroscopes offer a wide range of advantages such as: signal stability, low aging rate, manufacturing reproducibility, and good temperature stability [2].

The final of the devices to be discussed but the main focus of this dissertation is the quartz crystal resonator. Quartz crystal resonators are located in almost every electronic device. Typical smart phones have four to five quartz resonators, typically applications in phones are as frequency references for sending and receiving calls, or as

frequency references for GPS. The main reason that quartz crystals still dominate the market is due to its great properties shown in Table 1.2.

A.2 Quartz Crystal Resonators Created By Laser Assisted Wet Etching Technology

This section will cover some of the results of quartz crystal resonators created using the laser assisted wet etching technology discussed in Chapter 4. There are various structures that can be created in quartz crystals such as mesa and inverted mesa structures. The resonators created for this dissertation are all inverted mesa structures. The inverted mesa structure is the more practical of the structures to be created using the laser assisted wet etching technology.

The first set of resonators created was to show how the size of the device affects the quality factor and signal strength. Therefore these resonators are all created with the same fundamental frequency. The signal strength of the quartz resonator must be strong enough in order to stand out from background systems. If the resonator does not have a large enough signal, the sending signal will lock on to the background system. The quality factor of the quartz crystal resonators fabricated is quite low compared to the commercially available resonators. This can be explained in Equation 1.3, where the quality factor of the resonators is limited by the largest losses in the overall system. Table 1.4 lists the typical problems where large losses are incurred for quartz crystal resonators. The mounting setup of the resonators created for this dissertation is considered the point of where the largest amount of energy is being lost, thus degrading the quality factor.

The drive level for all crystals measured is at 0dBm which is about 10 microwatts of power applied to the resonators, which is not large enough to affect the frequency of the resonators. The geometry of the crystal and electrode could be a possible problem in the quality factor of the resonator. Typically commercialized resonators have beveled edges which allow more energy to be trapped inside the crystal. Without the equipment and proper safety mechanisms in place the quartz crystals were not beveled. Other than being beveled most quartz crystal resonators are circular and not square or rectangle like the crystals created in this dissertation.

Table A.1 shows the results for resonators with different shapes and sizes but all have a fundamental frequency around 3.334MHz with an average variation of 50Hz. The table shows the feature size of the resonators, the quality factor, signal strength, and unwanted spurious modes.

Table A.1 Quality Factor Versus Size

| Feature Size | Frequency | Quality Factor | Signal Strength | Spurious Modes |
|--------------|-----------|----------------|-----------------|----------------|
| 4mmX4mm | 3,339,193 | 30,440 | -33.863 dB | 4 |
| 8mmX8mm | 3,340,750 | 58,445 | -35.824 dB | 1 |
| 12mmX12mm | 3,339,000 | 49,393 | -35.211 dB | 1 |

The three resonators in Table A.1 have silver electrodes that were coated via dc sputtering. The larger feature sizes were best at eliminating the spurious modes. The 12mm and 8mm sample had the better signal strength as well as a higher quality factor

than the 4mm sample. The 8mm sample size was chosen due to it being the best when compared to all attributes measured for the resonator.

Inverted mesa resonators that were created using the laser assisted wet etching process will now be discussed. The inverted mesa resonators were created in frequencies ranging from 3.5MHz to 11.2MHz. All the resonators have roughly 100nm thin films of silver on each side of the quartz crystal used as electrodes. The reason for choosing silver as the electrode material will be discussed briefly. A figure of merit can be given to electrode material as the ratio of the electrical conductivity to density [40]. The figure of merit for commonly used metals as quartz electrodes is shown in Table A.2.

Table A.2 [40] Figure of Merit for Electrode Material

| Electrode Material | Density [kg/m ³] | Electrical Conductivity [10 ⁻⁷ S/m] | Figure of Merit S*m ² /kg |
|--------------------|------------------------------|--|--------------------------------------|
| Aluminum | 2,700 | 3.8 | 14,074 |
| Copper | 8,920 | 5.9 | 6,614 |
| Silver | 10,400 | 6.2 | 5,962 |
| Gold | 19,300 | 4.5 | 2,332 |
| Palladium | 12,023 | 1 | 832 |
| Platinum | 21,090 | 0.94 | 446 |

Aluminum is the best material to used as an electrode according to this figure of merit. Silver was used as the electrode due to its ease of dc sputtering. Aluminum oxidizes vary rapidly during sputtering and therefore requires a turbo pump for proper sputtering. The Denton Vacuum dc sputtering system on hand in the laboratory did not have a turbo pump. Silver had the best figure of merit of the electrode materials that could be sputtered without a turbo pump. Silver has a figure of merit double that of gold.

Figure A.1 shows an inverted mesa resonator's frequency versus gain magnitude (dB) response.

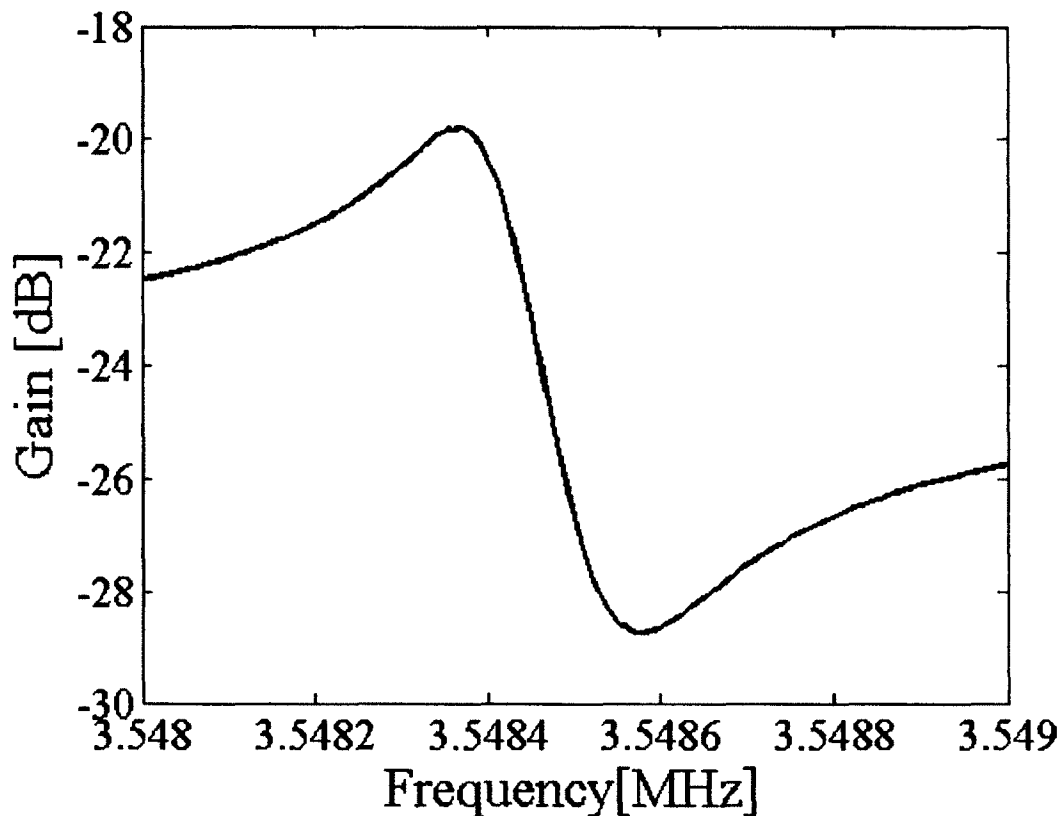


Figure A.1 Frequency Response of Resonator Etched by 30 μ m

The resonator response shown in Figure A.1 is a 500 μ m thick quartz crystal that has been etched using laser assisted wet etching process. The frequency can be calculated using Equation 1.5 from Chapter 1. For Figure A.1 the quality factor was measured to be 47,175 and a total signal strength of 8.970 dBm.

One of the problems with most metals is the fact that they do not bond with quartz crystals. Due to this problem, chromium and titanium 5nm thick layers are used as adhesion layers. Both chromium and titanium both require turbo pumps for sputtering;

therefore for quick experimentation they were not used. Silver and gold films less than 150nm will adhere to the quartz crystal without an adhesion layer. Figure A.2 is the same resonator; however, more silver has been added to it. It was calculated that the added mass was roughly a 15nm thick silver layer.

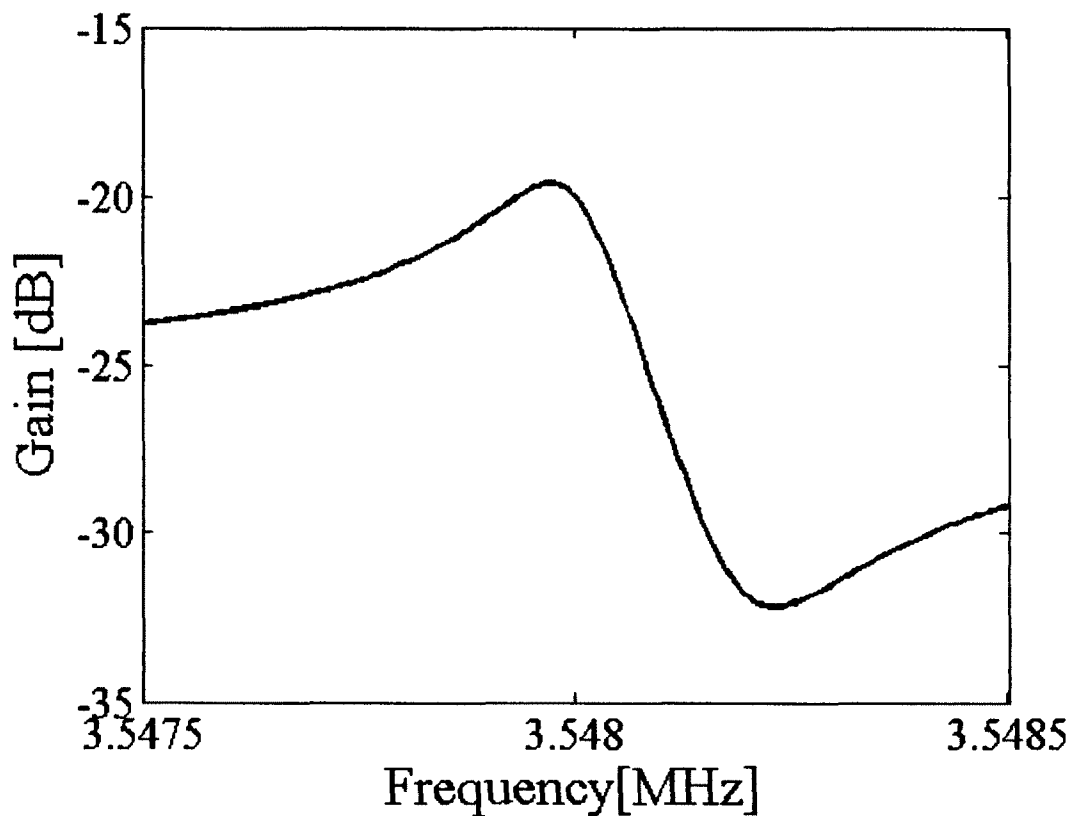


Figure A.2 Same Sample From Figure A.1 But with Added Electrode Mass

With the small amount of metal added to the quartz crystal resonator, there was a slight increase in quality factor (100) and there was a signal strength increase of 3.6dBm. The total signal strength for the new resonator with added mass is 12.591 dBm. This increase is significant in the fact that with only 15nm added electrode thickness the output of the resonator's signal increased more than double. Figure A.2 does not seem

larger due to the graph making it look distorted. Figure A.3 shows the comparison between the resonator with 100nm versus 115nm of silver electrode material.

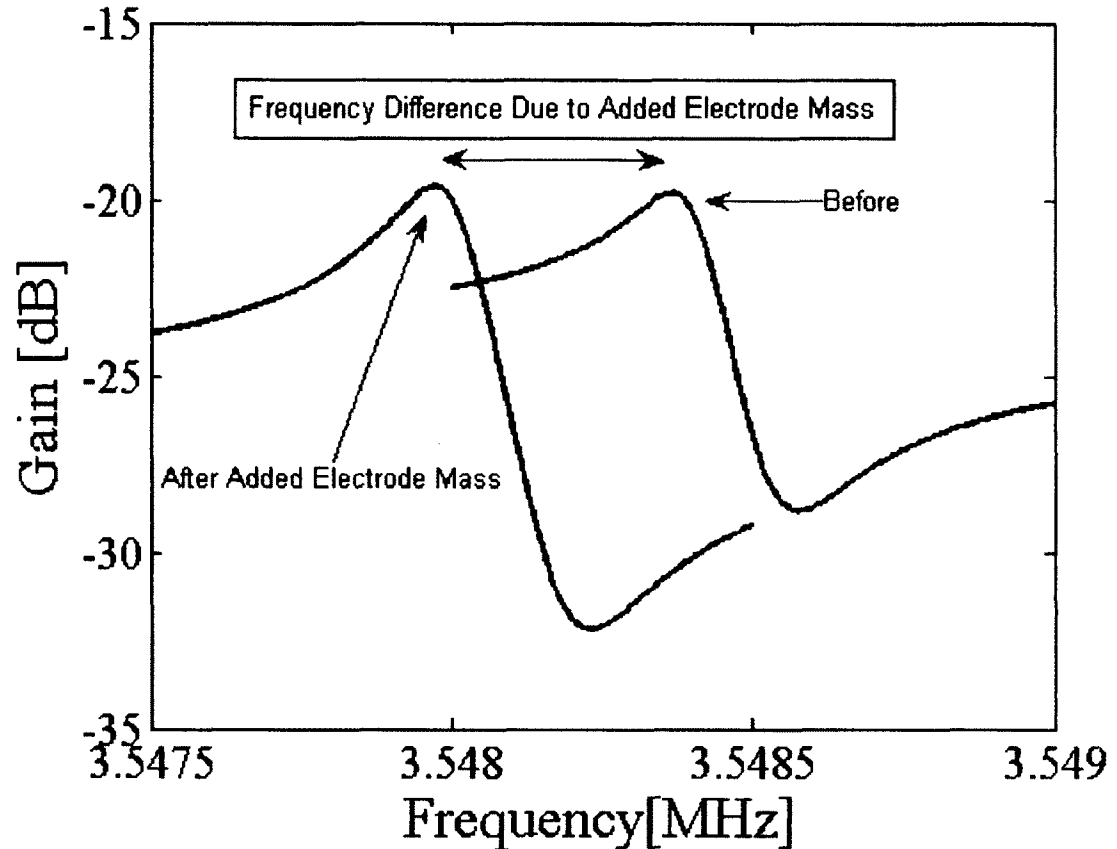


Figure A.3 The 3.5MHz Sample Compared Before and After Adding Addition Mass.

Figure A.3 clearly shows that adding electrode mass to the resonator will increase the signal strength and quality factor, while also lowering the frequency. The next step of this research involves increasing the frequency of the resonators produced. This is done by etching more of the quartz crystal, which follows the relationship expressed in Equation 1.5. The next couple of graphs are in the 4MHz range, which all still use silver as the electrode material. Figure A.4 shows an inverted mesa resonator response curve

with a center frequency around 4.4MHz, corresponding to an etch depth of 121 μm from the starting thickness of 500 μm .

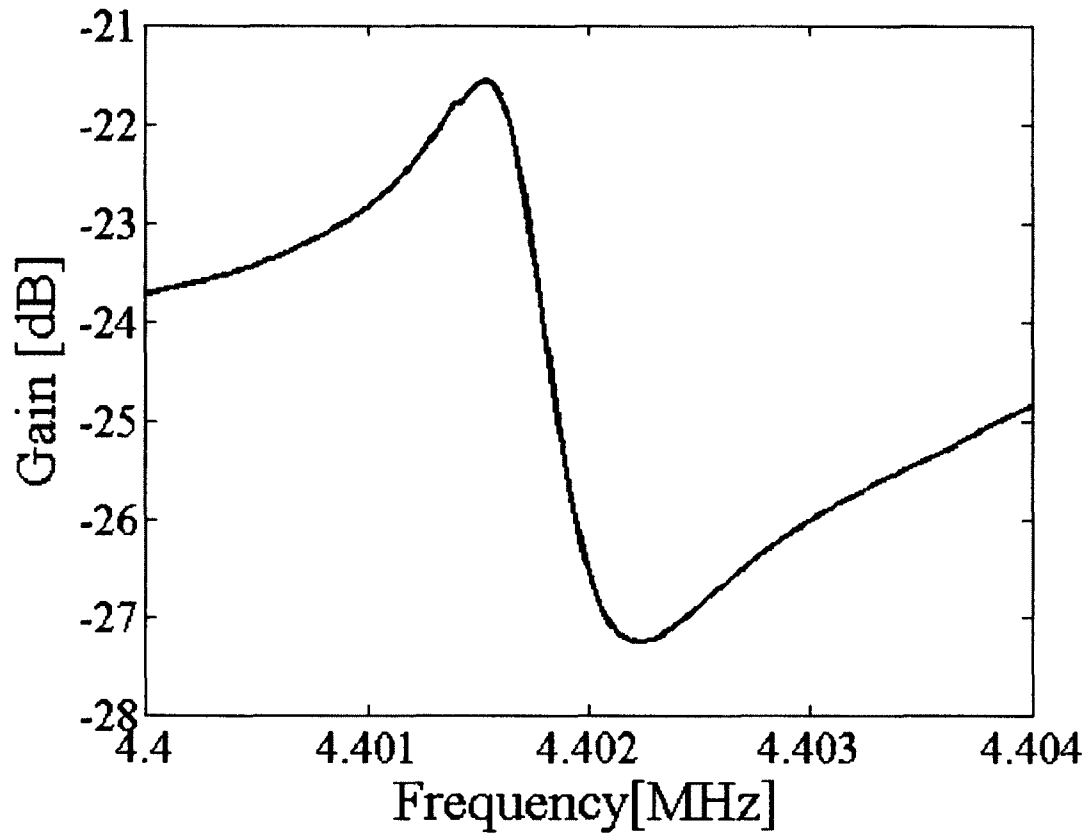


Figure A.4 Inverted Mesa Resonator at 4.4MHz

Figure A.4 had a quality factor of 16,156 with a signal strength of 5.684 dBm. All of the resonator plots show the great qualities of quartz crystals and why they are the preferred material for resonator applications. Even with a non-commercial holder for the crystals there is hardly any distortion. Figure A.5 shows a resonator with a frequency of 4.8 MHz.

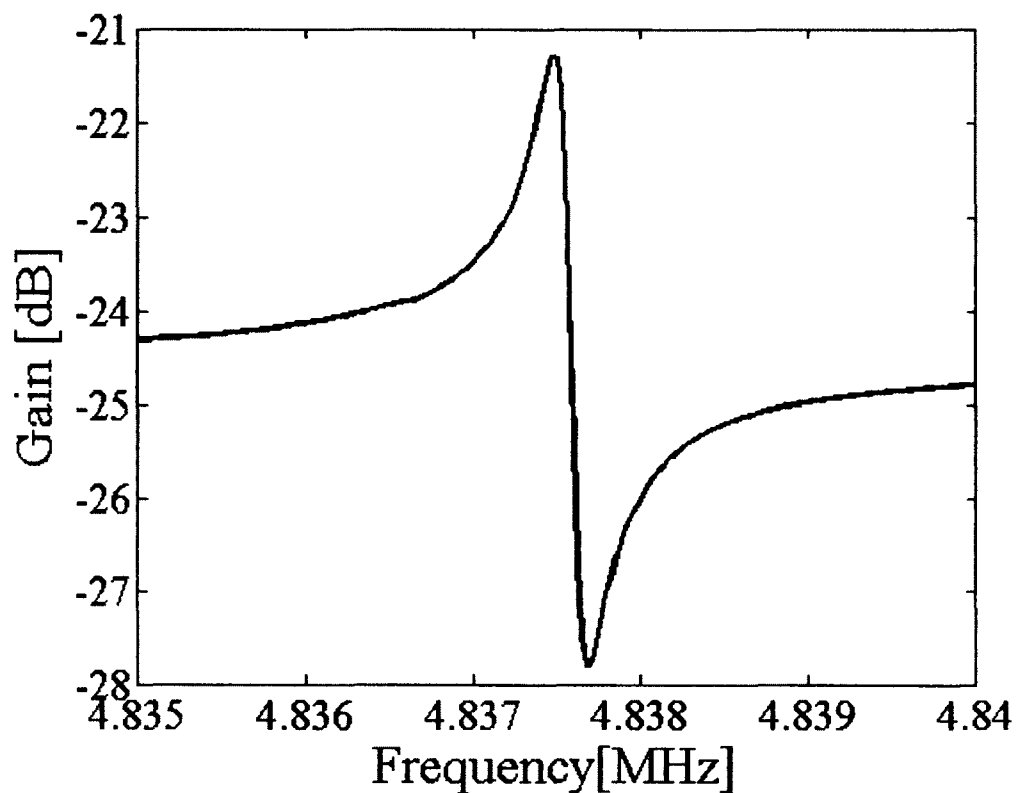


Figure A.5 Inverted Mesa Crystal Resonator

The properties of inverted resonator in Figure A.5 were a quality factor of 48,619 with a signal strength of 6.598 dBm. The next set of resonators to discuss are in the 5MHz frequency range. Figure A.6 shows an inverted mesa resonator at a frequency of 5.57MHz corresponding to a vibrating thickness of 300 μm , with the starting crystal thickness of 500 μm .

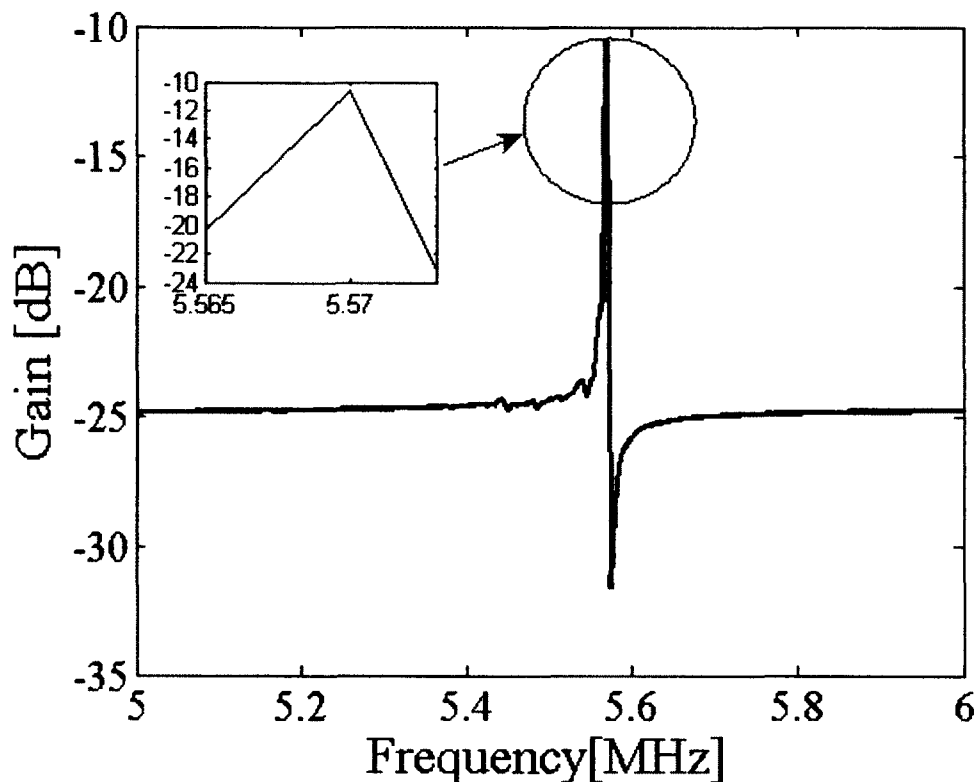


Figure A.6 5.57MHz Resonator with a Q factor of 29,077.

The 5.57 MHz inverted mesa resonator had a quality factor 29,077 with a signal strength of 21.065 dBm. The resonator shown in Figure A.6 had a very high signal strength, however, the quality factor is only 29,077. More electrode mass could be added to the resonator, or the electrode shape could be optimized in order to increase the quality factor. This researcher feels that improvement on the resonator holder system would eliminate a large amount of losses that occur in operation. Using a commercially designed holder system could allow for eliminating the large losses. The next frequency range to discuss of inverted mesa resonators created with the laser etching system is around 8 MHz. Figure A.7 shows a crystal resonator at 8MHz corresponding to a vibrating thickness of 207 μm .

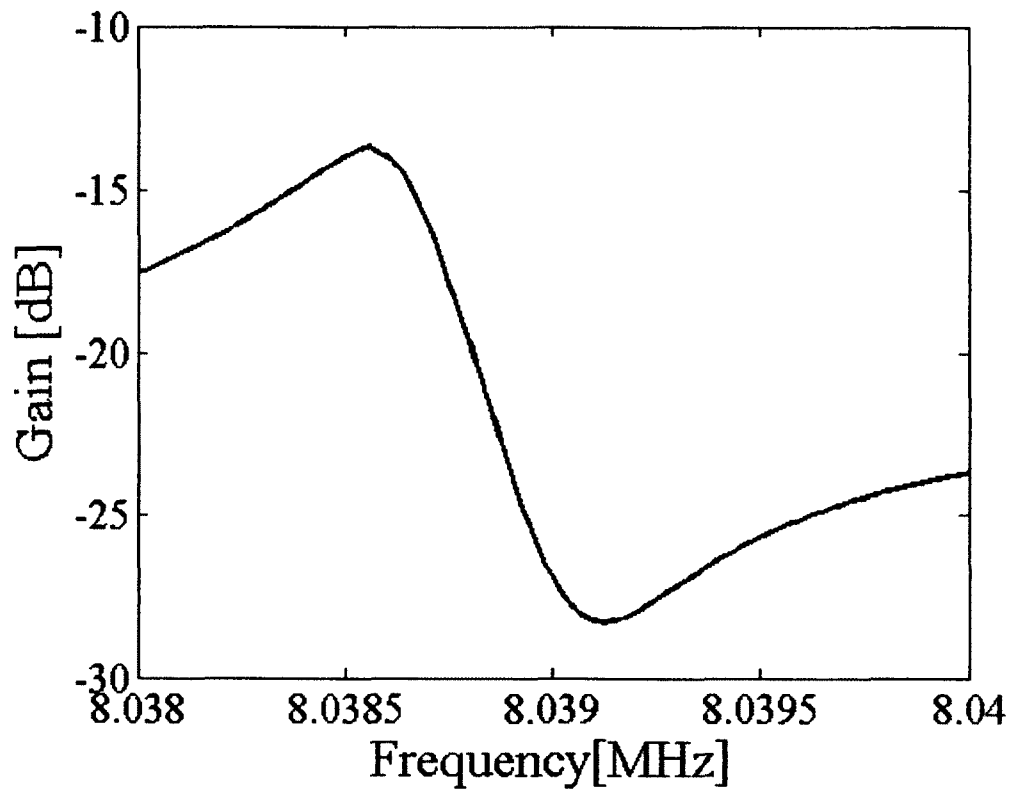


Figure A.7 8MHz Inverted Mesa Resonator

The 8MHz resonator shown in Figure A.7 had a quality factor 50,654 with a signal strength of 14.578dBm. Figure A.8 is the response of a 10MHz resonator sample with a vibrating thickness of 165 μm .

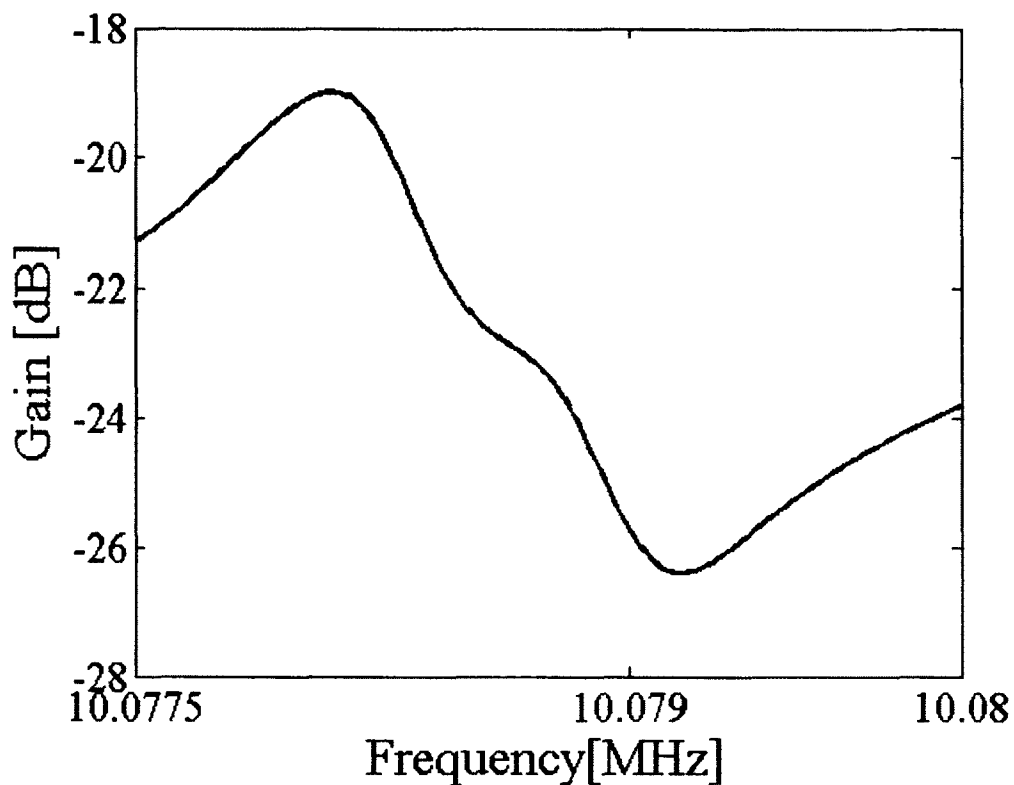


Figure A.8 10 MHz Resonator

The 10MHz crystal resonator had a quality factor 26,803, with a signal strength 7.397dBm. Once again all of these samples started with a initial quartz thickness of 500 μm . The thicker substrate gives more strength to the quartz crystals and allows for easier mounting. The final frequency of resonators created were in the 11 MHz range. The next two figures will show the sensitivity of the quartz crystals at 11MHz. Figure A.9 shows a 11.2 MHz crystal resonator with a vibrating thickness of 148 μm .

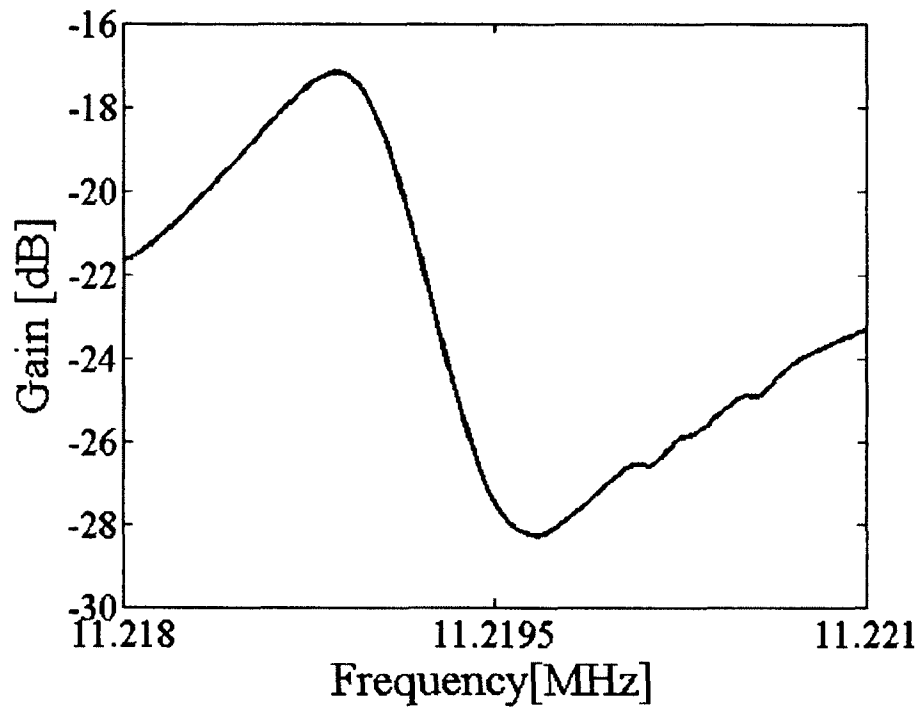


Figure A.9 11.2 MHz Resonator Before Added Mass

The 11.2 MHz had a quality factor of 40,0358 and a signal strength of 11.104dBm. Figure A.10 is the same resonator with added electrode mass.

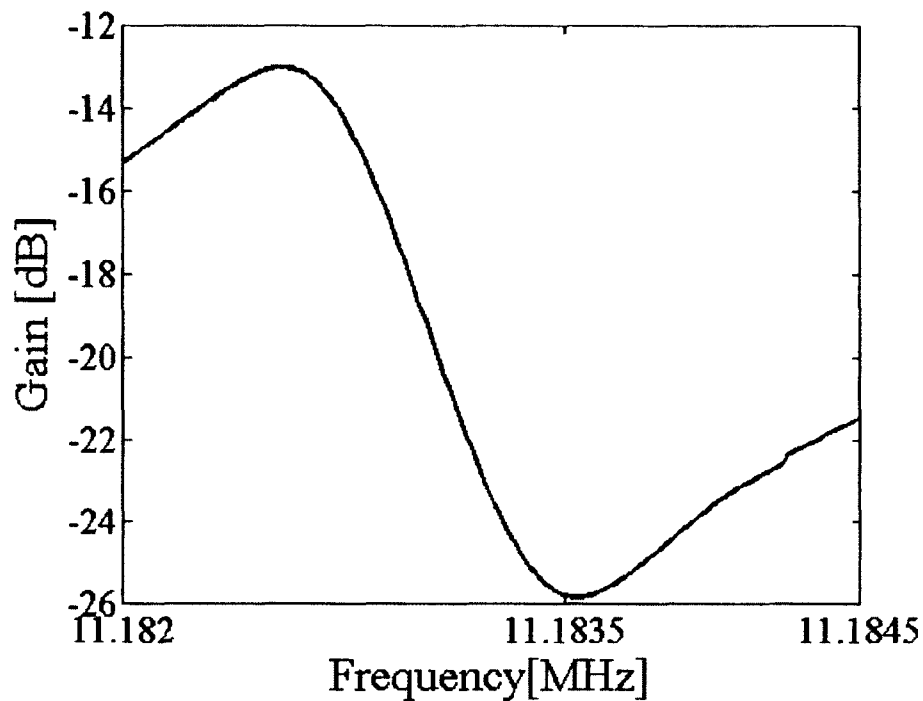


Figure A.10 11MHz Resonator with Added Mass

The results from the added mass of the resonator produced a decrease in quality factor down to 34,037. However, the signal strength was increased to 12.824dBm. The reason for the increase in signal strength is from increasing the amount of energy being trapped by the electrode. The decrease in the quality factor is due to increasing the impedance of the quartz crystal with the added mass of the electrode.

This section covered some inverted mesa resonators created using the laser etching process created in this dissertation. The frequencies ranged from 3.5MHz to 11.2MHz representing typical resonator frequencies used in the various devices. Further improvement can occur by changing the quartz resonator holder. As discussed previously, one poor mechanism can significantly lower the overall quality factor of the device. To further explain Equation 1.5, if a resonator had a quality factor an intrinsic quality factor of 100,000 and through holder losses the quality factor was 10,000, then

the maximum quality factor would be 9,091. Future work will include improving upon the holder system.

APPENDIX B
INCOHERENT LIGHT SOURCES

Chapters 2 and 4 show work that was carried out with coherent light sources (Lasers). Prior to the work in Chapter 4, the effects of incoherent light sources on the etch rate of quartz crystals was investigated. Coherent light sources have very narrow electromagnetic spectrum. The laser used in Chapter 4 had a wavelength of 808nm +/- 3nm. The coherence of lasers allows for the ability to be focused down to its diffraction limit. Also, coherent light is in phase, whereas incoherent light is out of phase. Incoherent light sources in this work have a broad electromagnetic spectrum. All of the incoherent light sources are off the shelf devices that can be easily found. This allows for increasing the etch rate of quartz crystals while maintaining the ability to keep the cost of each individual crystal equal to current market prices.

B.1. Quartz Resonator Fabrication using LEDs

The first set of experiments used an 850nm IR LED. In comparison to Laser diodes, LEDs are cheaper to fabricate due to their simple design. There are no resonant cavities or other optical elements located inside the LED. The main problem with LEDs is the fact that they have a very broad electromagnetic spectrum output. Another problem is the fact that LEDs are not collimated light sources. Collimated light sources can be focused down until they reach the diffraction limit. Since, LEDs are not collimated light sources and are therefore difficult to focus. However, experiments were conducted in order to test if it was possible to etch quartz crystals with LEDs.

The experiments were conducted with 850nm NIR LEDs. The etching setup is the same as the laser experimental setup except for using LEDs instead of using a laser. The 850nm LED built by OSRAM with the specifications shown in Table B.1.

Table B.1 Properties of LED

| | |
|--------------------|------------------------------|
| Wavelength | 850nm |
| Forward DC-Current | 100mA |
| Forward DC-Voltage | 1.5V |
| Radiant Intensity | Minimum at 100mA is 630mW/sr |
| Total Radiant Flux | 70mW |
| Viewing Angle | 6° |

The DC forward current and voltage are the recommended values to run the LEDs. An OceanOptics spectrum analyzer was used to measure the spectrum of the LED. The spectrum of the 850 IR LED is shown in Figure B.1.

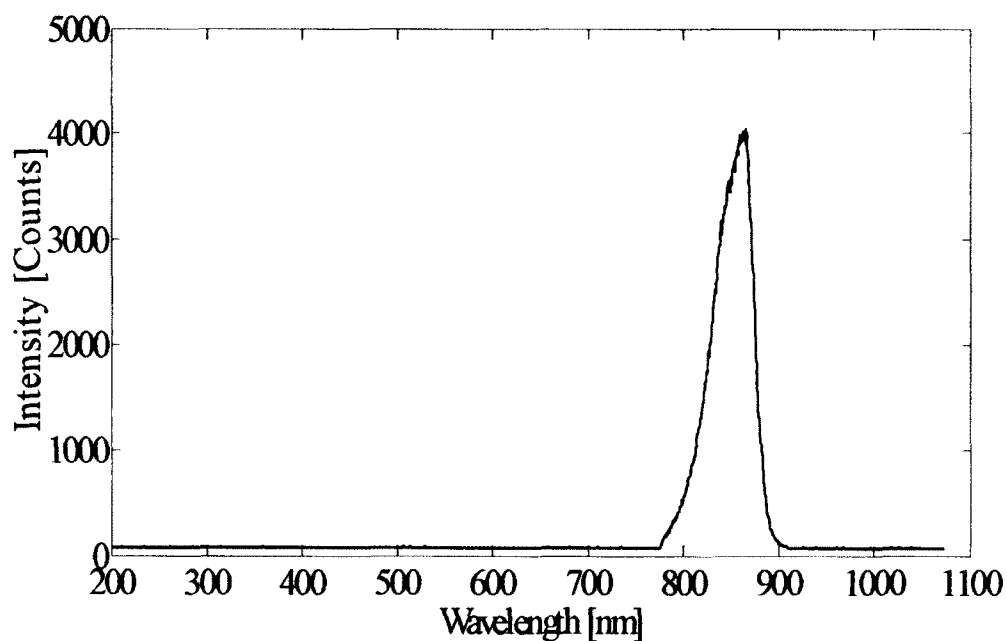


Figure B.1 Spectrum of LED Using OceanOptics Spectrometer

Figure B.1 shows the 850nm LED wavelength output and it has a much wider bandwidth than a laser, which varies by about 3nm. However, this LED's highest intensity varies by about 30nm. Another issue involves the power output of LEDs.

Commercial applications that use LEDs require very minimum power output. The LEDs used in this research are typically used in T.V. remote controllers. The power output for the 850nm LED was measured using a power meter and the results are shown in Figure B.2. The power meter used to measure the power output of the LED was a Coherent LABTOP Max.

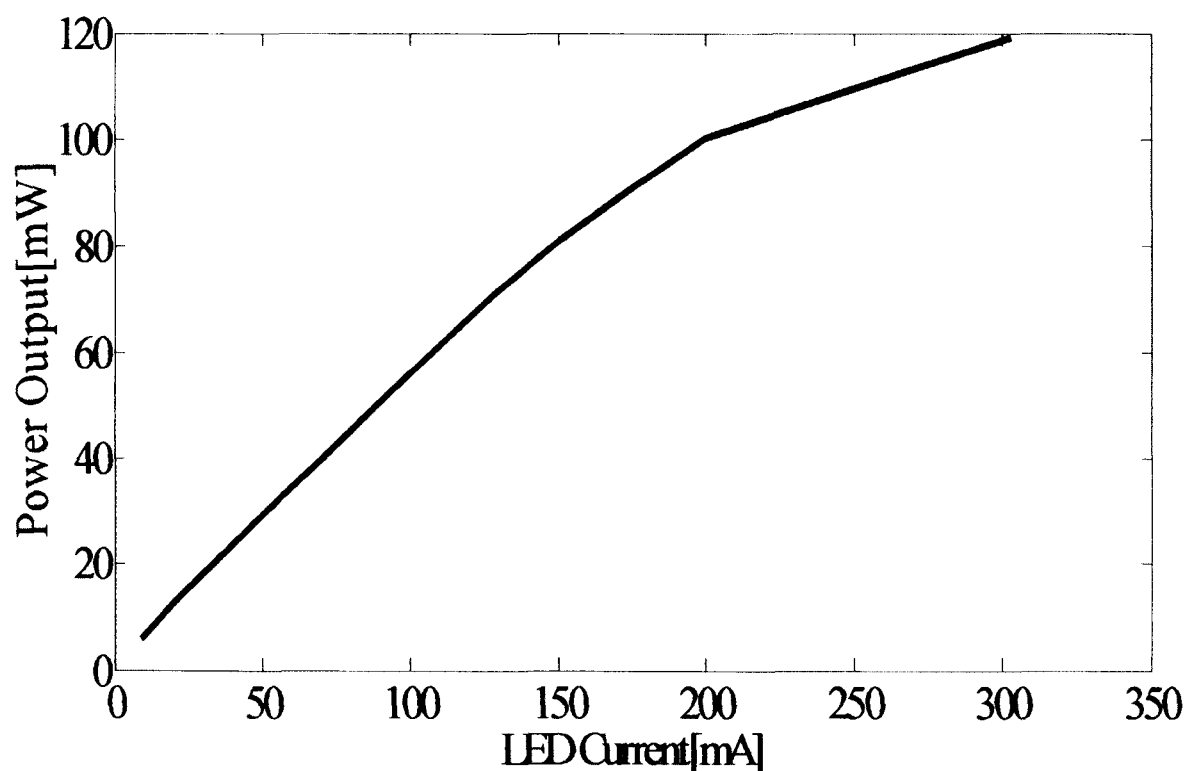


Figure B.2 Optical Power Output versus LED Current

The power output of the LED is for a typical 850nm LED used in the experiments. During this research the LED was voltage bias in order to maintain a current flow of 100mA. At 100mA the power output was around 60mW. The IR LED can be bias to have larger amounts of current to flow through the diode in order to increase the power output. However, the larger current flow beyond the recommend

current limits will decrease the life of the LED. Since LEDs are cheap it is possible to bias the LEDs beyond recommended limits. The etch rate results for the 850nm LED versus the reference is shown in Figure B.3.

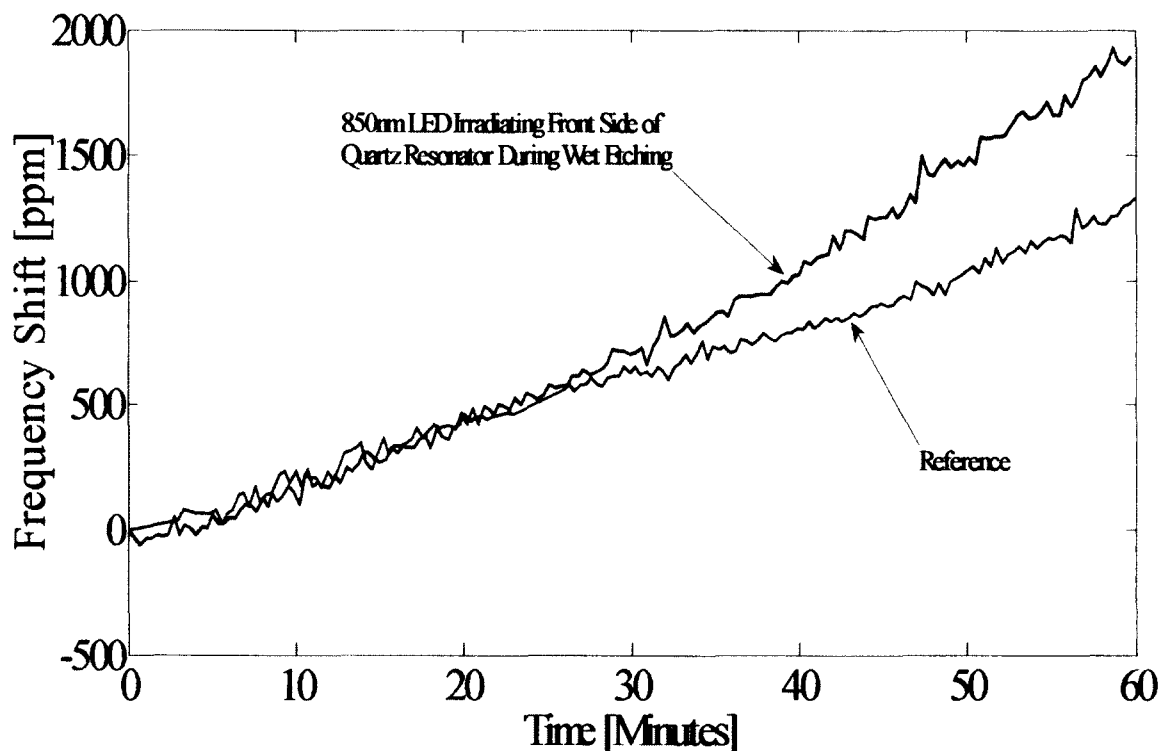


Figure B.3 Two Resonators Wet Etched, One with LED and a Reference

The 850nm LED increased the etch rate by 39% beyond the reference. The etch rate of the sample being irradiated by the 850nm LED followed previous results reported where the etch rate remained similar until the 30minute mark. There are other incoherent sources that were experimented with such as incandescent light bulbs. The next section will discuss experiments with 150, 500, and 1000 Watt incandescent light bulbs.

B.2. Incandescent Light Bulbs w/o IR Filter

This work looked into etching quartz crystals with incandescent light bulbs. Experiments were conducted with 150, 500, and 1000 Watt incandescent light bulbs. There were two experiments with the 150 Watt incandescent light bulb. The first experiment used only the 150W light. The second experiment also used an IR filter in series to block out the visible light. Figure B.4 shows the transmission percentage that the IR filter will allow to pass through it.

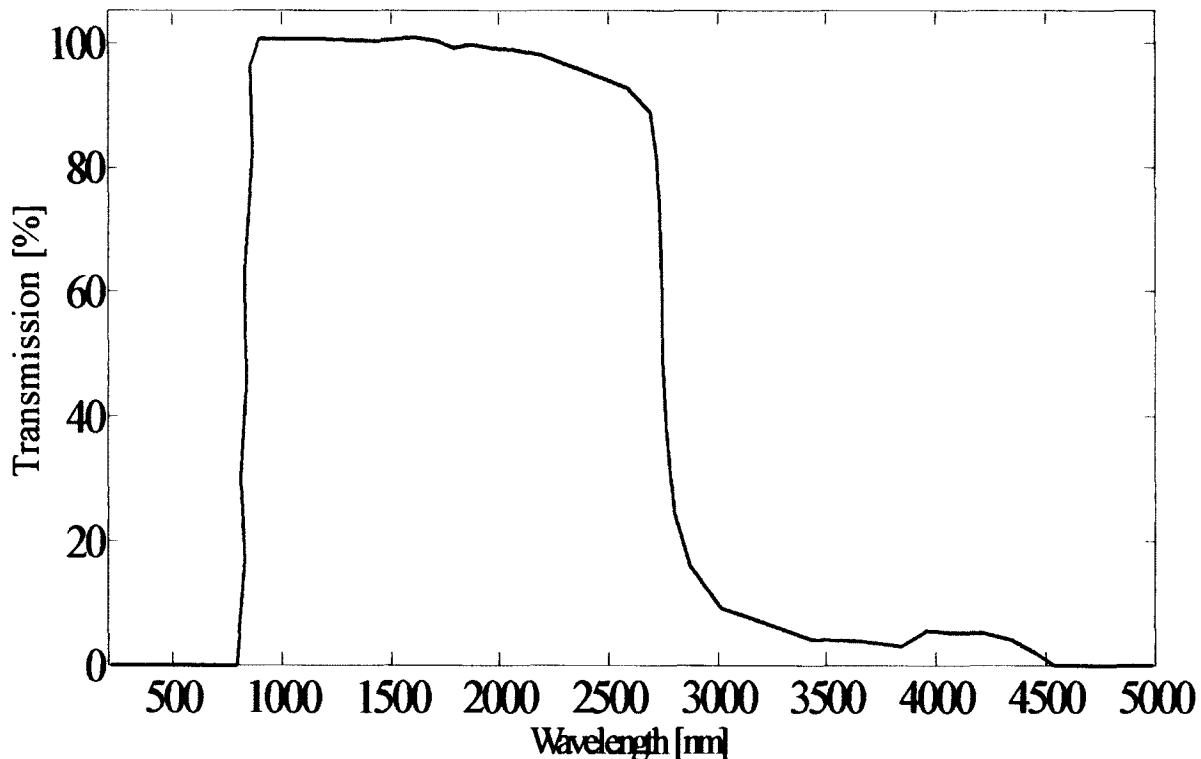


Figure B.4 Transmission Spectrum for IR Bandpass Filter

Figure B.4 shows that the IR filter will block out all of the visible light and allow only IR radiation from 830 to 4500nm. The cutoff wavelength for the IR filter is 830 +/-

9nm. Table B.2 shows the etch rate results for the different incandescent light bulbs compared to the 850nm IR LED.

Table B.2 Etch Results From Various Sources

| Irradiation Source | Etch Rate [$\mu\text{m/hr}$] | Percentage Difference From Reference [%] |
|--------------------------------------|--|---|
| 850nm IR LED | 0.973 | 39 |
| 150 Watt Light | 2.754 | 294 |
| 150 Watt Light with IR Filter | 1.518 | 118 |
| 500 Watt Light | 4.429 | 535 |
| 1000 Watt Light | 5.389 to 69.78 | 672 to 9898 |

Experiments were conducted with both a 500W and a 1000W incandescent light bulb. The etch rate can be increased significantly with the incandescent light bulbs. The 1000W incandescent bulb created a max etch rate of 69.78 $\mu\text{m/hr}$. The main problem with incandescent light bulbs is that they typically only emit 10% of their power in the form of light. Incandescent light bulbs lose more energy than laser diodes. It is much easier to mass produce using laser diodes instead of incandescent light bulbs due to the large size of the bulbs. Even though it is possible to increase the etch rate of quartz crystals using incandescent light bulbs it does not make practical sense to use these light bulbs in industry.

BIBLIOGRAPHY

- [1] TXC Corption, "2011 Company Overview," 2011.
- [2] Epson Toyocom, "Epson Toyocom QMEMS," [Online]. Available:
<http://www.epsontoyocom.co.jp/english/special/qmems/index.html>. [Accessed May 2012].
- [3] J. R. Vig, "IEEE Ultrasonics, Ferroelectrics, and Frequency Control Society," April 2012. [Online]. Available: www.ieee-uffc.org/frequency_control/teaching.asp. [Accessed July 2012].
- [4] M. S. McCorquodale, "Michael S. McCorquodale, Ph.D.," 5th April 2007. [Online]. Available: web.eecs.umich.edu/~mmccorq/seminars/mccorquodaleWIMS07.pdf [Accessed July 2012].
- [5] S. Cadel, "Electroiq," 22 Feburary 2012. [Online]. Available: www.electroiq.com/articles/stm/2012/02/mems-oscillators-occupy-1-timing-market-lure-more-makers.html. [Accessed June 2012].
- [6] F. Ayazi and R. Abdolvand, "Piezo-on-Diamond Resonators and Resonator Systems." Atlanta, GA, USA Patent 20080297281, 04 12 2008.
- [7] V. Kaajakari, Practical MEMS, Las Vegas, NV: Small Gear Publishing, 2009.

- [8] J. Nosek, "Drive level dependence of the resonant frequency in BAW quartz resonators and its modeling," *IEEE Transactions on Ultrasonics, Ferroelectrics, and Frequency Control*, pp. 823-829, July 1999.
- [9] F. Wantanabe and T. Watanabe, "Convex quartz crystal resonator of extremely high Q in 10MHz-50MHz," in *2002 IEEE Proceedings Ultrasonics Symposium*, Munich, Germany, 2002.
- [10] SiTime, "SiTime," [Online]. Available: www.sitime.com. [Accessed June 2012].
- [11] M. McCorquodale, "Self-referenced, trimmed and compensated RF CMOS harmonic oscillators as monolithic frequency generators," in *IEEE International Frequency Control Symposium*, Honolulu, HI, 2008.
- [12] M.S. McCorquodale, "A 25MHz all-CMOS reference clock generator for XO-replacement in serial wire interfaces," in *ISCAS 2008 IEEE International Symposium on Circuits and Systems*, Seattle, WA, 2008.
- [13] R. Ramus, "Alpha Quartz," *IEEE Potentials*, vol. 8, no. 4, pp. 9-12, 1989.
- [14] R.F. Milsom, D. Elliott, S. Terry-Wood and M. Redwood, "Analysis and design of coupled-mode miniature bar resonators and monolithic filters," *IEEE Transactions on Sonics and Ultrasonics*, vol. 30, no. 3, pp. 140-155, May 1983.
- [15] J.R. Vig, J. Lebus and R. Filler, "Chemically Polished Quartz," in *31st Annual Symposium on Frequency Control*, Fort Monmouth, NJ, 1977.
- [16] A. Zumsteg and P. Suda, "Properties of a 4 MHz Miniature Flat Rectangular Quartz Resonator Vibrating in a Coupled Mode," in *30th Annual Symposium on Frequency Control*, Fort Monmouth, NJ, 1976.

- [17] M.Deleuze, O. Cambon, A. Goiffon, A. Ibanez and E. Philippot, "Controlled dissolution of quartz material. Part I. Controlled dissolution of quartz plates in potassium and hydroxides: chemical thinning down of SC cuts," *Journal De Physique IV*, pp. 79-83, February 1994.
- [18] O.Cambon, M. Deleuze, J. Michel, J. Aubry, A. Goiffon and E. Philippot, "Controlled dissolution of quartz material. Part II. Quartz chemical etching applied to blanks industrial manufacturing," *Journal De Physique IV*, pp. 85-91, Feb 1994.
- [19] T. Abe, V. N. Hung and M. Esashi, "Inverted Mesa-Type Quartz Crystal Resonators Fabricated by Deep-Reactive Ion Etching," *IEEE Transactions on Ultrasonics, Ferroelectrics and Frequency Control*, pp. 1234-1236, July 2006.
- [20] K. Hjort, G. Thomell and J.-A. Schweltz, "Quartz micromachining by lithographics control of ion track etching," *Applied Physics Letters*, pp. 3435-3436, 1996.
- [21] H. Iwata, "Measured resonance characteristics of a 2GHz fundamental quartz resonator," *IEEE Transactions on Ultrasonics, Ferroelectrics, and Frequency Control*, pp. 1026-1029, August 2004.
- [22] M.Tanaka, "An overview of quartz MEMS devices," in *2010 IEEE International Frequency Control Symposium*, Newport Beach, CA, 2010.
- [23] J.K.Vondeling, "Fluoride-based etchants for quartz," *Journal of Materials Science*, pp. 304-314, 1983.
- [24] W.P.Hanson, "Chemically Polished High Frequency Resonators," in *37th Annual Symposium on Frequency Control*, Philadelphia, PA, 1983.

- [25] P.Suda, A. Zumsteg and W. Zingg, "Anisotropy of etching rate for quartz in ammonium bifluoride," in *33rd Annual Symposium on Frequency Control*, 1979.
- [26] A.J.Bernot, "Etching Study of AT-Cut Cultured Quartz Using Etchants Containing Fluoride Salts, Hydrofluoric Acid, and Ammonium Bifluoride," in *39th Annual Symposium on Frequency Control*, 1985.
- [27] O.Vallin, "Polishing of Quartz by Rapid Etching in Ammonium Bifluoride," *IEEE Transactions on Ultrasonics, Ferroelectrics and Frequency Control*, pp. 1454-1462, July 2007.
- [28] R.J.Brandmayr and J. Vig, "Chemical Polishing in Etching Solutions That Contain Surfactants," in *39th Annual Symposium on Frequency Control*, 1985.
- [29] S. L.Brantley, S. R. Crane, D. A. Crerar, R. Hellmann and R. Stallard, "Dissolution at dislocation etch pits in quartz," *Geochimica et Cosmochimica Acta*, pp. 2349-2361, 1986.
- [30] C.R.Tellier, "Effect of Crystal Orientation on the Surface Texture of Chemically Etched Quartz Plates, the Case of Cuts Close to the AT Cut," in *39th Annual Symposium on Frequency Control*, 1985.
- [31] J.R.Hunt, "Etch Pits and Channels in Swept AT- and SC-Cut Quartz," in *41st Annual Symposium on Frequency Control*, 1987.
- [32] J.R. Vig, "Etching Quartz Crystals," in *4th Annual Quartz Crystal Conference*, Kansas City, MO, 1982.
- [33] J.R. Vig, R. Brandmayr and R. Filler, "Etching Studies on Singly and Doubly Rotated Quartz Plates," 1979.

- [34] C.R.Tellier, "Experimental Study and Numerical Simulation of Quartz Crystal Etched Figures," in *40th Annual Symposium on Frequency Control*, 1986.
- [35] O.Ishii, T. Morita, T. Saito and Y. Nakazawa, "High frequency fundamental resonators and filters fabricated by batch process using chemical etching," in *IEEE International Frequency Control Symposium*, 1995.
- [36] T. Watanabe, "Mass production of quartz high speed chemical etching applied to at-cut wafers," in *IEEE International Frequency Control Symposium and PDA Exhibition*, 2001.
- [37] C.R.Tellier, "Some results on chemical etching of at-cut quartz wafers in ammonium bifluoride solutions," *Journal of Materials Science*, pp. 1348-1354, May 1982.
- [38] C.R.Tellier, "Etch Figures and Etch Rates in AT,BT,X and Y Cut Quartz Plates," in *38th Annual Frequency Control Symposium*, 1984.
- [39] J.J.Martin, "Electrodiffusion(Sweeping) of Ions in Quartz-A Review," *IEEE Transactions on Ultrasonics,Ferroelectrics and Frequency Control*, pp. 288-296, May 1988.
- [40] C.Wuthrich, S. D. Piazza, U. Ruedi and B. Studer, "Batch fabrication of AT-cut crystal resonators up to 200 MHz," in *Proceedings of the 1999 Joint Meeting of the European Frequency and Time Forum and the IEEE International Frequency Control Symposium*, 1999.

- [41] W.Clower, E. Rodrigue, C. Wilson and V. Kaajakari, "Electrical control for wet etching of quartz resonators," in *IEEE International Frequency Control Symposium, 2009 Joint with the 22nd European Frequency and Time Forum*, Bascon, France, 2009.
- [42] C. T. Kilian, *Modern Control Technology Components and Systems 3rd Edition*, Clifton Park, NY: Delmar Thomson Learning, 2006.
- [43] V. McNeil, "An investigation of the electrochemical etching of (100) silicon in CsOH and KOH," in *IEEE 4th Technical Digest Solid-State Sensor and Actuator Workshop*, 1990.
- [44] A. Gorecka-Drzazga, "Micro and nanostructurization of surfaces techniques and applications," *Optica Applicata* , vol. XXXVII, no. 4, pp. 341-357, 2007.
- [45] T.Trifonov, "Two- and three-dimensional microstructures produced by electrochemical etching of silicon," in *2005 Spanish Conference on Electron Devices*, 2005.
- [46] P.Kleimann, "Formation of three-dimensional microstructures by electrochemical etching of silicon," *Applied Physics Letters*, vol. 79, no. 11, pp. 1727-1730, 2001.
- [47] B.Kloeck, S. Collins, N. de Rooij and R. Smith, "Study of electrochemical etch-stop for high-precision thickness control of silicon membranes," *IEEE Transactions on Electron Devices*, vol. 36, no. 4, pp. 663-669, 1989.
- [48] H.Seidel, "The mechanism of anisotropic, electrochemical silicon etching in alkaline solutions," in *IEEE 4th Solid-State Sensor and Actuator Workshop*, 1990.

- [49] J.C.Flakea, "Electrochemical Etching of Silicon in Nonaqueous Electrolytes Containing Hydrogen Fluoride or Fluoroborate," *Journal of Electrochemical Society*, vol. 146, no. 5, pp. 1960-1965, 1999.
- [50] E. Conway, "Electrochemical characterization of Si in TMAH and TMAH:Triton-X-100 solutions under white light effects," *Journal of Micromechanics and Microengineering*, vol. 12, no. 2, pp. 136-148, 2002.
- [51] R. Jarimaviciute-Zvalioniene, V. Grigaliunas, S. Tamulevicius and A. Guobiene, "Fabrication of porous silicon microstructures using electrochemical etching," *Materials Science (Medziagotyra)*, vol. 9, no. 4, pp. 317-320, 2003.
- [52] R. Voss, H. Siedel and H. Baumgartel, "Light-controlled, electrochemical, anisotropic etching of silicon," in *1991 International Conference on Solid-State Sensors and Actuators, Digest of Technical Papers TRANSDUCERS '91*, San Francisco, CA, 1991.
- [53] H. C. Kim, D. H. Kim and K. Chun, "Photo-assisted electrochemical etching of a nano-gap trench with high aspect ratio for MEMS applications," *Journal of Micromechanics and Microengineering*, vol. 16, no. 5, pp. 906-913, 2006.
- [54] B.Lesche, F. Garcia, E. Hering, W. Margulis, I. Carvalho and F. Laurell, "Etching of silica glass under electric fields," *Physical Review Letters*, vol. 78, no. 11, pp. 2172-2175, 1997.
- [55] R. Powell and G. Derbenwick, "Vacuum Ultraviolet radiation effects in SiO₂," *IEEE Transactions on Nuclear Science*, vol. 18, no. 6, pp. 99-105, 1971.

- [56] C. Hedlund, U. Lindberg, U. Bucht and J. Soderkvist, "Anisotropic etching of Z-cut quartz," *Journal Micromechanical Microengineering*, vol. 3, pp. 65-73, 1993.
- [57] F. Ernsberger, "Structural effects in the chemical reactivity of silica and silicates," *Journal of Physics and Chemistry of Solids*, vol. 13, no. 3-4, pp. 347-351, 1960.
- [58] S.-P. Choong, "Influence of Magnetic Fields and X-rays on the Etching of Quartz," *Nature*, vol. 201, no. 4922, pp. 910-911, 1964.
- [59] S.-P. Choong, "Influence of Ultra-Violet Radiations on the Etching of Quartz," *Nature*, vol. 154, no. 3912, pp. 516-517, 1944.
- [60] Stanford Research Systems, 2012. [Online]. Available: <http://www.thinksrs.com/products/PS300.htm>. [Accessed September 2012].
- [61] Oxford Instruments, [Online]. Available: <http://www.oxford-instruments.com>.
- [62] S. Kothan and M. Tungjai, "An estimation of x-radiation output using mathematic model," *American Journal of Applied Science*, vol. 8, no. 9, pp. 923-926, 2011.
- [63] J. Riddell, J. Chervenak and V. van Lint, "Ionization-Induced Breakdown and Conductivity of Satellite Dielectrics," *IEEE Transactions on Nuclear Science*, vol. 29, no. 6, pp. 1754-1759, Dec 1982.
- [64] M. Block, O. Mancini and T. McClelland, "Performance of Rubidium and quartz clocks in space," in *IEEE Frequency Control Symposium and PDA Exhibition*, 2002.
- [65] R. Belser and W. Hicklin, "Stability studies of quartz crystals for satellites," in *IEEE 15th Annual Symposium on Frequency Control*, 1961.

- [66] M. Bloch, O. Mancini and T. McClelland, "Effects of radiation on performance of space-borne quartz crystal oscillators," in *2009 IEEE International Frequency Control Symposium Joint with the 22nd European Frequency and Time Forum*, 2009.
- [67] G. Cibiel, B. Boizot, J. Boy, J. Carlotti, O. Cambon, S. Devautour-Vinot, V. Candelier, J. Lamboley, P. Guibert, A. Largeteau, C. Inguibert and D. Piccheda, "Ultra stable oscillators dedicated for space applications: oscillator and quartz material behaviors vs radiation," in *IEEE International Frequency Control Symposium and Exposition*, 2006.
- [68] M. Treadaway, C. Mallon, T. Flanagan, R. Denson and E. Wenaas, "The effects of high energy electrons on the charging of spacecraft dielectrics," *IEEE Transactions on Nuclear Science*, vol. 26, no. 6, pp. 5101-5106, 1979.
- [69] J. Lefevre, S. Devautour-Vinot, O. Cambon, J.-J. Boy, P. Guibert, R. Chapoulie, C. Inguibert, D. Piccheda, A. Largeteau, G. Demazeau and G. Cibiel, "Characterization of unswept and swept quartz crystals for space applications," *Journal of Applied Physics*, vol. 105, no. 11, pp. 113523-113523(8), 2009.
- [70] R. Hughes, "Transient x-ray induced conductivity in single crystal fused quartz," in *IEEE 27th Annual Symposium on Frequency Control*, 1973.
- [71] T. Ahrens and F. Wooten, "Electrical conductivity induced in insulators by pulsed radiation," *IEEE Transactions on Nuclear Science*, vol. 23, no. 3, pp. 1268-1272, June 1976.

- [72] J. Martin, S. Doherty, L. Halliburton, M. Markes, N. Koumvakalis and W. Sibley, "Radiation induced mobility of interstitial ions in synthetic quartz," in *IEEE 33rd Annual Symposium on Frequency Control*, 1979.
- [73] R. Hughes, "Electronic and ionic charge carriers in irradiated single crystal and fused quartz," *Radiation Effects*, vol. 26, no. 4, pp. 225-235, 1975.
- [74] L. Halliburton, "Defect models and radiation damage mechanisms in alpha quartz," *Crystal Lattice Defects and Amorphous Materials*, vol. 12, pp. 163-190, 1984.
- [75] R. Poll and S. Ridgway, "Effects of pulsed ionizing radiation on some selected quartz oscillator crystals," *IEEE Transactions on Nuclear Science*, vol. 13, no. 6, pp. 130-140, Dec 1966.
- [76] D. Nichols and A. van Lint, "Theory of Transient electrical effects in irradiated insulators," *IEEE Transactions on Nuclear Science*, vol. 13, no. 6, pp. 119-126, Dec 1966.
- [77] F. Euler, P. Ligor, A. Kahan, P. Pellegrini, T. Flanagan and T. Wrobel, "Steady state radiation effects in precision quartz resonators," in *IEEE 32nd Annual Symposium on Frequency Control*, 1978.
- [78] J. King and H. Sander, "Transient change in q and frequency of at-cut quartz resonators following exposure to pulse x-rays," *IEEE Transactions on Nuclear Science*, vol. 20, no. 6, pp. 117-125, Dec 1973.
- [79] T. Flanagan and T. Wrobel, "Radiation effects in swept synthetic quartz," *IEEE Transactions on Nuclear Science*, vol. 16, no. 6, pp. 130-137, Dec 1969.

- [80] A. Nowick and H. Jain, "Electrical Conductivity and Dielectric Loss of Quartz Crystals Before and After Irradiation," in *IEEE 34th Annual Symposium on Frequency Control*, 1980.
- [81] K. Byrappa and M. Yoshimura, *Handbook of Hydrothermal Technology-A Technology fo Crystal Growth and Materials Processing*, Park Ridge, New Jersey: Noyes Publications, 2001.
- [82] H. Bahadur and R. Parshad, "Effect of Irradiation on Crystal Defects in Quartz," *IEEE Transactions on Nuclear Science*, vol. NS-32, no. 2, pp. 1169-1179, 1985.
- [83] A. Müller, J. E. Wanvik and P. M. Ihlen, "Petrological and Chemical Characterization of High-Purity Quartz Deposits with Examples from Norway," in *Quartz: Deposits, Mineralogy and Analytics*, Heidelberg, New York, Dordrecht, London, Springer, 2012, pp. 71-118.
- [84] D. Hart, J. Frank, D. Smith, J. Martin and J. Gualtieri, "A study of the electrodiffusion process in quartz," in *Proceedings of the 44th Annual Symposium on Frequency Control*, 1990.
- [85] J. Martin, R. Bossoli, L. Halliburton, B. Subramaniam and J. West, "Electrodiffusion of Charge-Compensating Ions in Alpha-Quartz," in *37th Annual Symposium on Frequency Control*, 1983.
- [86] G. Gibson and R. Vogel, "Migration of Lithium and Several Multicharged Ions through Quartz Plates in an Electric Field. II," *Journal of Chemical Physics*, vol. 18, no. 8, pp. 1094-1098, 1950.

- [87] J. Brice, "Crystals for quartz resonators," *Reviews of Modern Physics*, vol. 57, no. 1, pp. 105-148, 1985.
- [88] D. Koehler, "Radiation-Induced Frequency Transients in AT, BT and SC Cut Quartz Resonators," in *33rd Annual Symposium on Frequency Control*, 1979.
- [89] M. Bloch, O. Mancini and T. McClelland, "Effects of Radiation on Performance of Space-Borne Quartz Crystal Oscillators," in *IEEE International Frequency Control Symposium 2009 Joint with the 22nd European Frequency and Time Forum*, Besancon, France, 2009.
- [90] E. Rodrigue and V. Kaajakari, "Electrochemical etching of crystalline quartz," *Electrochemical and Solid-State Letters*, vol. 12, no. 1, pp. D1-D2, 2009.
- [91] E. Rodrigue and V. Kaajakari, "Electrochemical etching of quartz," in *IEEE Ultrasonics Symposium*, 2007.
- [92] S. White, "Ionic diffusion in quartz," *Nature*, vol. 225, pp. 375-376, Jan 24 1970.
- [93] J. Verhoogen, "Ionic diffusion and electrical conductivity in quartz," *American Mineralogist*, vol. 37, pp. 637-655, 1952.
- [94] A. Kronenberg and S. Kirby, "Ionic conductivity of quartz: DC time dependence and transition in charge carriers," *American Mineralogist*, vol. 72, pp. 739-747, 1987.
- [95] D. Koehler, "Radiation-Induced Conductivity and High Temperature Q Changes in Quartz Resonators," in *35th Annual Frequency Control Symposium*, 1981.
- [96] R. McGinnis, "Rad Pro Calculator," [Online]. Available: <http://www.radprocalculator.com/Index.aspx>. [Accessed July 2012].

- [97] H. Wenden, "Ionic diffusion and the properties of quartz I. The direct current resistivity," *The American Mineralogist*, pp. 859-888, Nov-Dec 1957.
- [98] J. Wang, H. Niino and A. Yabe, "Micromachining Quartz Crystal with Excimer Lasers by Laser-Induced Backside Wet Etching," *Applied Physics A Materials Science & Processing*, vol. 69, pp. 271-273, 1999.
- [99] H. Varel, D. Ashkenasi, A. Rosenfeld, M. Wahmer and E. Campbell, "Micromachining of Quartz with Ultrashort Laser Pulses," *Applied Physics A Materials Science & Processing*, vol. 65, no. 4/5, pp. 367-374, 1997.
- [100] J. Ihlemann, B. Wolff and P. Simon, "Nanosecond and Femtosecond Excimer Laser Ablation of Fused Silica," *Applied Physics A Solids and Surfaces*, vol. 54, pp. 363-368, 1992.
- [101] G. Kopitkovas, T. Lippert, C. David, A. Wokaun and J. Gobrecht, "Fabrication of Micro-Optical Elements in Quartz by Laser Induced Backside Wet Etching," *Microelectronic Engineering*, vol. 67-68, pp. 438-444, 2003.
- [102] S. Matsuo, Y. Tabuchi, T. Okada, S. Juodkazis and H. Misawa, "Femtosecond Laser Assisted Etching of Quartz: Microstructuring From Inside," *Applied Physics A*, vol. 84, pp. 99-102, 2006.
- [103] OEM Laser Systems, Inc, "OEM Laser Specs Reference," 2004-2013. [Online]. Available: <http://www.oemlasersystems.com/product-catalog/continuous-wave-laser-systems/801nm-900nm-laser-systems/808nm-diode-laser-systems/5000mw-808nm-diode-laser-system-5-power-stability-detail>. [Accessed April 2013].

- [104] C. H. Henry, "Theory of Spontaneous Emission Noise in Open Resonators and its Application to Lasers and Optical Amplifiers," *Journal of Lightwave Technology*, vol. LT-4, no. 3, pp. 288-297, 1986.
- [105] H. Sun, *Laser Diode Beam Basics, Manipulations and Characterizations*, Springer Netherlands, 2012.
- [106] RPC Photonics, 2007-2013. [Online]. Available: www.rpcphotonics.com/engineered.asp. [Accessed 2nd July 2013].
- [107] M. Polyanskiy, "Refractive Index Database," 2008 to 2013. [Online]. Available: <http://refractiveindex.info>. [Accessed July 2013].
- [108] K. Sugioka, M. S. Brown and C. B. Arnold, "Fundamentals of Laser-Material Interaction and Applications to Multiscale Surface Modification," in *Laser Precision Microfabrication*, Verlag, Berlin, Heidelberg, Springer, 2010, pp.91-120.
- [109] COMSOL® Inc, "COMSOL Showroom: Laser Heating- A Self Guided Tutorial," 2013. [Online]. Available: <http://www.comsol.com/showroom/gallery/12317/>. [Accessed July 2012].
- [110] D. L. Shealy and J. A. Hoffnagle, "Beam Shaping Profiles and Propagation," in *SPIE Conference Laser Beam Shaping VI*, 2005.
- [111] COMSOL Multiphysics, *Heat Transfer Module User's Guide*, COMSOL, May 2012.
- [112] Filmetrics, *Advanced Thin-Film Measurement Systems*, San Diego, CA, 2012.